INFORMATION TO USERS

This manuscript has been reproduced from the microfilm master. UMI films the text directly from the original or copy submitted. Thus, some thesis and dissertation copies are in typewriter face, while others may be from any type of computer printer.

The quality of this reproduction is dependent upon the quality of the copy submitted. Broken or indistinct print, colored or poor quality illustrations and photographs, print bleedthrough, substandard margins, and improper alignment can adversely affect reproduction.

In the unlikely event that the author did not send UMI a complete manuscript and there are missing pages, these will be noted. Also, if unauthorized copyright material had to be removed, a note will indicate the deletion.

Oversize materials (e.g., maps, drawings, charts) are reproduced by sectioning the original, beginning at the upper left-hand corner and continuing from left to right in equal sections with small overlaps.

Photographs included in the original manuscript have been reproduced xerographically in this copy. Higher quality 6" x 9" black and white photographic prints are available for any photographs or illustrations appearing in this copy for an additional charge. Contact UMI directly to order.

Bell & Howell Information and Learning
300 North Zeeb Road, Ann Arbor, MI 48106-1346 USA

UMI®
800-521-0600

SILANES AND ALLYLSILANES AS POSSIBLE PRECURSORS FOR TRANSITION METAL-STABILIZED SILYLIUM IONS.

By

RAFFAELE RUFFOLO, B. Sc.

A Thesis

Submitted to the School of Graduate Studies

in Partial Fulfillment of the Requirements

for the Degree

Doctor of Philosophy

McMaster University

SILANES AND ALLYLSILANES AS POSSIBLE PRECURSORS FOR TRANSITION METAL-STABILIZED SILYLIUM IONS.

To Nonno Mario

who always believed in me

DOCTOR OF PHILOSOPHY (1997) McMaster University

(Chemistry) Hamilton Ontario

TITLE: Silanes and Allylsilanes as Possible Precursors for Transition Metal-Stabilized Silylium Ions

AUTHOR: Raffaele Ruffolo, B. Sc. (McMaster University)

SUPERVISOR: Professor M. J. McGlinchey and Professor M. A. Brook

NUMBER OF PAGES: xiv, 140

ABSTRACT

Extended Hückel molecular orbital calculations on silicon cations $[HC{\equiv}C\text{-}Si(CH_3)_2)Co_2(CO)_6]^+$ reveal that the favored geometry for this silylium ion requires the SiH_2 group to lean towards a $Co(CO)_3$ vertex. This parallels the known behavior of carbocations with metal cluster vertices whereby the electron-deficient center is stabilized by a direct interaction with an organometallic fragment. These calculations also show that replacement of $Co(CO)_3$ vertices by isolobal $CpMo(CO)_2$ groups noticeably enhances the stabilization of the silylium moiety.

The most successful approach for the synthesis of silylium ions reported to date has been the removal of hydride from a suitable silane precursor. In the attempt to generate a metal-stabilized silylium ion the silane, $(CH_3)_3Si\text{-}C{\equiv}C\text{-}Si(C_6H_5)_2H[Mo_2(CO)_4Cp_2]$, was treated with triphenylmethyl tetrafluoroborate; however, the cluster compound was recovered unchanged. It is apparent from the X-ray structure that the dimetallic cluster and the two phenyl groups inhibit the approach of the trityl for reaction with the Si-H group.

The next strategy used in the study involved construction of a tetracoordinate silicon with an alkynyl, two alkyl substituents and a fourth group possessing a reactive site, outside the steric sphere, capable of being removed when treated with the appropriate reagent. In our studies, protonation of an alkynyl-allylsilane (free, or metal-complexed alkyne) with either HBF_4 or triflic acid readily occurs with elimination of propene and formation of the corresponding silyl fluoride or triflate. A competition reaction between free and metal-

complexed alkynyl-allylsilanes with a limiting amount of acid showed no discrimination between free alkynes or their metal complexed analogues.

The study of precursor compounds which contain both a carbocation site (i.e., alcohol or isopropenyl) and an allylsilane yielded initially the metal stabilized carbocation which subsequently underwent allyl transfer with concomitant formation of a fluorosilane. In contrast, replacement of a cobalt tricarbonyl vertex by $Fe(CO)_3$ fragment gave, upon treatment with HBF_4, the corresponding fluorosilane that was characterized by X-ray crystallography.

ACKNOWLEDGEMENTS

I wish to express my sincere gratitude to my supervisors Dr. M. J. McGlinchey and Dr. M. A. Brook for the guidance that they provided throughout the course of the work as well as their initial support before I was accepted into Graduate school. Dr. M. J. McGlinchey: thanks for the many discussions we had about chemistry (or whatever the topic may have been) and the encouragement I received when chemistry wasn't quite working out. Dr. Brook: I would like to express my appreciation for you support, guidance, and inspiring words.

I would also like to thank my supervisory committee, Dr. W. J. Leigh and Dr. L. Li for their time and input into my thesis research. Special thanks go to Dr. Luc Girard, Dr. Andreas Decken and Dr. Hari Gupta who all helped me in my first graduate year while my supervisors were in Europe on sabbatical.

I appreciate the assistance from Dr. Don Hughes and Mr. Brian Sayer in the NMR facility. I would also like to thank Dr. Richard Smith and the all mass spec. support team. A note of thanks to Dr. Jim Britten for helping me obtain several crystal structures and answering the many questions I always had on crystallography. Without the help and expertise of the above mentioned people, characterization of compounds that I found to be routine would have been hell. I would also like to thank the ladies in the Chemistry Departments Office.

To everyone with whom I worked in ABB-357, Andreas, Luc, Lisa, Hari, Pippa, Suzie, Jamie, Mark, Dave Pole and Stacey: thank-you for putting up with my antics and making my time in the lab enjoyable. To everyone in ABB-466, JJ, Graham, Courtney, Mike, Tom, Grant, David Valentini, Dave Bayles, Denny, Christophe, Vasso, Rodica, Sonia, Frank, Mustafa, Giles and Gang: thank you for your friendship and chemical expertise.

I must also mention some other people in the department whom made my time at McMaster a very memorable one. I thank John Valliant, Christine, Nick, Bruce, Rabah, John Pezacki, Dave Lavorato, Chooch, Mark Fava, Erin, Randy and Buck, for the many discussions, baseball and/or basketball games and beers that we shared at the Phoenix.

I particularly want to thank Jamie and Mark my goalie and defensive partner (respectively): thanks for being good friends and covering up for me. I would also like to thank my old friends Pippa, John Valliant and Christine, for the many great times and useful discussions.

A very special thanks goes out to Adrienne, who means everything to me. Thanks for your loving support. Lastly, many thanks to my parents, my grandmother, Rosaria, my sister, Rosemary, my aunt, uncle and cousins, Laura and Michelle (oh yes, I forgot Uncle Guido), for their support throughout my graduate career.

Table of Contents

List of Figures

List of Schemes

List of Tables

1. INTRODUCTION

1.1. Comparison of Silicon and Carbon

The proximity of silicon to carbon in Group 14 of the Periodic Table has led to many comparative studies on the chemistry of the two elements. For many years, a variety of silicon analogues of carbon-based functionalilties were considered to be unlikely structural entities. For example, it was only relatively recently reported that compounds containing multiple bonds to silicon could be prepared.[1] By analogy to the well-studied R_3C^+ ions in organic chemistry, many investigators have attempted to prove the existence of R_3Si^+ ions as intermediates in reactions.

Silicon atoms are about 50 % larger than carbon and this increased size has several ramifications, including lower barriers to silicon-element bond rotations and also less stable π–bonds. There are, further, two major properties that distinguish silicon from carbon; first, their respective electronegativities and, second, the common coordination numbers of each. The respective electronegativities of carbon and silicon are 2.5 and 1.8 (Pauling Scale),[2] and lower electronegativity of silicon should result in more polar silicon-element bonds compared to carbon. This bond polarity contributes to strong silicon bonds (e.g., to oxygen and halides) and provides the driving force in reactions (i.e., the formation of very stable products). The Pauling electronegativity of silicon is actually similar to that of some of the first-row transition metals. The difference in electronegativity between silicon and carbon would suggest that formation of R_3Si^+ ions by heterolytic cleavage of $Si^{\delta+}$- $X^{\delta-}$ bonds (X = C, halogen, etc.) should be easier than the formation of the corresponding R_3C^+ species. This is indeed the case in the gas phase.[3]

The types of available carbon and silicon environments also differ markedly as shown in Figure 1-1. Silicon differs from carbon in that it forms fewer stable multiple bonds but more stable derivatives with more than four bonds than carbon; carbon generally will carry a maximum of four single covalent bonds, though it is known to exist in some organometallic (transition metal) carbide derivatives with five or more nearest neighbors.[4]

The lack of multiple bonds seriously hampers synthetic strategies in silicon chemistry in comparison to the possibilities available in carbon chemistry. This is counterbalanced, however, by the ease of formation of hypervalent species which translates into relatively low activation energies for nucleophilic substitutions at silicon compared to carbon, and a greater range of reaction pathways at tetrahedral silicon centers than are accessible to their carbon analogues.

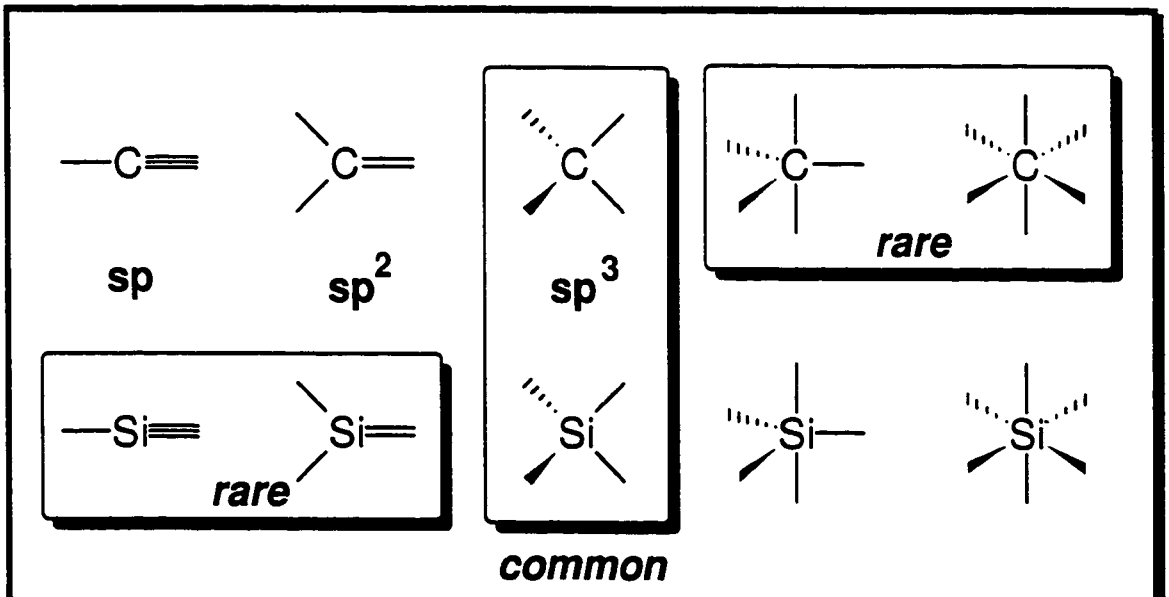

Figure 1-1: Common environments of Si and C.

1.2. Examples of metal stabilized carbocations

The ability of neighbouring atoms to provide anchimeric assistance to electron-deficient centers is well-established in conventional organic chemistry. For instance, the rate of hydrolysis of 2,2′-dichlorodiethyl sulfide, **1**, (the mustard gas of World War I) is enormously enhanced compared to that found for ordinary primary alkyl halides. This occurs because the neighboring sulfur atom can provide a lone pair of electrons to alleviate the developing cationic charge on carbon; rapid nucleophilic attack on the sulfonium ion intermediate, **2**, leads to product formation.[5]

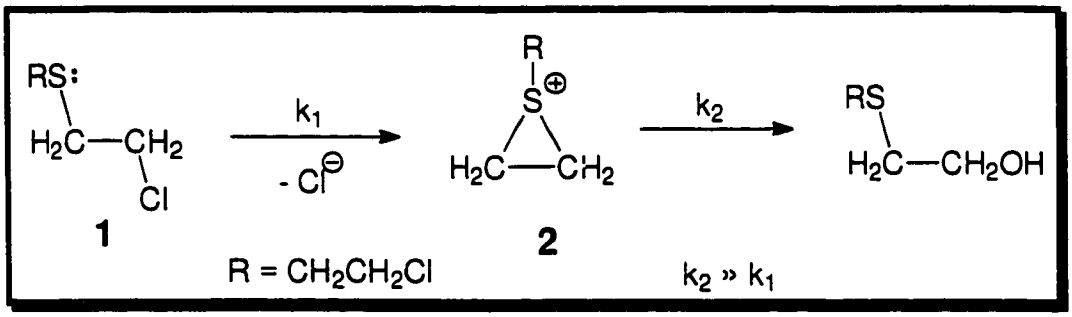

Analogously, a wide variety of organometallic moieties, such as ferrocenyl,[6] (cyclobutadienyl)$Fe(CO)_3$,[7] (cyclobutadienyl)$Co(C_5H_5)$,[8] and (cyclopentadienyl)-$Cr(CO)_2NO$,[9] have been shown to provide neighboring group assistance to developing cationic centers; this pioneering work has been reviewed previously.[10] Typically, the 100,000-fold rate enhancement of benzyl halides, when π-complexed to $Cr(CO)_3$, has been attributed to stabilization of the intermediate cation by interaction with the electron-rich metal center.[11] Indeed, in recent years, cationic intermediates, such as **3**, have been characterized by NMR spectroscopy.[12-15] Even more convincingly, the structure of the

ferrocenylmethyl cation, **4**, has been determined by X-ray crystallography,[16, 17] and the 22° bend of the sp^2-hybridized carbocationic center towards the metal atom has been rationalized in terms of a fulvene ligand coordinated to a $(C_5H_5)Fe^+$ moiety.[18]

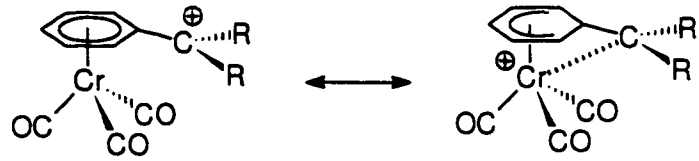

3a **3b**

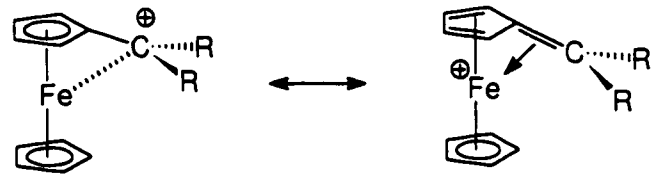

4a **4b**

In light of these observations, it is perhaps not unexpected that metal clusters should be capable of alleviating the positive charge on proximally attached atoms or molecular fragments which are not part of aromatic systems.[19-21] Indeed, the capacity of metal clusters for cation stabilization is almost unsurpassed.

1.2.1. Molecular Orbital Calculations.

Our understanding of the bonding in these cluster-stabilized cations derives principally from extended Hückel molecular orbital calculations carried out initially by Schilling and Hoffmann.[22] In a now classic paper they described the interactions of the frontier orbitals of triangular M_3L_9 fragments with a variety of capping groups. The orbital

pattern of an $Fe_3(CO)_9$ triangle can be constructed from suitable symmetry-adapted combinations of the three constituent $Fe(CO)_3$ moieties.[23]

As shown in Figure 1-2, each $M(CO)_3$ fragment contributes three frontier orbitals to the triangular unit. The lowest of these is primarily d_{xy} hybridized towards the missing sites of the octahedron from which the fragment was formally derived. These three in-plane orbitals yield a doubly degenerate *1e* set and a high-lying a_2 orbital. The former are filled and provide good metal-metal bonding interactions while the latter (which is an entirely out-of-phase combination) is also in the plane of the metals but is normally vacant. The combination of d_{z^2} orbitals from the three constituent $M(CO)_3$ fragments produces the classic a_1 π-type orbital as well as the doubly degenerate π* set of *e* symmetry; this orbital level pattern is analogous to that of the π manifolds found in cyclopropenium and related systems. It is noteworthy, however, that these d_{z^2} combinations do not overlap well with orbitals of the capping group which are aligned along the C_3 axis of the cluster. However, this role is more than adequately filled by the in-phase combination of the remaining orbitals of the $M(CO)_3$ fragment; each of these is a mixture of *s*, p_z and d_{z^2} and their bonding combination is oriented perfectly to interact with the capping atom.[22]

To summarize, therefore, metal triangles such as $[Fe_3(CO)_9]$, **5**, or $[Co_3(CO)_9]^{3+}$, **6**, give rise to a low-lying set of three filled orbitals (*1e* + $1a_1$) and, at somewhat higher energy, a set of three vacant orbitals ($2a_1$ + *2e*) which serve to accept electron density from capping ligands. In light of the EHMO analysis presented above, it is apparent that a carbyne moiety (represented formally as HC^{3-}) has a filled *sp*-hybrid orbital ideally oriented to interact with

the vacant $2a_1$ combination of the $[Co_3(CO)_9]^{3+}$ triangle. Moreover, the two occupied π-orbitals of the carbyne have the correct symmetry to overlap with the degenerate *2e* acceptor pair, as shown in Figure 1-3.

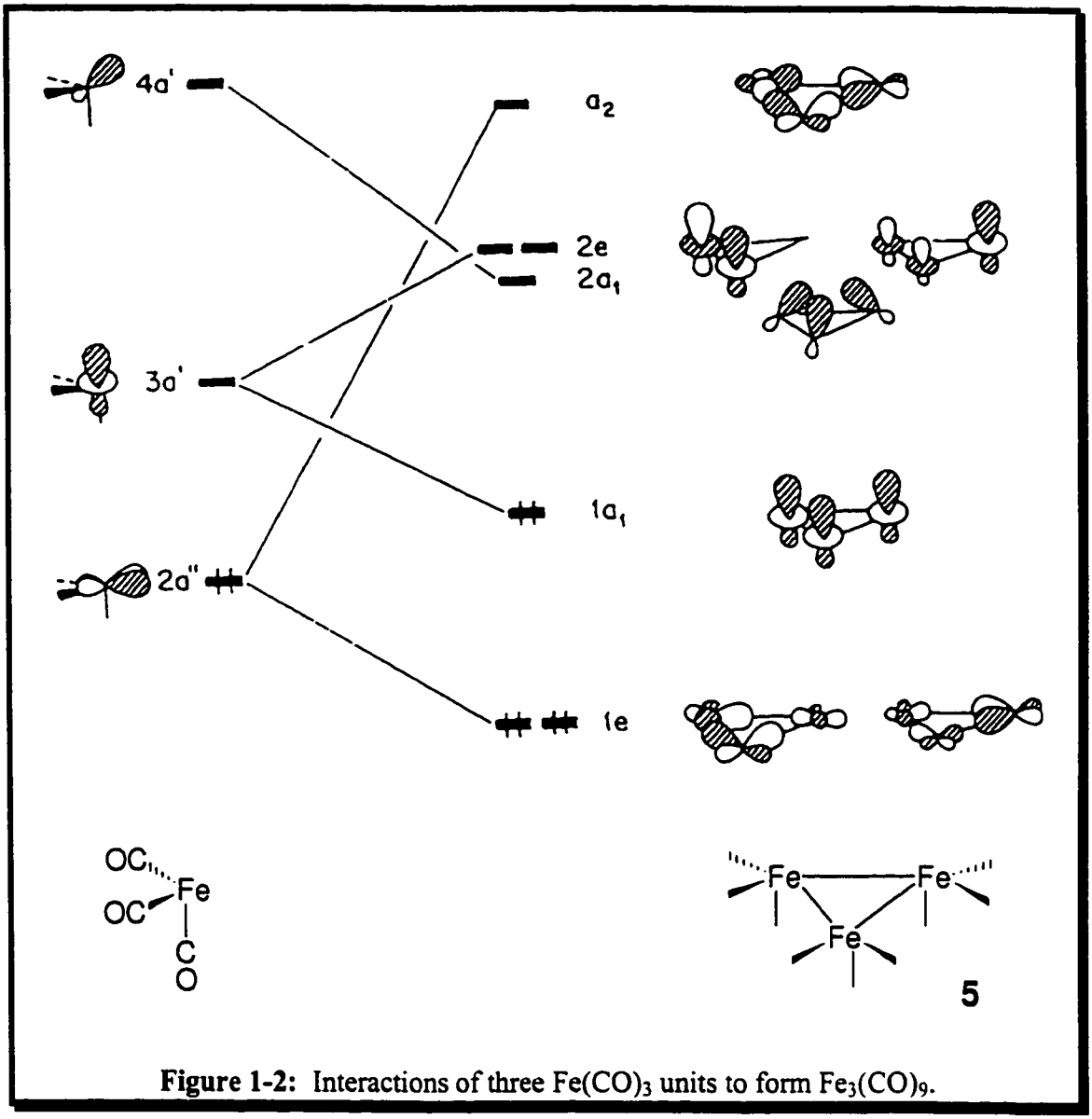

Figure 1-2: Interactions of three $Fe(CO)_3$ units to form $Fe_3(CO)_9$.

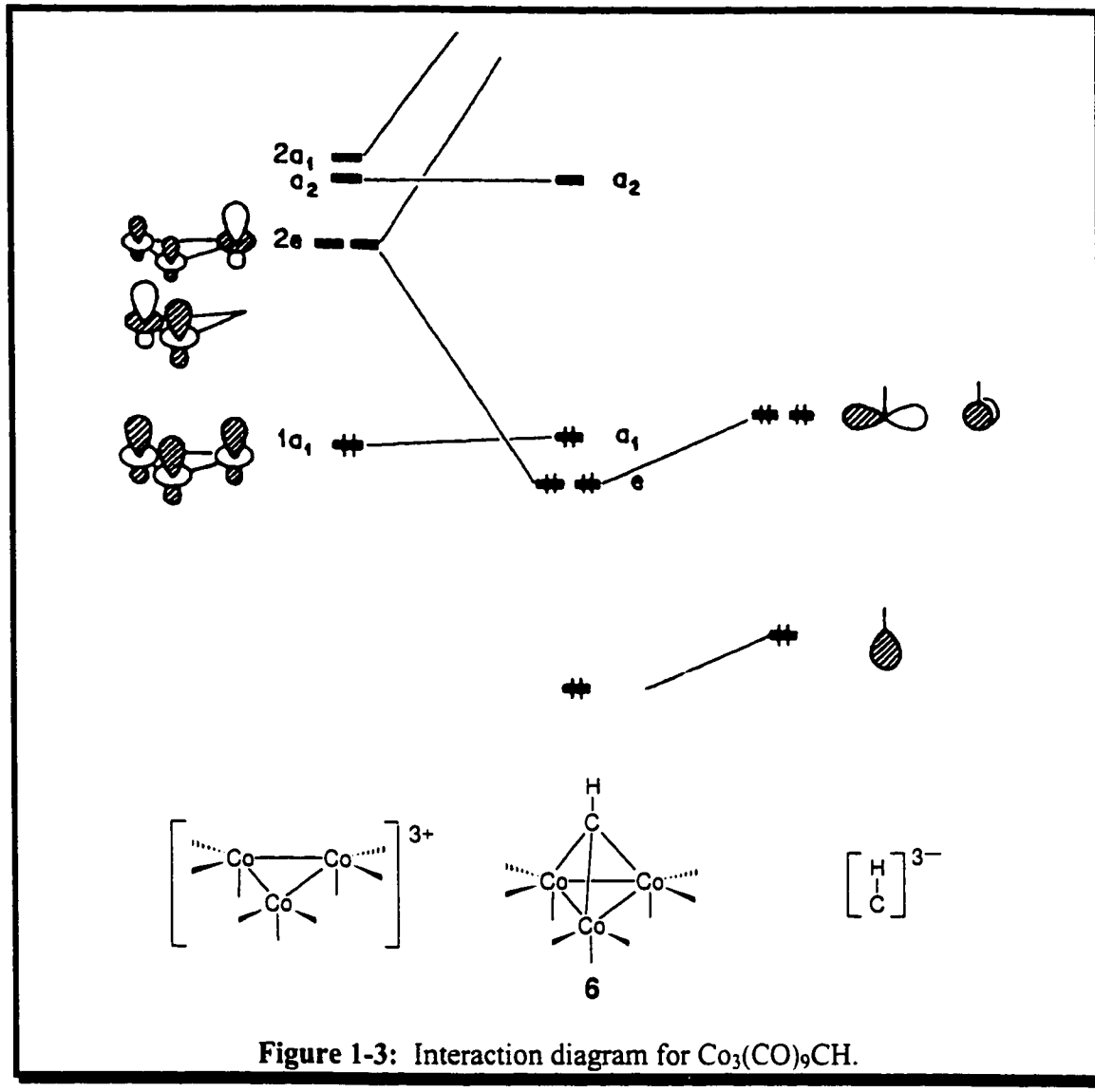

Figure 1-3: Interaction diagram for $Co_3(CO)_9CH$.

Schilling and Hoffmann extended these concepts to the cluster carbocations prepared by Seyferth.[22] In particular, they examined the conformations available to the alkyl cation $[Co_3(CO)_9C{=}CH_2]^+$, **7**. They were able to show that the linear cation **7a** is actually an energy maximum with essentially no barrier to rotation of the CH_2 group relative to the basal plane. Moreover, the minimum energy structure **7b**, in which the vinylidene cap bends towards a cobalt atom, is stabilized because of a very favorable interaction

between the symmetrical component of the *2e* set of the metal triangle and the π orbital of the $C=CH_2$ unit. This latter orbital is well-localized on the methylene carbon and creates direct bonding between this carbon and a cobalt atom (see Figure 1-4); as a result, the gap between the highest occupied molecular orbital (HOMO) and the lowest unoccupied molecular orbital (LUMO) increases markedly on bending the $C=CH_2$ moiety towards a $Co(CO)_3$ vertex.

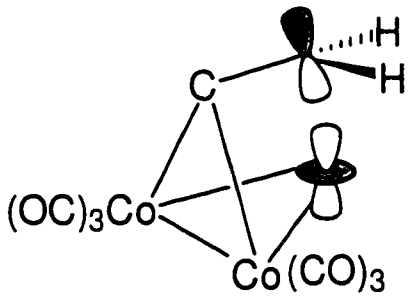

Figure 1-4: The interaction of a vacant p_z orbital on the cationic carbon with a fill d_{z^2} orbital on cobalt.

Schilling and Hoffmann also noted that when the vinylidene cap is oriented towards a cobalt-cobalt bond, as in **7c**, there is a somewhat weaker interaction of the methylene p_z orbital with the antisymmetric component of the *2e* set of the tricobalt fragment.[22] In this conformation, the methylene hydrogens are oriented in an upright manner relative to the basal plane. Since molecule **7c** lies about 4 kJ mol^{-1} above the favored structure **7b**, it represents a saddle point in the antarafacial migration process which allows the vinylidene cap to bond to each cobalt center successively, as in Figure 1-5.

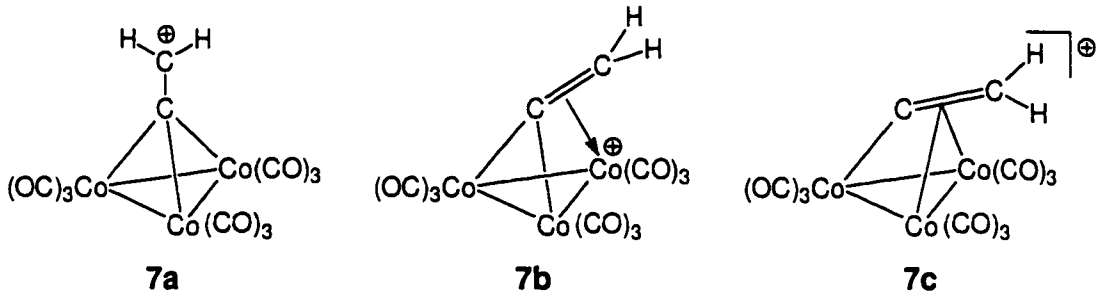

Figure 1-5: Migration of the vinylidene fragment around the metal triangle in $[Co_3(CO)_9C=CH_2]^+$ (7).

1.2.2. Examples of Metal-stabilized Carbocations

The ready isolation of dimolybdenum cations suggested that in a direct competition between $CpMo(CO)_2$ and $Co(CO)_3$ vertices a cationic center would be preferentially stabilized by the molybdenum. This was first investigated by D'Agostino *et al.* who prepared the mixed metal clusters $CpMCo(CO)_5(HC{\equiv}CCH_2OH)$, **8**, M = Mo or W, which upon protonation furnished the cations $[CpMCo(CO)_5(HC{\equiv}CCH_2)]^+$, **9**, as seen in Figure 1-6.[24] The ^{13}C NMR chemical shifts of the metal carbonyls indicated strongly that the positive charge was partially delocalized onto the molybdenum (or tungsten) atom while the cobalt carbonyls were little affected. [It is straightforward to assign ^{13}CO ligands bonded to tungsten by means of the satellite peaks caused by the 14% abundant ^{183}W isotope.]

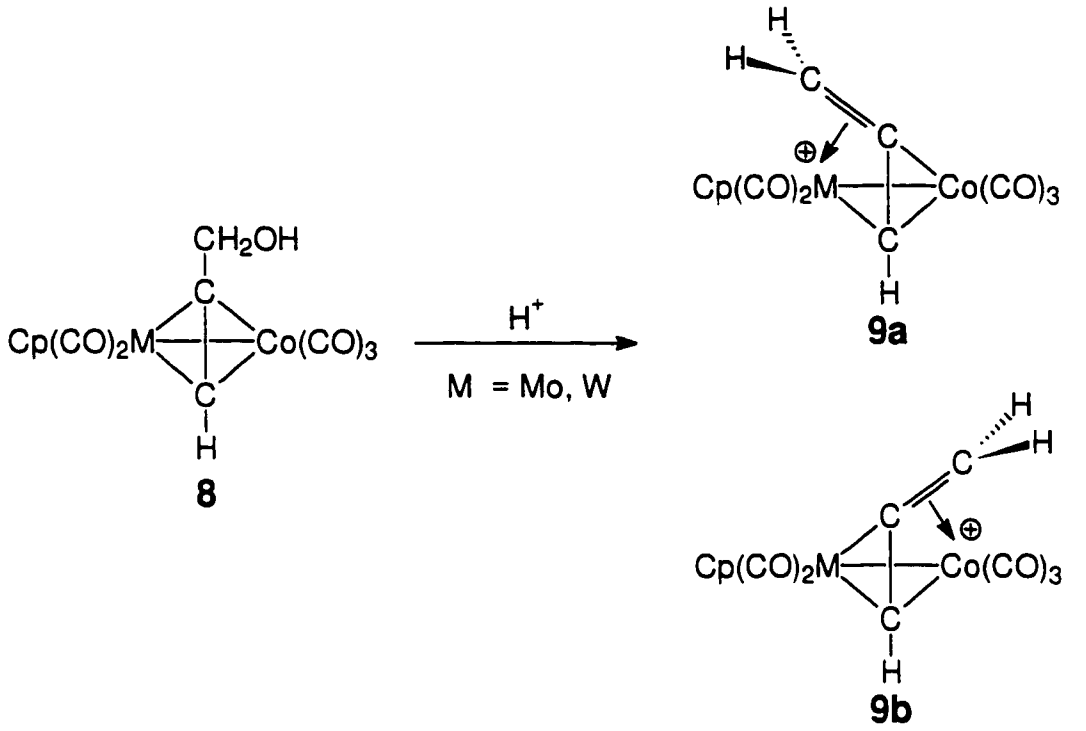

Figure 1-6: Metal-stabilized carbocation on mixed metal cluster.

These spectroscopic data were supplemented by EHMO calculations (see Figure 1-7) which likewise indicated a more favorable interaction with the Mo vertex, **9a**, rather than with the $Co(CO)_3$ group, **9b**. Variable-temperature NMR studies indicated that these were not fluxional molecules; unlike the homo-dimetallic systems, $[Co_2(CO)_6(HC{\equiv}CCH_2)]^+$ or $[Cp_2Mo_2(CO)_4(HC{\equiv}CCH_2)]^+$ for which the antarafacial migration pathway has been firmly established, there was no evidence for the formation of a cobalt-stabilized isomer, **9b**.[25-32]

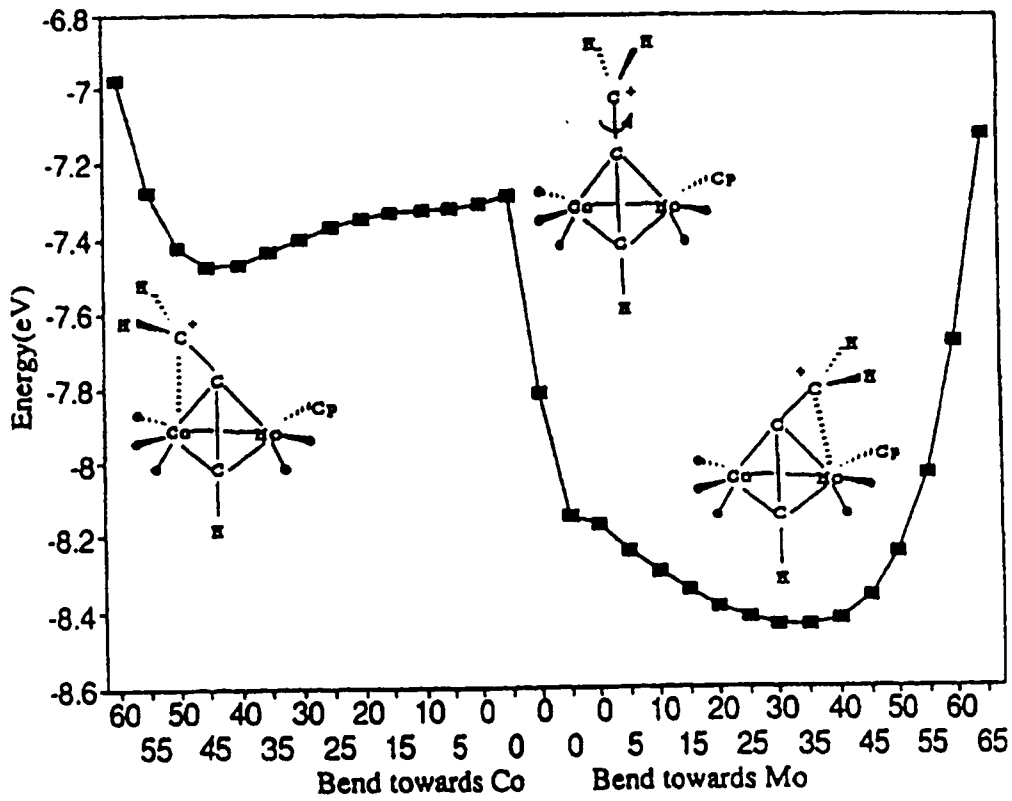

Figure 1-7: EHMO-calculated energy profile depicting the preferential interaction of a methylene fragment with a $CpMo(CO)_2$ vertex (as in 9a) rather than with a $Co(CO)_3$ unit.

Interestingly, when the secondary alcohol $CpWCo(CO)_5$-(HC≡CCH(Et)OH), **10**, was protonated, two diastereomers **11a** and **11b** were observed in a 2:1 ratio, as seen in Figure 1-8.[24] Moreover, an important series of experiments by Nicholas revealed an even more striking example of diastereoselectivity. It had been shown already that substitution of a carbonyl ligand in a $Co(CO)_3$ vertex by a phosphine enhanced the stabilizing ability of the cluster to such an extent that the vinylidene capping fragment interacted preferentially with the $Co(CO)_2PR_3$ vertex.[33] When the diastereomers of $Co_2(CO)_5PPh_3$-(HC≡C-CH(*t*-Bu)OH,

12a and **12b** were protonated, only a single cation **13a** was produced. It is apparent that the structure of this product minimizes the steric interactions between the *tert*-butyl group and the other cluster vertices, but the routes to this product from two isomeric precursors must be different.[34]

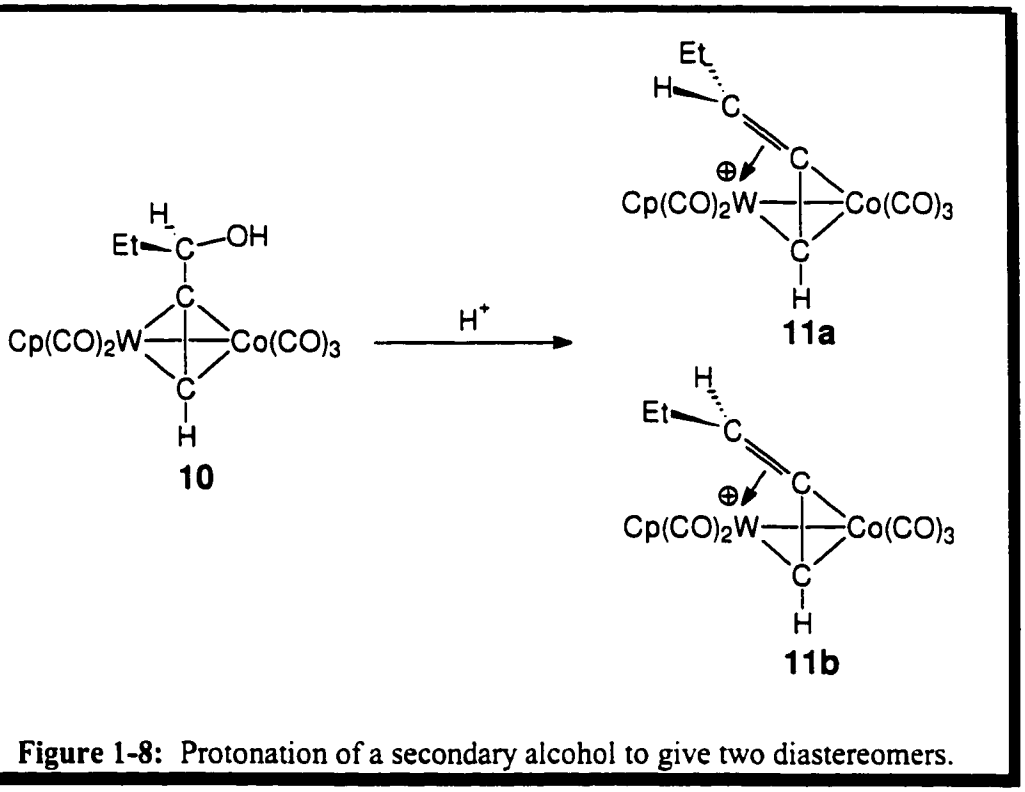

Figure 1-8: Protonation of a secondary alcohol to give two diastereomers.

The explanation which has been advanced for this phenomenon is depicted in Scheme 1-1.[35] It is assumed that these cations are generated by initial protonation of the alcohol precursor and that loss of water occurs with anchimeric assistance from a metal center which is *antiperiplanar* with respect to the leaving group. Certainly, this mechanism is well established for $Cr(CO)_3$-stabilized benzyl cations[36] or ferrocenyl-methyl cations[37] which undergo substitution with retention of configuration, as exemplified in Scheme 1-2.

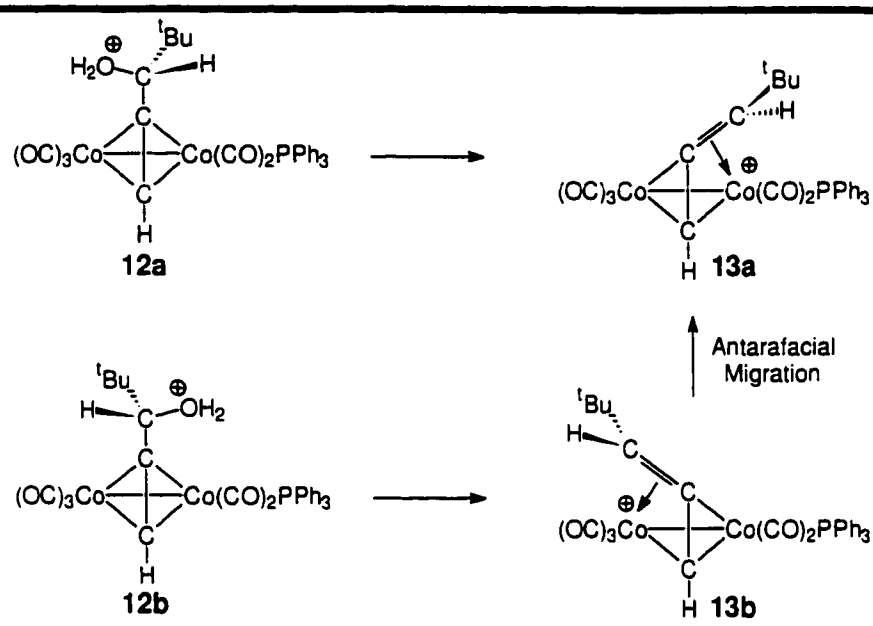

Scheme 1-1: Proposed mechanism to account for the observation of a single diastereomer **13a** generated *via* antiperiplanar elimination of water from two isomeric precursors **12a** and **12b**.

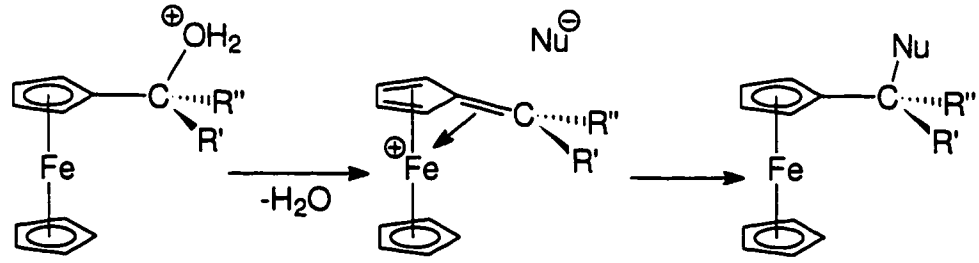

Scheme 1-2: Nucleophilic substitution in a chiral ferrocenylmethanol occurs with retention of configuration.

Now, if one assumes that elimination of water can be assisted either by the $Co(CO)_2PR_3$ or by the $Co(CO)_3$ vertex, then clearly two isomeric cations can result. However, if cation **13b** (which is stabilized by the $Co(CO)_3$ moiety) can undergo irreversible antarafacial migration to the more stable isomer **13a**, then only a single product will result. This same reasoning may be applied to the Co-W cations **11a** and **11b**, whereby the minor percentage of cation generated in a cobalt-assisted transition state can irreversibly isomerize to the favored W-stabilized diastereomer.[24, 35]

These data allow us to begin constructing a hierarchy of organometallic fragments in terms of their ability to stabilize carbocationic centers. A number of organometallic cations have been isolated and characterized spectroscopically and/or structurally. Typically, it has been shown by NMR and X-ray crystallography that in the cluster $[(C_5H_5)Fe(C_5H_4)\text{-}CH\text{-}(C{\equiv}CR)Mo_2(CO)_4Cp_2]^+$, **14**, it is the molybdenum cluster rather than the ferrocenyl fragment which preferentially stabilizes the electron-deficient center.[27] It is perhaps more realistic to visualize these metal-stabilized carbocations as vinylidene groups coordinated to an M_3 or M_2C triangle.[22, 40] We are aware of several other systems, **15** through **19**,[40-43] in which a C=CR′R″ moiety can selectively bind to its preferred metal fragment. Thus, in a preliminary fashion, we can begin to arrange metal vertices in order of their ability to stabilize carbocationic centers: molecules **15** and **16** tell us that: $Cp_2Mo_2(CO)_4(RC{\equiv}C\text{-})$ > ferrocenyl > $Co_2(CO)_6(RC{\equiv}C\text{-})$. Furthermore, we can see from molecules **17** through **19**, and also from **11** and **13**, that CpRu > CpFe, and that $Ru(CO)_3$ > $Fe(CO)_3$ > $CpW(CO)_2$ > $Co(CO)_2PPh_3$ >$Co(CO)_3$.

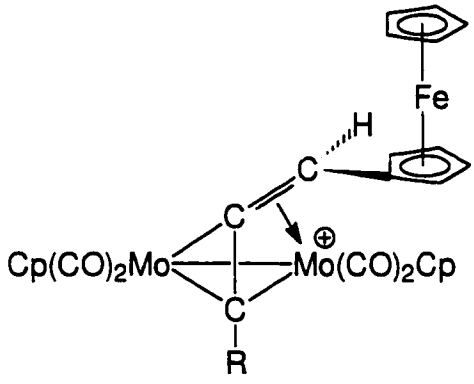
Fe
H
C
C
Cp(CO)2Mo
Mo(CO)2Cp
C
R

15

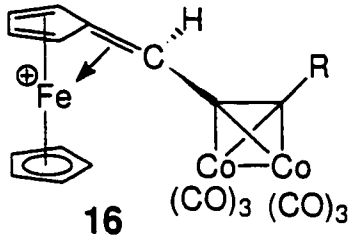
H
C
R
Fe
Co—Co
(CO)3 (CO)3

16

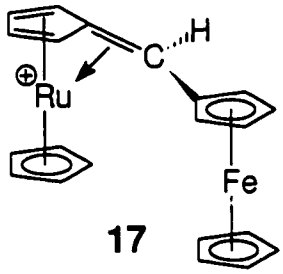
H
C
Ru
Fe

17

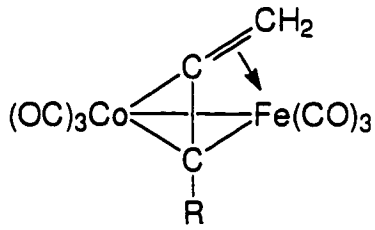
CH2
C
(OC)3Co
Fe(CO)3
C
R

18

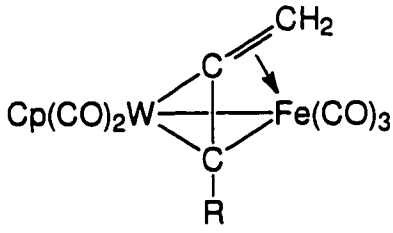
CH2
C
Cp(CO)2W
Fe(CO)3
C
R

19

1.3. Silicon Cations: An ongoing controversy

Organosilicon chemists have long searched for a system in which silylium ions* are stable. Early attempts to generate R_3Si^+ species concentrated on methods of preparation and identification that had been successful in carbon chemistry. For example, much work has been carried out to determine whether Ph_3SiX compounds (X = halogen or OH) will give conducting solutions in suitable solvents such as pyridine or liquid SO_2 similar to those found for Ph_3CX analogues. Attempts to use super-acid media such as FSO_3H-SbF_5-SO_2 to prepare R_3Si^+ cations have also been made, and numerous reactions in which R_3Si^+ ions might be expected as intermediates have been investigated.[44,45] Perhaps the greatest controversy in organosilicon chemistry in recent years has centered around the work of Lambert *et al.*,[46] who have presented results that proposed the ionization of simple silyl perchlorates (e.g. $(^iPrS)_3SiOClO_3$ and $Ph_3SiOClO_3$) in solvents such as CH_2Cl_2 and sulfolane, to give R_3Si^+ and ClO_4^- ions. Despite the considerable work on silyl perchlorates, there is still a lack of unambiguous evidence for their ionization to give R_3Si^+ in the investigated media.†

There is absolutely no controversy about the existence of silylium ions in the gas phase, and there is also strong evidence that they exist as reactive intermediates in solution. Hence, true three coordinate silylium ions should be thermodynamically stable, but they are also reactive (kinetically) such that their isolation is difficult in condensed phases.

* For the purpose of this document I will use the terms silylium ions, silicon cations and silyl cation interchangeably.

† There is no evidence indicating that partial hydrolysis did not occur, therefore the measurement may be somewhat misleading.

One question arises: why is it so difficult to generate a silicon cation (or silylium ion) when there are numerous documented examples of stable carbocations? The major factor is that silicon can easily adopt a higher coordination number than its counterpart, carbon. If silicon is required to take on a positive charge, then it can easily remove this charge by going to a higher coordination. This can be achieved by one of the following: *i)* by coordination of one or more solvent molecules, *or ii)* coordination of a counter-ion to the silicon. This counter-ion may be present in the medium, or may be abstracted from an anion.

Even under the conditions developed for the preparation and study of stable carbocations (low-nucleophilicity system, low temperatures), the extreme affinity of silicon for oxygen, fluorine and chlorine usually results in the reaction of solvents (even SO_2, or SO_2ClF) and/or reagents (Lewis acid halides, superacid systems) with the developing electrophilic silicon center (for example, to yield silyl fluorides, fluorosulfates, trifluoromethyl sulfates, etc.).

1.4. Characterization of Silicon Cations:

The main techniques used to investigate the structures of silyl perchlorates in solution were conductance measurements and multi-NMR spectroscopy.[47] Conductance measurements are perhaps the most obvious means of determining whether or not a compound is ionized in solution. However, there are many problems associated with this technique, since the conductance of a solution can rarely be attributed to only one compound in solution. Olah and co-workers have demonstrated that the conductance of dilute solutions of silyl perchlorates can arise from the hydrolysis of perchlorates by

residual water in the "dry" solvents used.[48,49] This result shows the difficulty of ascribing conductivity to a specific component in solution.

The most valuable analytical tool employed to study carbocations has been ^{13}C NMR spectroscopy since this permits direct observation of the cationic center. The sensitivity of ^{13}C chemical shifts and coupling constants to changes in hybridization, geometry, and charge density gives specific information concerning the nature of the carbocation. In 1982 Olah and co-workers published a study where a correlation between ^{29}Si chemical shifts in silicon compounds and ^{13}C chemical shifts in the analogous carbon compounds was carried out.[50] Among structurally related silanes, there are trends in ^{29}Si chemical shifts that parallel the trends in ^{13}C shifts of analogous carbon compounds. For example, in carbon compounds, the development of positive charge causes a downfield shift of the charged center. Similarly, in a series of related silanes, the ^{29}Si chemical shifts were found to move downfield as the electron-withdrawing abilities of substituents increase. Olah concluded that if a silicon cation were to be present in solution, the ^{29}Si chemical shifts would be predicted to shift by some 100-150 ppm.[50] Neither conductance nor NMR can explicitly prove the presence of silicon cations.

The method of choice to determine, unambiguously, the presence of a silicon cation would be X-ray diffraction. This method would yield information about the silicon environment, i.e., its coordination number (3,4,5 etc.). As well, the degree of cationic character can be obtained easily by examining the average C-Si-C bond angle. In a true silicon cation the angle should be 120°. If the silicon cation is formed, the X-ray diffraction experiment would show the counter-anion in the unit cell packing, and would also give information as to whether the cation and counter-ion are interacting in an ionic or covalent fashion.

1.5. Solid State Evidence of Silicon Cations

The existence of silyl cations in the condensed phase continues to be a controversial topic.[51] Silylium ions are thermodynamically stable; they are readily produced in the gas phase and can be conveniently studied by mass spectrometry.[52] Recently, Lambert and co-workers reported the X-ray structure for a triethylsilylium tetrakis(pentafluorophenyl)-borate salt.[53] The structure contained several molecules of toluene in the unit cell, one of which was observed to occupy the fourth coordination site about the silicon atom, as seen in Figure 1-9. The closest bond distance between the silicon and the toluene was reported to be 2.18 Å (Si-C_{ipso}), which is longer than any previously known four-coordinate silicon carbon bond distance. The counter anion used, tetrakis(pentafluorophenyl)borate, shows no coordination to the $[Et_3Si\bullet\bullet\bullet toluene]^+$. The closest reported contact between the Si and a fluorine was 4.02 Å, which indicated that the anion is truly free. The average C-Si-C angle is 114° rather than the expected 120° for a true tricoordinate silicon cation. The reported ^{29}Si NMR shift for this compound was found to be 92.3 in benzene and 94.3 in the solid state, indicating that the compound has some silylium ion character.

Reed and coworkers reported the X-ray structure of a triisopropylsilylium salt with a hexabrominated *closo*-carborane counter-ion, as seen in Figure 1-10.[54] The geometry of this structure most closely approaches the ideal tricoordinate system. The average C-Si-C angle was found to be 117°, which is closer to the ideal angle than in Lambert's structure. In this case there is a weak contact to the counter anion; the Si-Br distance is reported to be 2.48 Å which is slightly longer than a normal Si-Br bond length. The ^{29}Si NMR chemical shift in the solid state was 109.8 ppm and 105 ppm in toluene. Reed and co-workers describe the molecule as "an ionic-like species that lies along a continuum that ranges from four-coordinated covalent to trigonal-planar ionic."

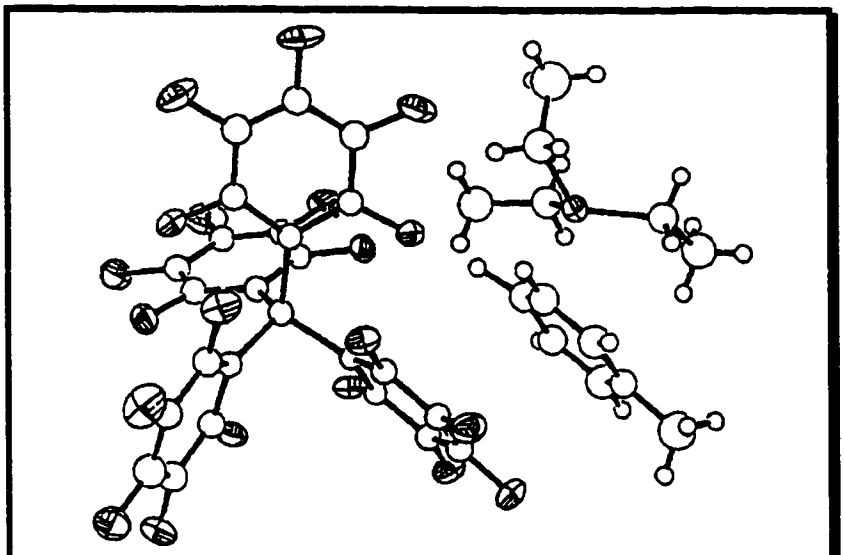

Figure 1-9: X-ray structure of $[Et_3Si\bullet\bullet\bullet toluene]^+$ reported by Lambert and co-workers

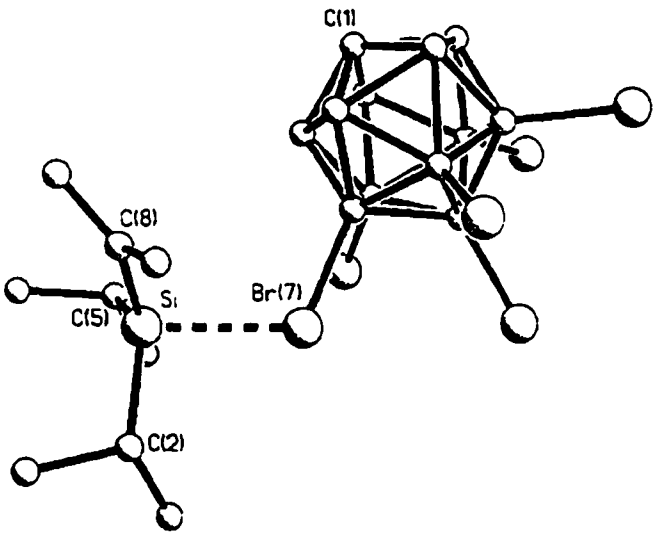

Figure 1-10: X-ray structure of $[i\text{-}Pr_3Si(Br_6\text{-}CB_{11}H_6]$ reported by Reed and co-workers.

The reports of both Lambert's and Reed's crystal structures have raised many questions. Although it was agreed upon that according to several criteria (C-Si-C bond angle, ^{29}Si NMR, high level calculations) neither structure represented a true three coordinated silylium ion, the establishment of some silylium ion character in both *i*-Pr_3Si (Br_6-$CB_{11}H_6$) and Et_3Si (toluene)$^+$ compound cannot be denied.

1.6. Defining the Project

The ability of transition metals to delocalize the positive charge from carbocationic ligands has been amply documented and we have already discussed numerous examples of such intermediates that are themselves not isolable in the condensed phase. Stable silicon cations have not been prepared in the condensed phase. The goal of this thesis is to establish if the stabilizing ability of transition metal cluster would allow the isolation of a silicon cation.

Initially, we present a theoretical investigation, by means of molecular orbital calculations at the extended Hückel level. This is followed by a series of synthetic studies discussing the preparation of suitable precursors leading directly or indirectly to stabilized silicon cation on dimetallic clusters.

2. TOWARDS SILICON CATIONS VIA SILANE PRECURSORS

2.1. Backgound

Numerous groups have attempted to generate silylium ions by traditional carbenium ion approaches involving the removal of electron-withdrawing groups such as halides or esters. Polar solvents are used and usually a Lewis acid is added to promote ionization. Since halogens are highly reactive towards silylium ions (a phenomenom refered to as silaphilicity) it is unlikely that this family type of approach can lead to free silylium ions.

In a now classic paper Bartlett *et al.* studied the mechanism of intermolecular hydride transfer involving carbenium ions and the carbon-hydrogen bonds of various hydrocarbons.[55] They found that reagents such as aluminum bromide catalyze the interchange of hydride and halide between substrates, as seen in Scheme 2-1. They interpreted their results in terms of an intermolecular hydride shift, by analogy with the already known intramolecular 1,2-hydride shift.

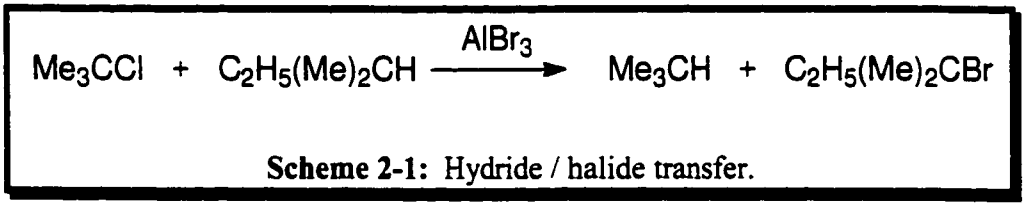

Scheme 2-1: Hydride / halide transfer.

This reaction appears to be well adapted for the production of silyium ions, because it is thermodynamically favorable. The trade of a weaker Si-H bond for the stronger C-H bond is the thermodynamic driving force for the reaction. Although silicon

generally has stronger bonds than carbon to electronegative elements such as oxygen, nitrogen, and halogens, which provide common leaving groups in carbocation chemistry, the reverse is true for the bond to hydrogen.[56]

In an attempt to obtain a better understanding of the interaction between silicon cations and dimetallic clusters, calculations at the extended Hückel molecular orbital level were carried out on model systems.

2.2. EHMO calculations

The suggestion by Seyferth that the vinylidene capping group in $[Co_3(CO)_9C\text{-}CR_2]^+$ would adopt the bent structure **7a** rather than the more symmetrical isomer **7b**, with its pseudo-3-fold axis,[38] has received both theoretical and experimental support.[22, 57] Extended Hückel molecular orbital calculations by Schilling and Hoffmann showed that, by allowing the α-carbon to lean towards a cobalt vertex, the vacant *p* orbital on the sp^2-hybridized - CH_2^+ fragment can accept electron density from a filled metal *d* orbital. The net result is not only enhanced stabilization of the cationic center, *via* delocalization of the positive charge onto the metal vertex, but also a larger HOMO-LUMO gap.[22, 39]

The replacement of the $Co(CO)_3$ vertices by isolobal $CpMo(CO)_2$ fragments yields cationic clusters, $[Cp_2Mo_2(CO)_4(RC{\equiv}C\text{-}CR_2)]^+$, many of which have been characterized by X-ray crystallography. Recently, an energy hypersurface for the migration of a $C{=}CH_2$ fragment over a $[Cp_2Mo_2(CO)_4CH]^+$ triangular base has been computed. It was shown that the structure in which the CH_2 group is oriented directly over a metal vertex lies at the bottom of the potential energy well.[58] Moreover, the calculated trajectory along which the

methylene group migrates from one metal vertex to the other is beautifully paralleled by a series of X-ray crystal structures of cations $[Cp_2Mo_2(CO)_4(RC{\equiv}CR'R'')]^+$, in which the groups R' and R" range from H, methyl and ferrocenyl to terpenoid and steroidal substituents.[58, 59]

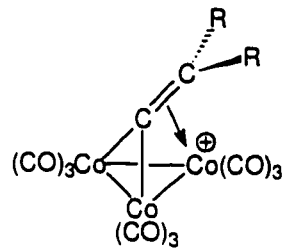

7a

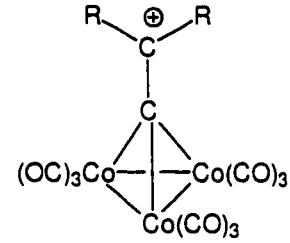

7b

We present here the analogous hypersurface for a $C{=}SiH_2$ fragment sited above a $[Co_2(CO)_6CH]^+$ basal triangle. The molecular geometry was based on a typical $(alkyne)Co_2(CO)_6$ cluster with Co-Co, Co-C, and C-C values of 2.49, 1.99 and 1.35 Å, respectively. To define the geometry of the cationic cluster which undergoes rearrangement, we place the origin, ⊙, of our coordinate system at the centroid of the Co(1)-Co(2)-C(3) basal triangle. The carbynyl capping atom, C(2), is defined by a vector starting at the origin and making an angle of 71° with the line C(3)-C ⊙. The distance was taken as 0.81 Å (for the Co_2C_2 clusters) and as 1.25 Å (for the Mo_2C_2 clusters).[30, 60] The coordinates of the α-EH_2 unit, where **E** = C or Si, are defined in terms of the C(2)-**E** distance (1.45 Å and 1.85 Å for CH_2 and SiH_2, respectively) and the three angles θ, ϕ, and ω. As shown in Figure 2-1, θ is the angle ⊙-C(2)-**E** which decreases from 180° as the CH_2 or SiH_2 unit is allowed to lean towards the metal-metal bond. As the EH_2 group swivels away from the mirror plane which bisects the metal-metal bond and contains C(1) and C(2),

the dihedral angle ϕ opens up from 0° towards 90° at which point the C(2)-**E** bond is parallel to the metal-metal vector. The third degree of freedom, the twist angle ω, defines the orientation of the $\mathbf{EH_2}$ plane with respect to the basal plane. When all three components of the $\mathbf{EH_2}$ unit lie in the molecular mirror plane ($\phi = 0°$), the ω values are 0° for H_{endo} and 180° for H_{exo}, where H_{endo} is defined as the hydrogen closer to the M-M vector. As the $\mathbf{EH_2}$ fragment swivels towards M(1), one might anticipate that the values $\omega(H_{endo})$ and $\omega(H_{exo})$ would gradually evolve towards 90° and -90°, respectively. To generate the hypersurface shown in Figure 2-2, the angles θ and ϕ were incremented in units of 2°; at each point defined by a (ϑ, ϕ) pair, the torsion angle ω was varied from 0° to 180° in 15° increments and the minimum energy ω value for each (θ, ϕ) position was plotted. These data not only allow the evaluation of a global minimum (i.e. the structure which presumably would be found by X-ray diffraction if the metal-stabilized silylium ion could be isolated as a single crystal), but they also yield the favored pathway by which the cation can migrate from one metal vertex to the other.

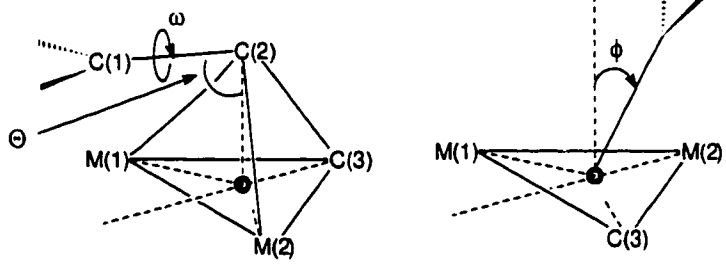

Figure 2-1: Definition of the coordinate system used in the EHMO calculations.

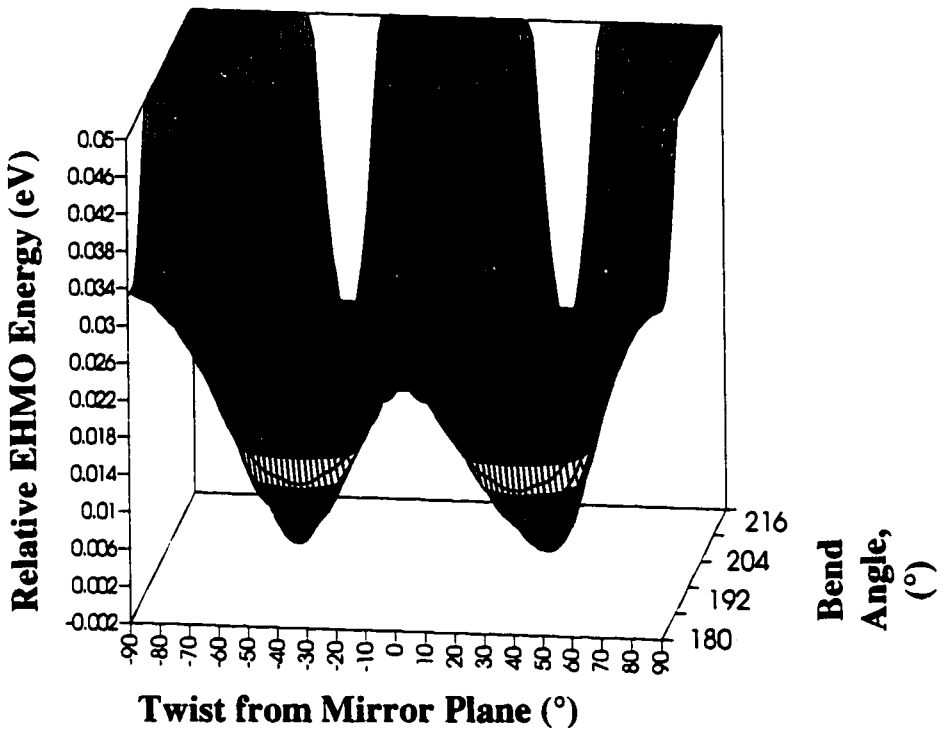

Figure 2-2: EHMO-calculated energy hypersurface for the migration of SiH_2 $[Co_2(CO)_6(HC{\equiv}C\text{-}SiH_2)]^+$.

In the molybdenum-stabilized carbocations previously studied both by EHMO calculations and by a Bürgi-Dunitz analysis of a series of X-ray crystal structures,[59] the α-CH_2 group is found to pass through a symmetrical transition state in which the methylene moiety lies in the molecular mirror plane and perpendicular to the Mo-Mo bond vector. By contrast, in $[Co_2(CO)_6(HC{\equiv}C\text{-}SiH_2)]^+$ the SiH_2 fragment can rotate freely about the C(2)-Si axis when $\phi = 0°$. At this point, the SiH_2 group is found to bend only slightly (6°) towards the Co-Co bond, presumably to allow some stabilization of the electron-deficient silicon center by both cobalt atoms. As ϕ increases and the SiH_2 unit moves towards one $Co(CO)_3$ vertex, the molecule falls into a potential well. As the cluster cation descends into this well, increases in ϕ are accompanied by a smooth decrease in the bend angle θ, from 174° at ϕ = 0°, to 164° at $\phi = 32°$ We have previously shown for the migration of the CH_2^+ group in $[(C_5H_4\text{-}C_5H_4)Mo_2(CO)_4(R\text{-}C{\equiv}C\text{-}CH_2)]^+$ that the migrating cation orients itself (as a function of ω) so as to best align the vacant *p* orbital with the nearest metal center; this behavior can also be seen in Figure 2-3. The EHMO-derived energetically most favorable structures for both carbenium and silylium ions stabilized on either a cobalt or molybdenum center are depicted in Figure 2-4.

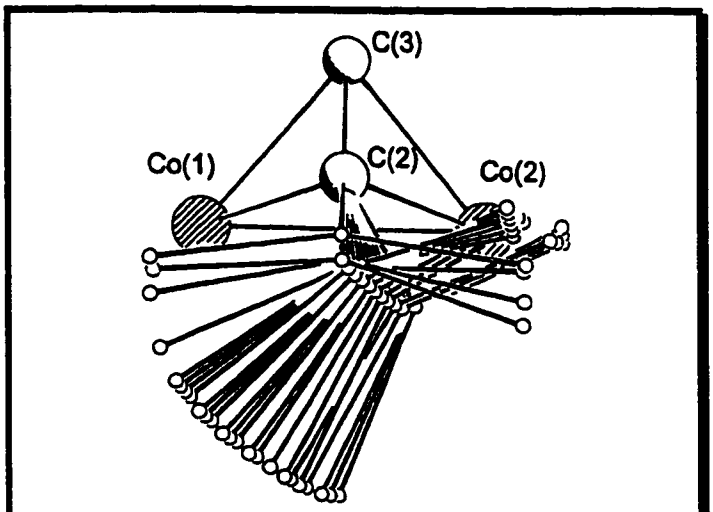

Figure 2-3: Migration pathway of the SiH_2^+ group on a cobalt cluster.

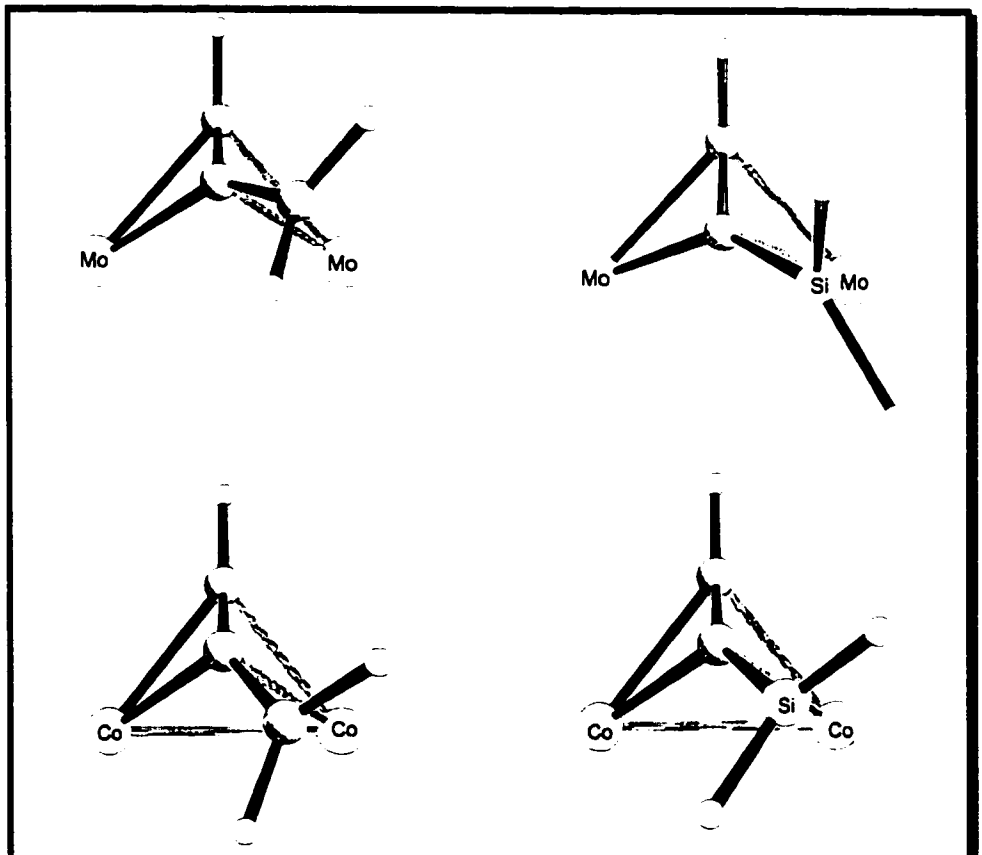

Figure 2-4: Calculated structure for carbenium and silylium ions stabilized by dimetallic clusters.

Another factor which was considered involved the pyramidalization of the EH_2 fragments when bonded to a transition metal center. It was shown previously that an 8° "folding-back" of the methylene hydrogens in $[(C_5H_4\text{-}C_5H_4)Mo_2(CO)_4(R\text{-}C{\equiv}C\text{-}CH_2)]^+$ led to a slight stabilization. In $[(C_5H_5)_2Mo_2(CO)_4(HC{\equiv}C\text{-}EH_2)]^+$, the system is stabilized by 5.8 kJ mol^{-1} or 5.0 kJ mol^{-1} for **E** = C or Si, respectively, relative to the cation sitting in an upright position. The corresponding values for the analogous $[Co_2(CO)_6(HC{\equiv}C\text{-}EH_2)]^+$ systems are 1.9 kJ mol^{-1} for the carbenium ion and zero for the SiH_2^+ complex. Overall, according to the EHMO calculations, the energetic advantage arising from allowing the EH_2^+ fragment to lean towards a metal vertex is 41 kJ mol^{-1} for $Mo_2\text{-}CH_2^+$, 22 kJ mol^{-1} for $Mo_2\text{-}SiH_2^+$, 24 kJ mol^{-1} for $Co_2\text{-}CH_2^+$, and 3 kJ mol^{-1} for $Co_2\text{-}SiH_2^+$. The predicted M-EH_2^+ distances for the above-listed cations are Mo-C 2.65 Å, Mo-Si 2.99 Å, Co-C 2.53 Å, and Co-Si 3.08 Å, respectively.

Of course, these EHMO-calculated energies should not be regarded as definitive values; however, such semi-empirical approaches are valuable indicators of trends. While computationally more demanding methods, such as Density Functional Theory, give more reliable energies, they are not amenable to the convenient generation of hypersurfaces. EHMO, Fenske-Hall calculations and other such approaches are still valuable components of the experimentalist's armory.

One can summarize the situation for metal-stabilized silylium systems as follows: the stabilization of a Si^+ center by a $CpMo(CO)_2$ fragment is comparable to that found for a $Co(CO)_3$-stabilized carbocation. In contrast, the anchimeric assistance provided to an Si^+

center by a $Co(CO)_3$ vertex is expected to be rather minimal. The calculations suggest that carbenium ions are better stabilized by metals than are silylium ions, and also that a $(C_5H_5)Mo(CO)_2$ vertex is more effective than a $Co(CO)_3$ group. This latter facet is amply illustrated by the recently reported X-ray crystal structure of the (2-propynylbornyl)$[Mo(CO)_2(C_5H_5)Co(CO)_3]^+$ cation in which the carbocationic charge is alleviated by direct interaction with the molybdenum atom.[61]

2.3. Synthetic Aspects - Results and Discussion

The $CpMo(CO)_2$ vertex is perhaps the most favorable organometallic fragment for the stabilization of carbocations as noted above.[61] These species may also be regarded as alkenes coordinated to a molybdenum cation, as in **9** or **15**. Similarly, the ruthenium-stabilized silene, $(C_5Me_5)Ru(H)(\eta^2\text{-}Ph_2Si{=}CH_2)P(C_6H_{11})_3$, **20**, has been synthesized and crystallographically characterized by Tilley.[62] These results suggest that a molybdenum-stabilized silylium moiety, **21**, might be a viable objective, and so our initial goal was to prepare a suitable precursor possessing a potential leaving group.

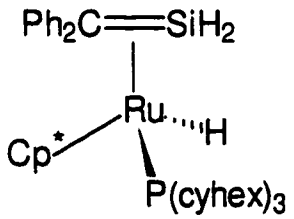

20

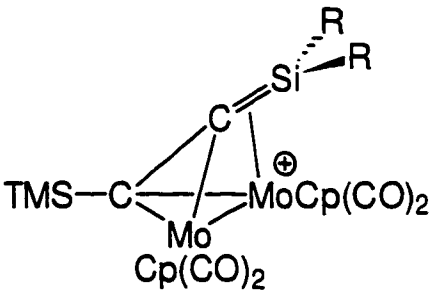

21

It is known that alkynylsilanes, such as Ph-C≡C-$SiMe_2H$ or Ph-C≡C-SiH(Me)CR, react with dicobalt octacarbonyl to yield the corresponding (alkyne)$Co_2(CO)_6$ tetrahedral clusters, **22**. However, one must take care to avoid the addition of excess $Co_2(CO)_8$ otherwise cleavage of the Si-H linkage leads to the formation of a silicon-cobalt bond, as in **23**. Furthermore, as shown in Scheme 2-2, these latter molecules are readily susceptible to nucleophilic attack, especially by alcohols, giving siloxy derivatives **24**.[63-65]

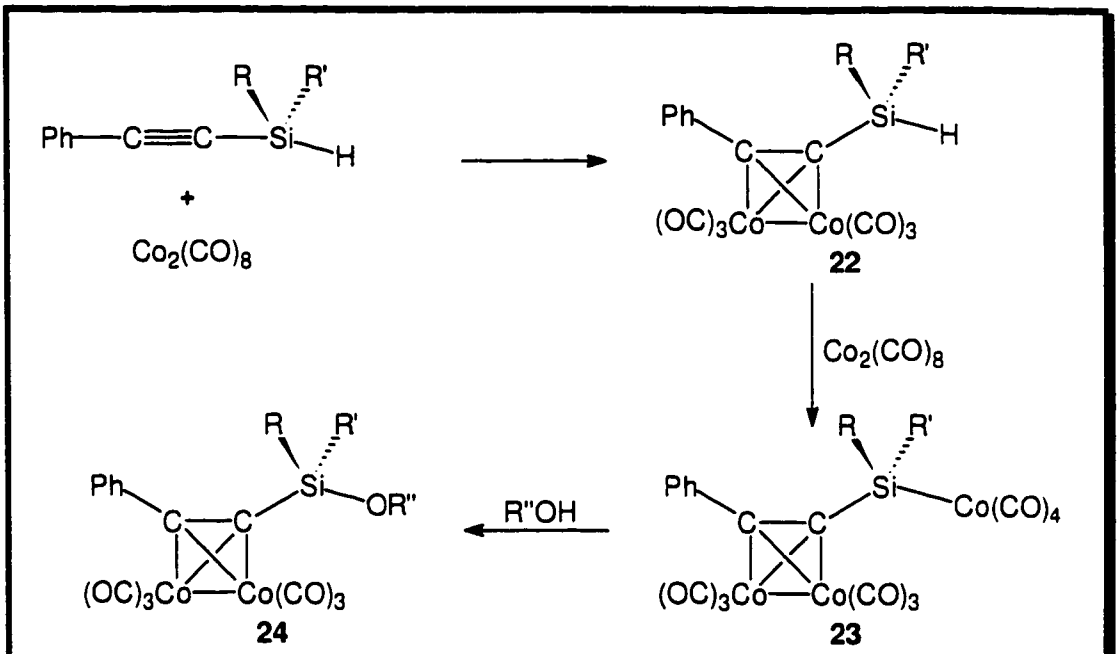

Scheme 2-2: Oxidative addition of $Co_2(CO)_8$ to silanes.

The reaction of the silyl-alkyne Me_3Si-C≡C-$SiPh_2H$ with $Co_2(CO)_8$ or with the metal-metal triple-bonded dimer $Cp(CO)_2Mo{\equiv}Mo(CO)_2Cp$ yields the tetrahedral clusters $Co_2(CO)_6(Me_3Si$-C≡C-$SiPh_2H)$, **25**, and $Cp_2Mo_2(CO)_4(Me_3Si$-C≡C-$SiPh_2H)$, **26**, which were readily identifiable by their ^1H, ^{13}C and ^{29}Si NMR spectra, and also by their

characteristic Si-H stretches at 2144 cm^{-1} and 2171 cm^{-1}, respectively. Recrystallization of the dimolybdenum complex, **26**, from THF/hexane gave red parallelepipeds suitable for an X-ray diffraction study. The silyl-alkyne cluster **26** crystallizes in the monoclinic space $P2_1/c$, and a view of the molecule appears as Figure 2-5. The Mo-C distances within the tetrahedral core vary from 2.142 Å to 2.237 Å and are within the normal range.[66] However, the complexed alkyne linkage, C(2)-C(3) = 1.420(5) Å, is rather long compared to analogous bonds found in other $Cp_2Mo_2(CO)_4(RC{\equiv}CR)$ clusters where the C≡C distances normally lie in the range 1.35 Å to 1.37 Å.[23] This effect presumably arises as a result of the bulk of the trimethylsilyl and diphenylsilyl substituents, and is also seen in the angles Si(1)-C(2)-C(3) and C(2)-C(3)-Si(4) which are 140° and 149°, respectively, rather than the normal C-C-R value of ≈ 137°. The lengthened C(2)-C(3) distance is counterbalanced by the rather short Mo(1)-Mo(2) distance of 2.783(1)Å which is considerably shorter than the Mo-Mo bond length of 2.97 Å normally found in these $Cp_2Mo_2(CO)_4(RC{\equiv}CR)$ clusters. The crystallographic data were of sufficient quality to allow the hydrogen attached to Si(4) to be located; it lies 4 Å from the nearest molybdenum and, apparently, there is no tendency towards a Si••H••Mo agostic interaction in this molecule. This observation is in accord with the ^{29}Si NMR data which yield a $^1J_{(Si\text{-}H)}$ value of 211 Hz; for comparison, in the free ligand, $Me_3Si\text{-}C{\equiv}C\text{-}SiPh_2H$, $^1J_{(Si\text{-}H)}$ is 212 Hz.

A common feature of $Cp_2Mo_2(CO)_4(RC{\equiv}CR)$ systems is the presence of one semi-bridging carbonyl and three clearly terminal CO ligands.[67] However, such is not the case in $Cp_2Mo_2(CO)_4(Me_3Si\text{-}C{\equiv}C\text{-}SiPh_2H)$, **26**; all four molybdenum-carbonyl linkages are

terminal with M-C≡O angles of 175° ± 2°. Indeed, when viewed along the metal-metal bond (see Figure 2-6), the $Cp_2Mo_2(CO)_4C_2$ moiety is seen to have almost idealized C_2 symmetry. Again, one may attribute the adoption of this structure to the presence of the two bulky substituents on the alkyne. This behavior is reminiscent of Knox's $Cp_2Mo_2(CO)_4(Me_3Si\text{-}C{\equiv}C\text{-}SiMe_3)$ cluster, which also adopts a C_2 structure with terminal carbonyls.[68]

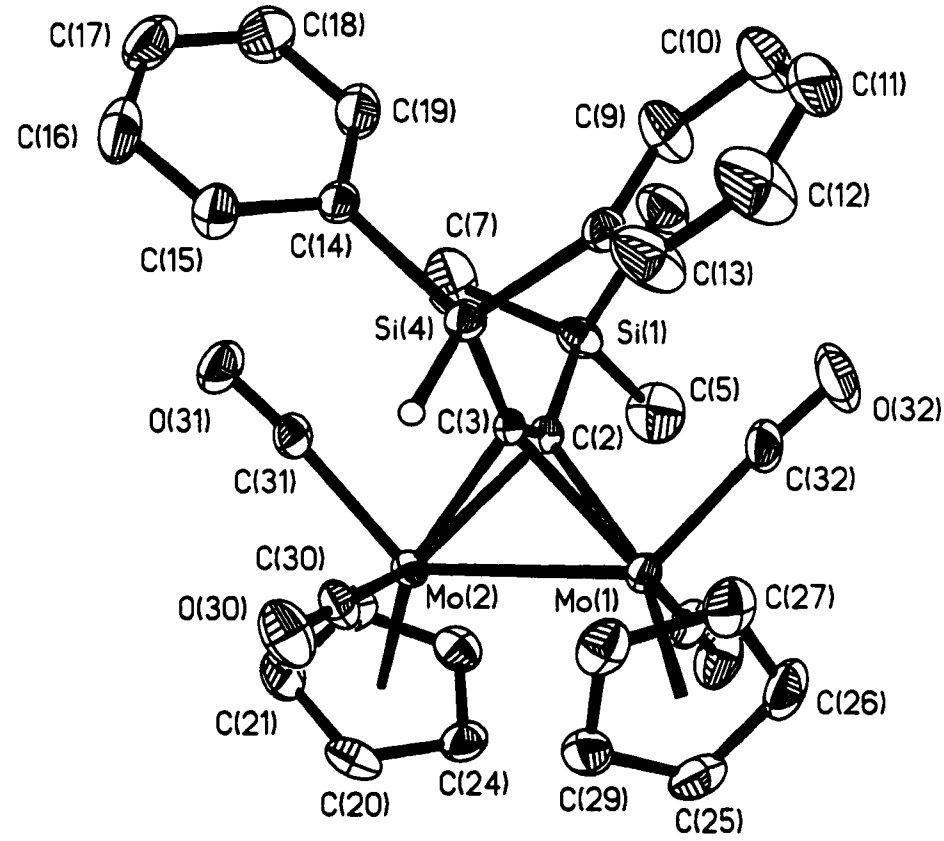

Figure 2-5: View of **26**, showing 30% probability ellipsoid and the atomic numbering.

Salient bond lengths(Å): Mo(1)-Mo(2) 2.783(1), Mo(1)-C(2) 2.223(3), Mo(1)-C(3) 2.142(3), Mo(2)-C(2) 2.146(3), Mo(2)-C(3) 2.237(3), C(2)-C(3) 1.420(5), C(2)-Si(1) 1.901(3), C(3)-Si(4) 1.923(3)

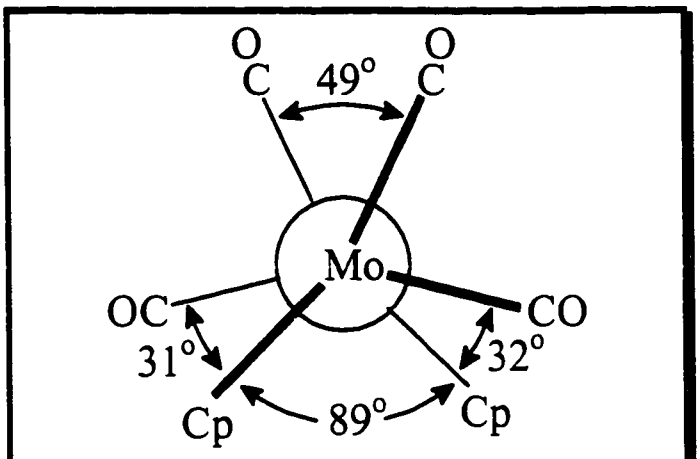

Figure 2-6: Newman projection of **26**, viewed along the molybdenum-molybdenum bond.

In an attempt to generate a molybdenum-stabilized silylium ion, $Cp_2Mo_2(CO)_4(Me_3Si\text{-}C{\equiv}C\text{-}SiPh_2H)$, **26**, was treated with $Ph_3C^+ BF_4^-$ but the complex was recovered unchanged. One can speculate that the steric problems engendered by the approach of the bulky trityl cation in its attempt to abstract a hydride from the Ph_2Si-H moiety in **26** thwarted the process. This result should be contrasted with the report by Corriu that the reaction of $Co_2(CO)_6(Ph\text{-}C{\equiv}C\text{-}SiMe_2H)$, **27**, with $Ph_3C^+ BF_4^-$ led to the isolation of the fluorosilane complex $Co_2(CO)_6(Ph\text{-}C{\equiv}C\text{-}SiMe_2F)$, **28**.[69] However, in the latter case, the potential steric problems are likely to be less severe than for **26**.

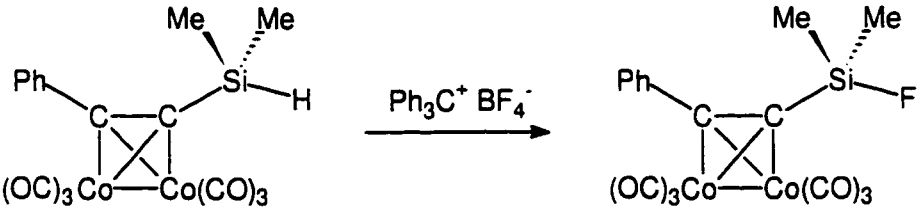

27 **28**

As shown in Scheme 2-3, addition of more than one equivalent of $Co_2(CO)_8$ to an alkynylsilane yields not only a Co_2C_2 tetrahedral cluster but also leads to the formation of a silicon-$Co(CO)_4$ linkage which is itself very susceptible to hydrolysis, and leads to siloxanes.[63-65] Furthermore, it has been noted that siloxanes are also obtained upon hydrolysis of cobalt clusters bearing $SiMe_2H$ or $SiMe_2CR$ substituents. The aqueous hydrolysis of $(XSiMe_2\text{-}C{\equiv}C\text{-}SiMe_2X)Co_2(CO)_6$, **29**, where X = H or CR, is reported to yield the cyclic dimer **30**, but only mass spectroscopic evidence is available. However, the free ligand, i.e. octamethyl-3,5,8,10-tetrasila-4,9-cyclodeca-1,6-diyne, **31**, has been crystallographically characterized.[70]

In the course of his pioneering studies, Seyferth described the syntheses of numerous alkynylsilanes (including $Me_3Si\text{-}C{\equiv}C\text{-}SiMe_2H$) and their general reaction to yield tetrahedral clusters when treated with $Co_2(CO)_8$.[71] However, no further mention was made of the product(s) derived from $Me_3Si\text{-}C{\equiv}C\text{-}SiMe_2H$. We find that treatment of 1-dimethyl-silyl-2-trimethylsilylethyne with an equimolar quantity of $Co_2(CO)_8$ in pentane yields the siloxane **32**. The product was initially identified by its NMR and mass spectra; the latter revealed the presence of two cobalt cluster fragments and their associated carbonyl ligands. Recrystallization from hexane gave black parallelepipeds suitable for an X-ray diffraction study. The siloxane cluster **32** crystallizes in the monoclinic space *C2/c*, and a view of the molecule appears as Figure 2-7.

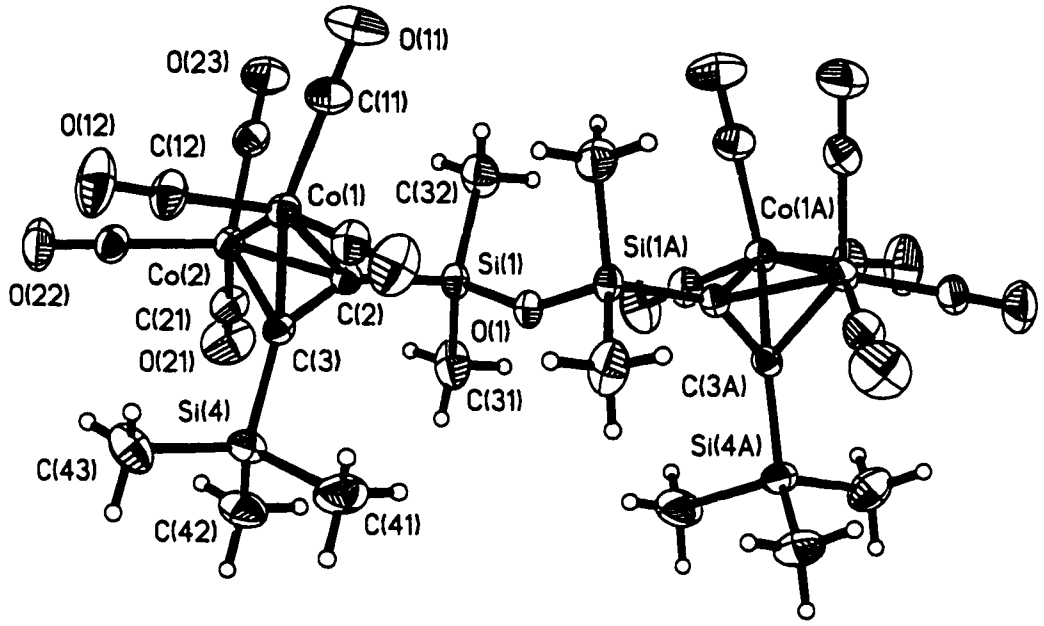

Figure 2-7: View of **32** showing 30 % thermal ellipsoidal and atomic numbering.

Salient bond lengths (Å): Co(1)-Co(2) 2.491(1), Co(1)-C(2) 1.991(2), Co(1)-C(3) 1.995(2), Co(2)-C(3) 1.991(2), C(2)-C(3) 1.326(3), C(2)-Si(1) 1.851(2),C(3)-Si(4) 1.853(2), Si(1)-O(1) 1.628(1).
Salient bond angles (deg): Si(1)-C(2)-C(3) 144.6(2), C(2)-C(3)-Si(4) 144.6(2).

The bond lengths within the Co_2C_2 tetrahedra (Co-Co, 2.491(1) Å; Co-C, 1.99 - 2.00 Å; C-C, 1.326(3) Å) are within the normal ranges for such molecules.[29] As with the dimolybdenum cluster, **26**, the Si-C≡C angles are wider than normal (144° vs ≈ 135°), but there are no unusual bond lengths. The Si-O-Si angle of 151.5° is typical of siloxanes bearing bulky substituents.[72] The molecule possesses a two-fold axis, and a view along the Si(1)•••Si(1a) vector is entirely analogous to a staggered ethane in which the largest substituents are aligned almost antiparallel. Figure 2-8 provides such a "Newman

projection" along the silicon•••silicon axis. The dihedral angle between the two cluster capping carbons, C(2) and C(2a), is 172°.

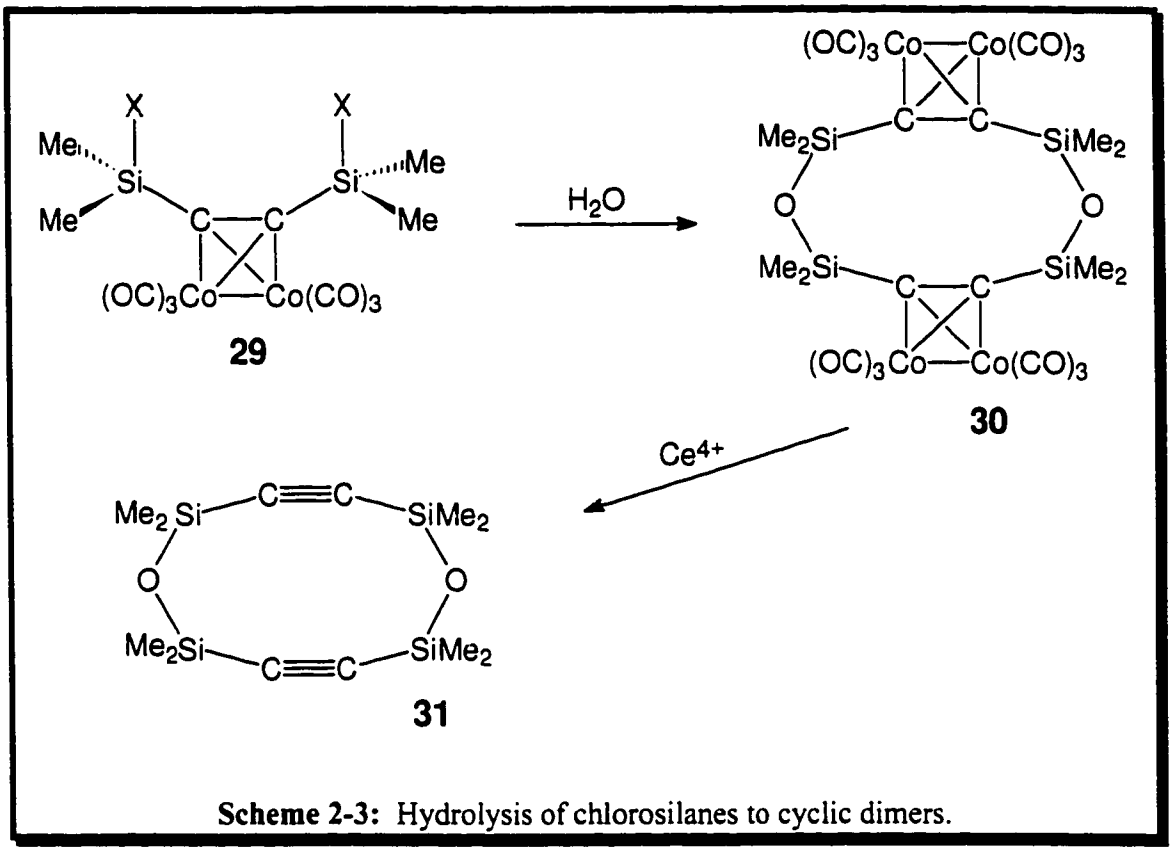

Scheme 2-3: Hydrolysis of chlorosilanes to cyclic dimers.

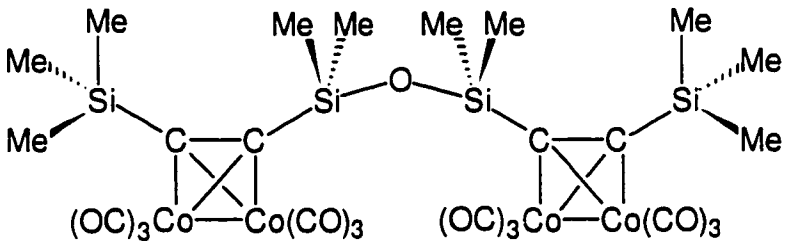

32

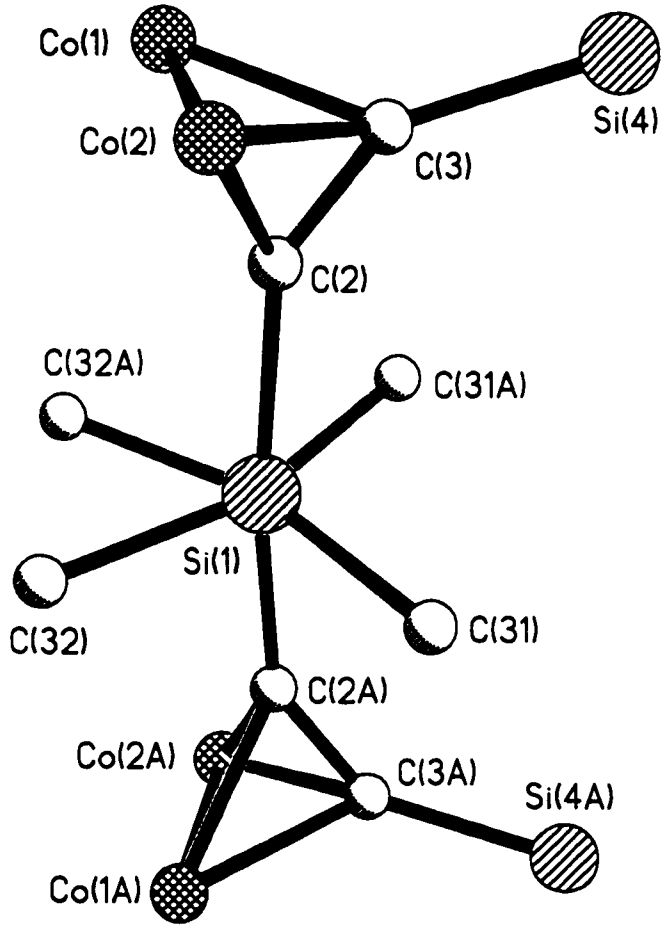

Figure 2-8: Newman projection of **32**, viewed along the silicon-silicon vector.

The closest structurally characterized analogue to **32**, of which we are aware, is $Co_2(CO)_6$(Ph-C≡C-SiCl(Me)$Co(CO)_4$). Its dimensions closely match those found for **32**.[65] One can readily envisage a route to **32** which involves generation of a tetrahedral cluster

$Co_2(CO)_6(Me_3Si\text{-}C{\equiv}C\text{-}SiMe_2H)$, oxidative addition to give $Co_2(CO)_6(Me_3Si\text{-}C{\equiv}C\text{-}SiMe_2\text{-}Co(CO)_4)$ and, finally, hydrolysis to the siloxane.

2.4. Summary

To conclude, we have presented evidence from molecular orbital calculations at the extended Hückel level that a silylium ion would be stabilized by interaction with a metal fragment; in this respect, a $(C_5H_5)Mo(CO)_2$ moiety is shown to be better able to alleviate the electron deficiency at silicon than is a $Co(CO)_3$ fragment. However, the stabilization of a SiR_2^+ unit will be less than that observed for carbocations.

We have also found that upon treating trimethylsilylethynyldimethylsilane, $Me_3Si\text{-}C{\equiv}C\text{-}SiMe_2H$, with dicobalt octacarbonyl the siloxane, **32**, is isolated in good yield. Repeated attempts to remove hydride from the organometellic precursor, $(Me_3Si\text{-}C{\equiv}C\text{-}SiMe_2H)[Mo_2(CO)_4(C_5H_5)_2]$, were unsuccessful. Presumably removal of hydride by use of the trityl cation is inhibited by the steric bulk around the silicon atom. Routes to metal-stabilized silylium systems require the juxtaposition of the organometallic fragment prior to generation of the silicon cation; subsequent removal of an appropriate leaving group should lead to silylium ion formation.

3. ALLYL-SILANES

3.1. New Approach: Extending the Gap.

As shown in chapter 2, we have achieved the syntheses of a series of metal cluster complexes, **33**, possessing an Si-H unit, which were possible precursors to silicon cations. However, attempts to generate a metal-stabilized silicon cation **34**, from **33** by hydride abstraction using the Ph_3C^+ cation were unsuccessful. Indeed, the X-ray crystal structure of **26** suggests that steric hindrance precludes the approach of the bulky trityl cation to the Si-H bond, as seen in Scheme 3-1.

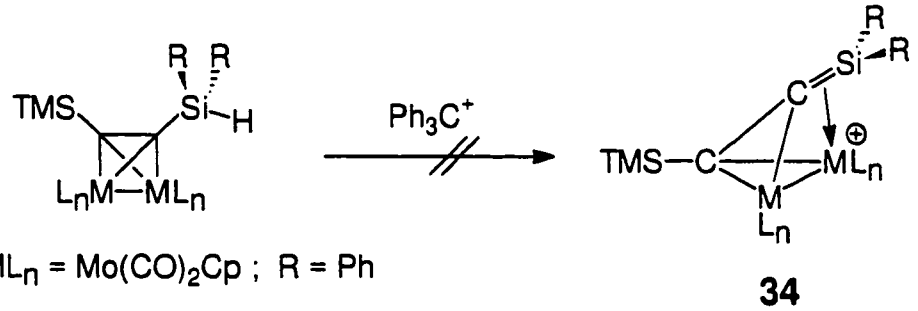

33 $ML_n = Mo(CO)_2Cp$; R = Ph

34

Scheme 3-1: Attempted removal of hydride, from silane precursor.

We describe herein the syntheses and reactivities of a series of allylsilane derivatives of metal clusters. These compounds should be subject to protonation at the γ-carbon with generation of a β-silyl-stabilized cation.[73] Cleavage of the silicon α-carbon bond and subsequent loss of propene can then lead to a silyl cation, as depicted in Scheme 3-2. This process could occur *via* an S_E2' mechanism as shown by Sakurai.[74] Protonation at the

terminal allylic carbon should alleviate the steric problems associated with direct electrophilic attack at the silicon center. In the carbocation series, Curtis has reported the X-ray crystal structure of the dimolybdenum dication $[Cp_2Mo_2(CO)_4(CH_2\text{-}C{\equiv}C\text{-}CH_2)]^{2+}$. One can envisage the possibility of preparing a disilylium analogue.[75]

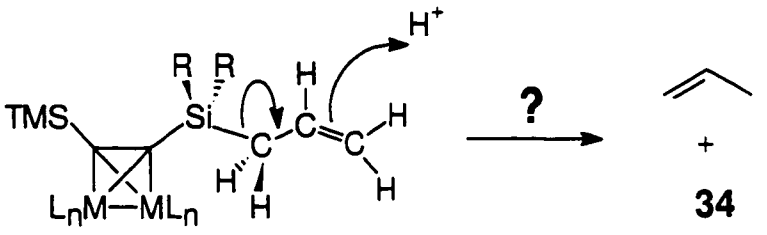

Scheme 3-2: A possible route to metal-stabilized silyl cations from allylsilanes.

3.2. Background

The syntheses, structures, and reactivities of carbocations have played a pivotal role in chemistry for many decades. As shown in Olah's pioneering investigations, such species can be generated in superacid media and studied at leisure.[76] Moreover, as with other normally short-lived intermediates such as carbynes or cyclobutadienes, transition metal complexes of carbocations, such as **35** or **36**, can be isolated and characterized by X-ray crystallography.[61, 77]

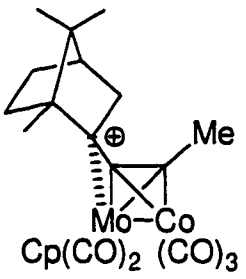

35

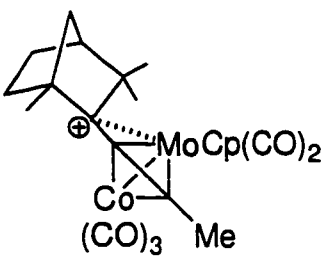

36

Transition metal cluster complexes of silyl poly-ynes have been the subject of several recent studies owing to their potential applications in materials science. Lang and co-workers have shown that η^1-metalloalkynes **37** are precursors to the mixed-metal clusters **38** which, when pyrolyzed, yield metal carbide ceramics, as depicted in Scheme 3-3.[78]

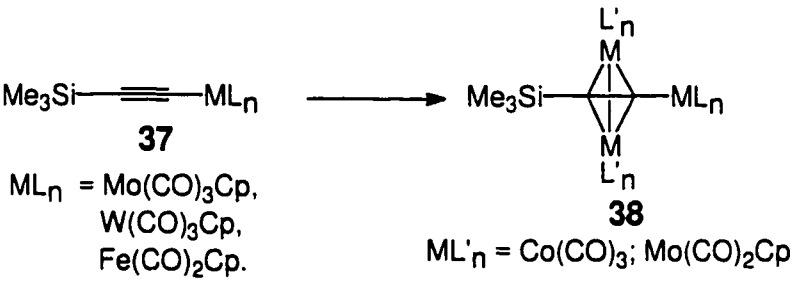

Scheme 3-3: Syntheses of clusters possessing η^1-ML_n substituents.

Cobalt, nickel, molybdenum and tungsten clusters have also been prepared from diynes and tetraynes.[79-81] Perhaps the most fascinating molecule in this series of poly-yne derivatives is $C_{18}[Co_2(CO)_4dppm]_3$, the tris-cluster complex derived from the nonayne cyclo[18]carbon.[82] Such clusters are also able to stabilize α-carbocations. We wanted to establish if they could also stabilize analogous silicon cations.

3.3. Preparation of AllylSilane Precursors.

As a prelude to the syntheses of a series of alkynylsilane clusters, the mono- and di-alkynyl silanes **39, 40,** and **41** were prepared by treatment of the appropriate lithio-alkyne with allyldimethylchlorosilane, as shown in Scheme 3-4.

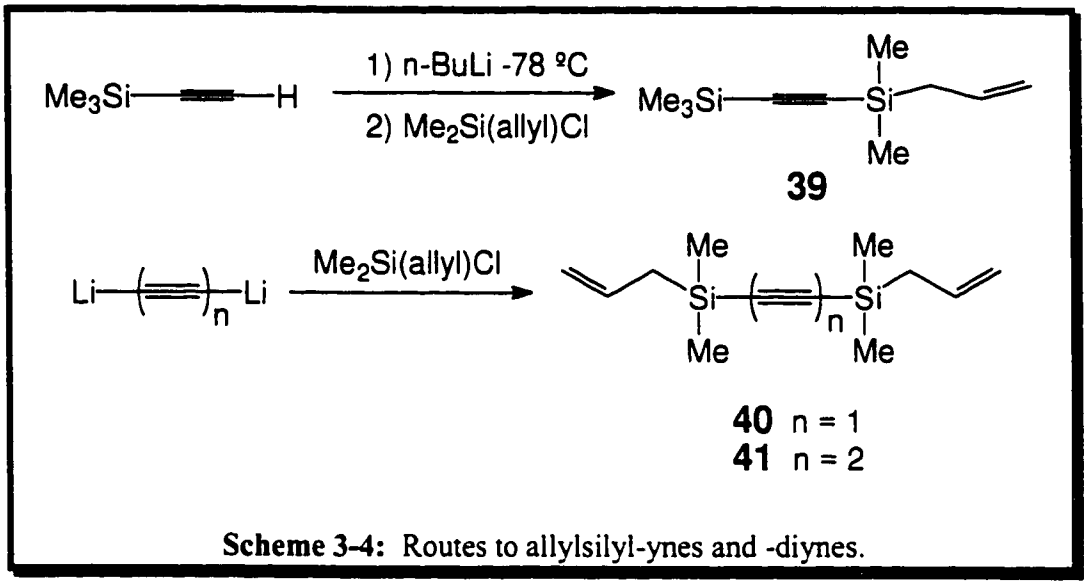

Scheme 3-4: Routes to allylsilyl-ynes and -diynes.

As depicted in Scheme 3-5, the mono-allyl system **39** reacts with $Co_2(CO)_8$ or $Cp_2Mo_2(CO)_4$ to yield the dimetallatetrahedranes **42** or **43**, respectively. These clusters were identified by the use of ^1H, ^{13}C, and ^{29}Si NMR, infrared spectroscopy and mass spectrometry; the dimolybdenum cluster **43**, was additionally characterized by X-ray crystallography. The structure of **43** appears in Figure 3-1 and the overall molecular geometry closely resembles those previously reported for the related systems $[Cp_2Mo_2(CO)_4](Me_3Si\text{-}C{\equiv}C\text{-}SiPh_2H)$, **26**, and $[Cp_2Mo_2(CO)_4](Me_3Si\text{-}C{\equiv}C\text{-}SiMe_3)$.[68] For our present purposes, however, we note that

the allyl fragment is oriented so as to leave the terminal methylene group entirely exposed and readily accessible to an incoming electrophile.

Treatment of the diallyl-monoalkyne and -dialkyne, **40** and **41**, respectively, with excess $Co_2(CO)_8$ or $Cp_2Mo_2(CO)_4$ yielded the clusters **44, 45** and **46**. The reaction of **41** with one equivalent of $Co_2(CO)_8$ led to the unsymmetrical product **47** which possesses both a free and complexed triple bond, as depicted in Scheme 3-6. The X-ray crystal structure of the diallyl double cluster **45** is shown in Figure 3-2. As with the bis-trimethylsilyl analogue, $(Me_3Si\text{-}C{\equiv}C\text{-}C{\equiv}C\text{-}SiMe_3)[Co_2(CO)_6]_2$, previously reported by Magnus,[80] the cluster core adopts the "staggered ethane" conformation illustrated in Figure 3-3. The torsion angle C(2)-C(1)-C(1A)-C(2A) is 162°.

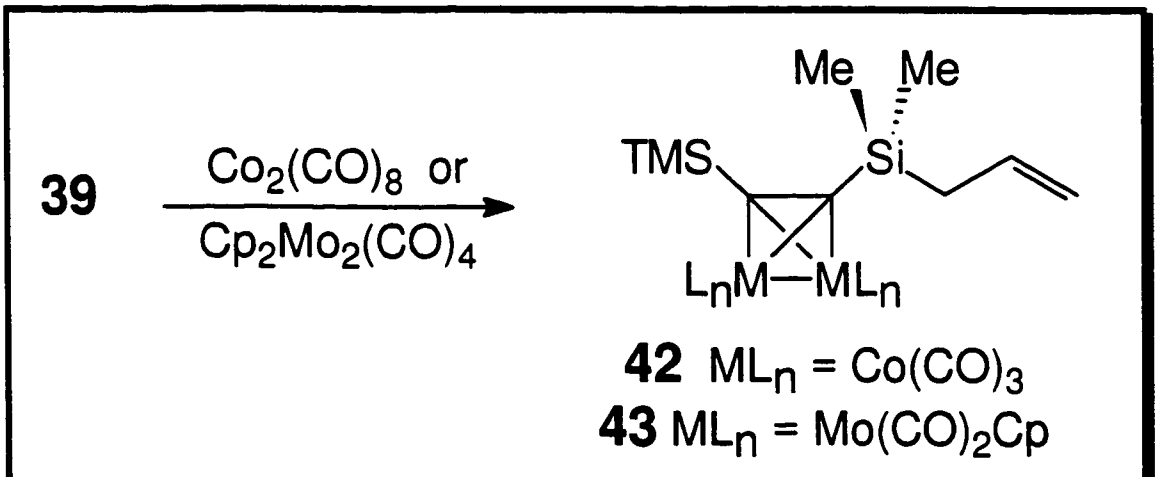

Scheme 3-5: Synthesis of allylsilyl dimetallic clusters.

One could envisage the incorporation of the diyne cluster **45** into a cyclodialkyne, perhaps *via* successive hydrosilylations.[83] However, the steric bulk of the double cluster hinders rotation about the central carbon-carbon bond and forces the two allyl substituents to maintain their approximate anti-periplanar orientation, a conformation from which cyclization could not readily be envisaged.

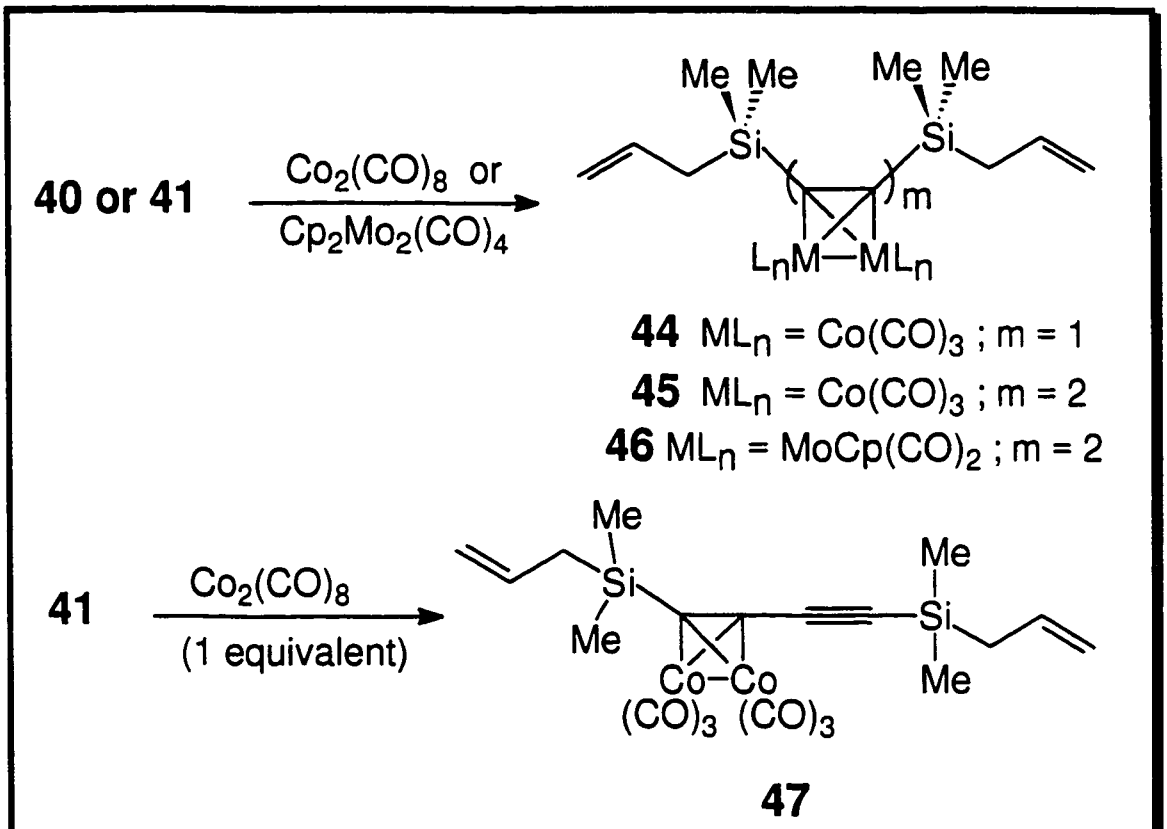

Scheme 3-6: Routes to allylsilane metal clusters.

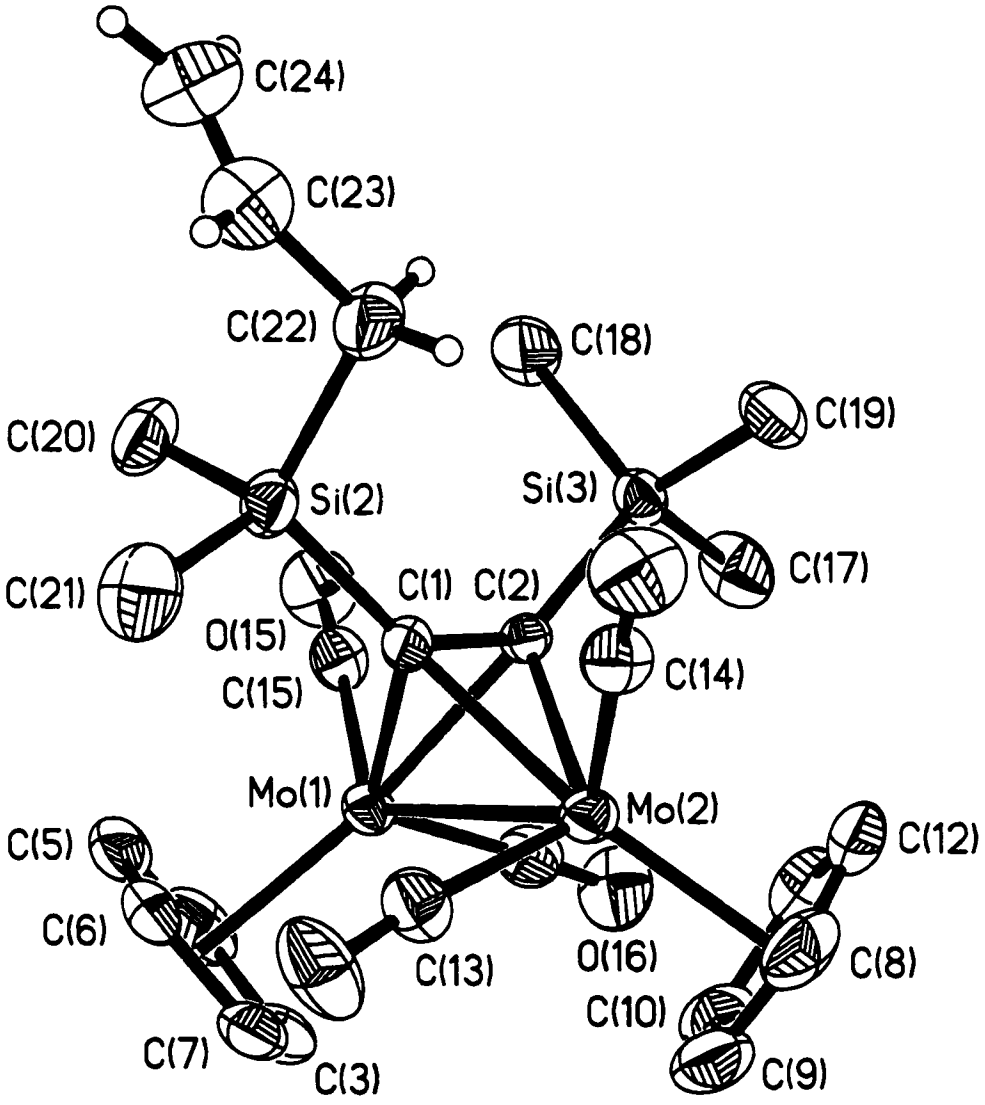

Figure 3-1: X-ray crystal structure of **43**, showing 30% thermal ellipsoids.

Salient bond lengths(Å): Mo(1)-Mo(2) 2.9290(8), Mo(1)-C(2) 2.257(4), Mo(1)-C(3) 2.322(5), Mo(2)-C(2) 2.183(4), Mo(2)-C(13) 1.959(5), C(1)-C(2) 1.353(5), C(2)-Si(3) 1.850(4), C(1)-Si(2) 1.858(4)

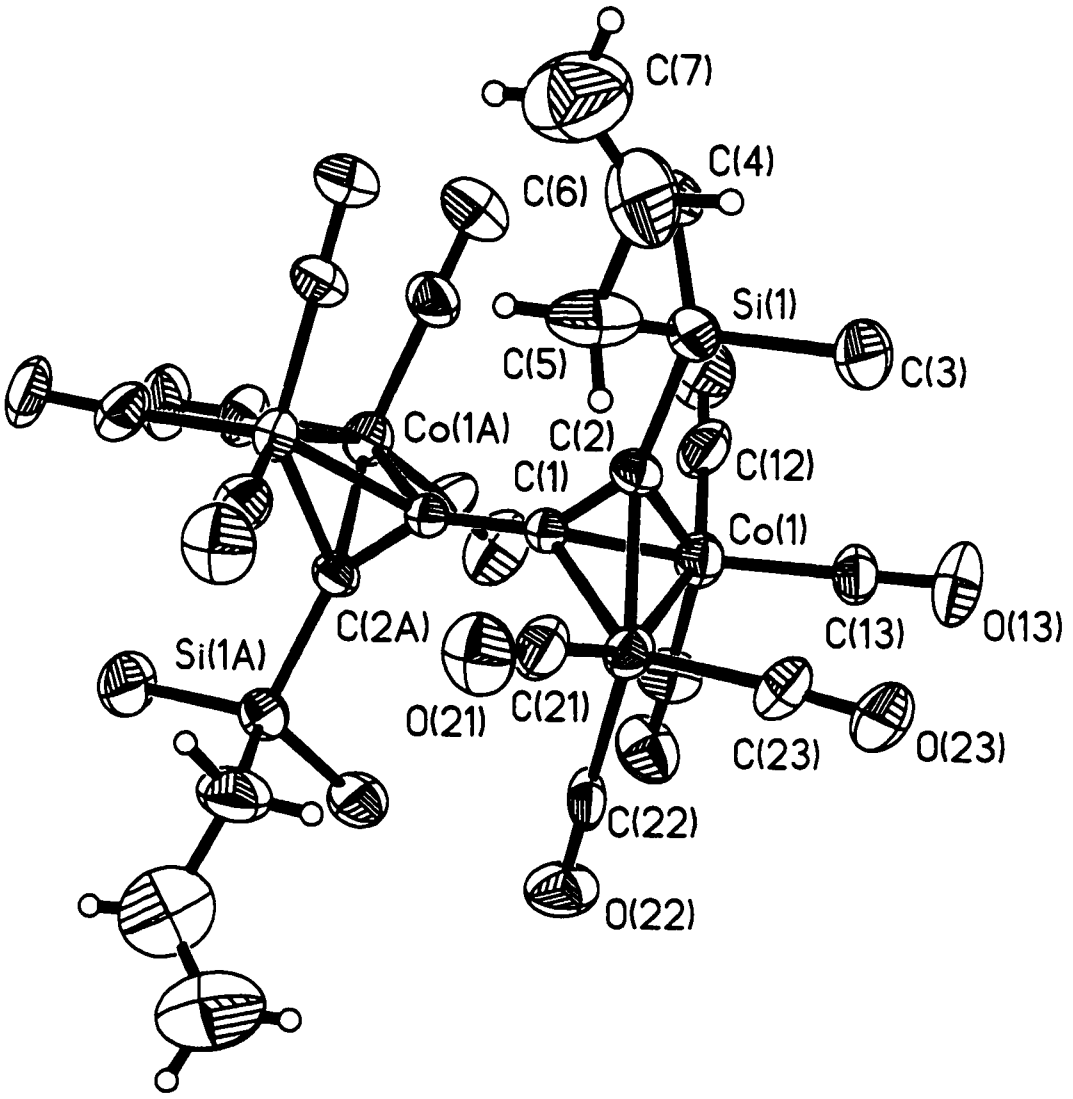

Figure 3-2: X-ray crystal structure of **45** showing 30% thermal ellipsoids.

Salient bond lengths(Å): Co(1)-Co(2) 2.460(3), Co(1)-C(2) 1.969(12), Co(1)-C(1) 1.962(12), Co(2)-C(1) 1.973(10), Co(2)-C(2) 2.023(12), C(1)-C(2) 1.331(14), C(1)-C(1a) 1.46(2), C(2)-Si(1) 1.832(12)

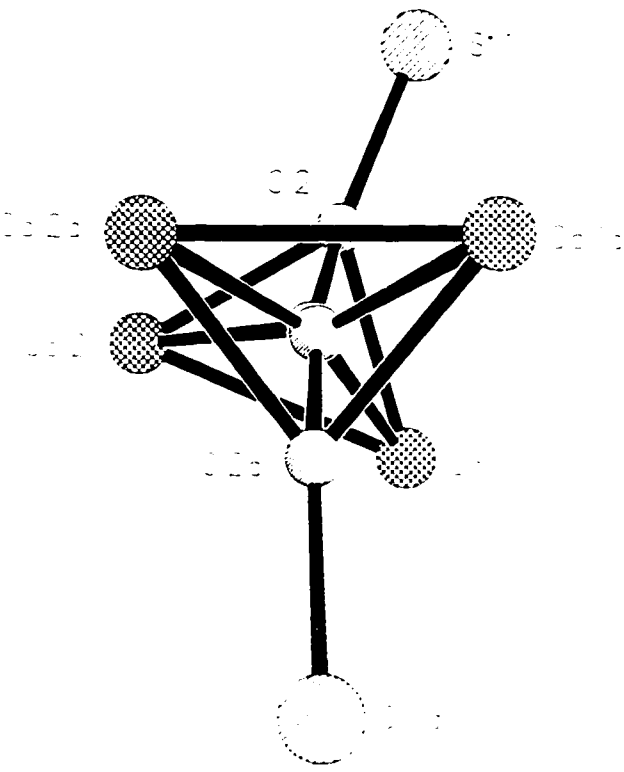

Figure 3-3: View along the C(1a)-C(1) bond in **45** showing the staggered conformation of the two cluster cores.

3.4. *Reactions of allyl clusters with HBF_4*

The protonation of $(Me_3Si\text{-}C{\equiv}C\text{-}SiMe_2\text{-}CH_2\text{-}CH{=}CH_2)Co_2(CO)_6$, **42**, with HBF_4 in an NMR tube at -90 °C was monitored by ^{13}C, ^{19}F and ^{29}Si NMR spectroscopy. At that temperature, the formation of the fluorosilane **48** was readily observable *via* the appearance of a 269 Hz silicon-coupled doublet in the ^{19}F spectrum, as shown in Figure 3-4. In addition, the ^{13}C NMR spectrum revealed peaks at 133.8, 115.1 and 74.7 ppm, characteristic of propene.[84] There was no evidence for the production of either a β-stabilized silyl cation, **49**, or a silylium

ion. We note that Lambert has very recently reported NMR data for a β-stabilized silyl cation.[73] If either of these species are produced, their lifetime must be very short under these reaction conditions. The most probable scenario involves protonation of the allyl unit with subsequent rapid, nucleophilic attack by fluoride ion at silicon, as depicted in Scheme 3-7.

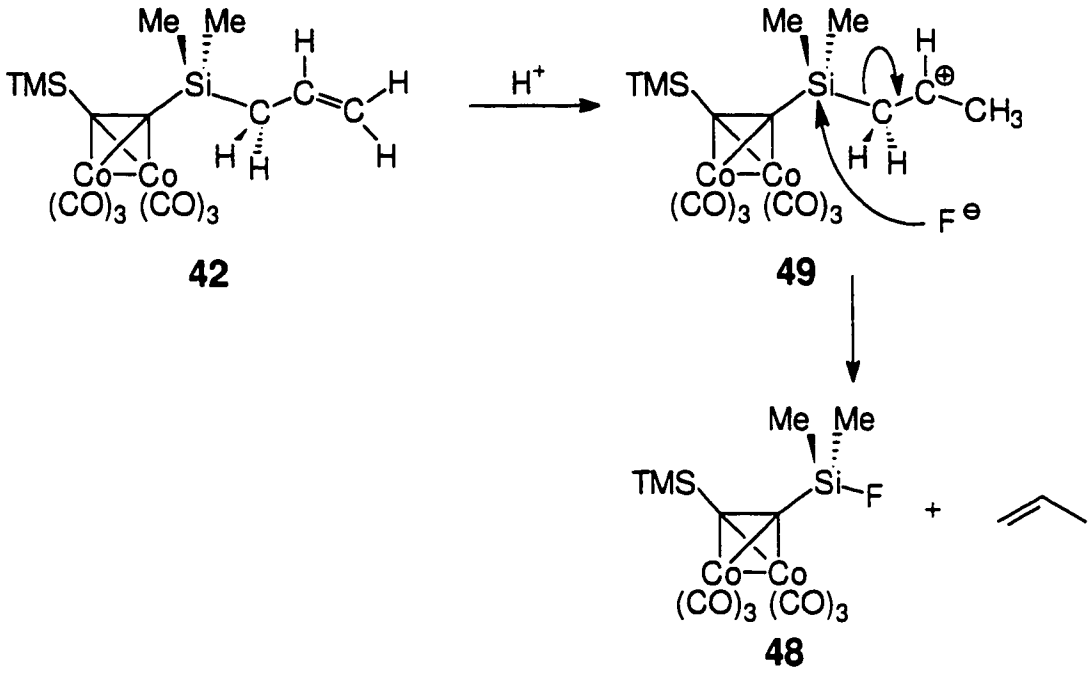

Scheme 3-7: Proposed mechanism for the formation of **48**, $Me_3SiC{\equiv}CSiMe_2F[Co_2(CO)_6]$.

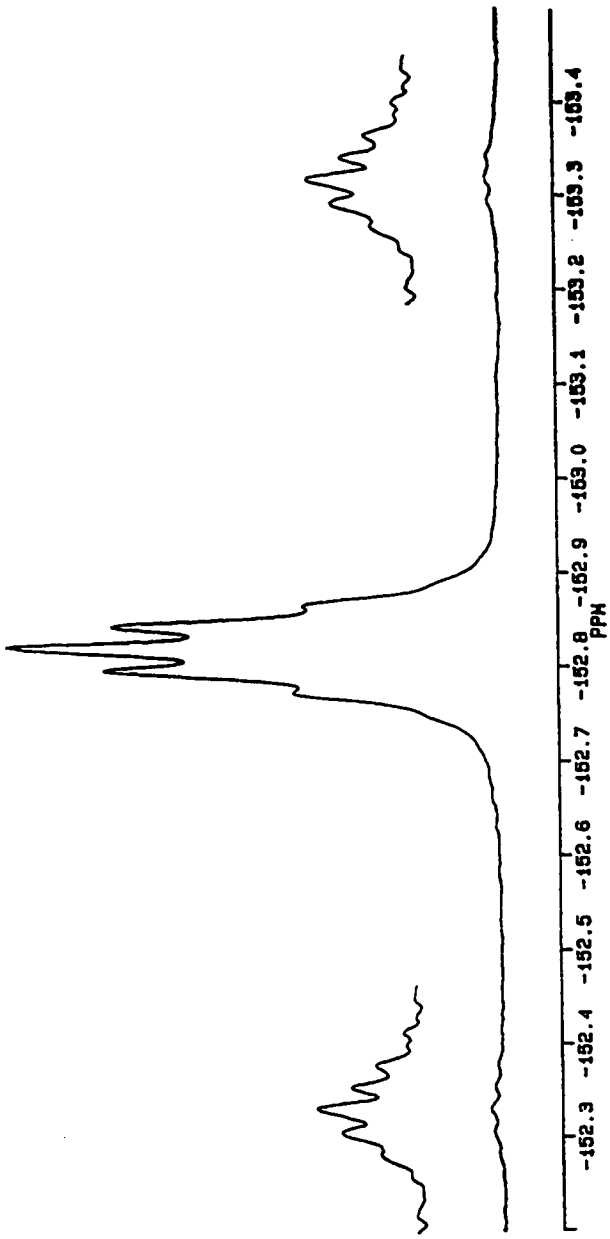

Figure 3-4: 282.42 MHz ^{19}F NMR spectrum of $(Me_3Si\text{-}C{\equiv}C\text{-}SiMe_2F)Co_2(CO)_6$, **48**, showing the ^{29}Si satellite peaks.

Analogously, the dimolybdenum allyl cluster **43**, and the free ligand **39**, both behave similarly with HBF_4 to give the corresponding fluorosilanes, **50** and **51**, respectively as depicted in Scheme 3-8. Treatment of the bis-allyl compounds **41**, **45** and **46** with one equivalent of HBF_4 gives the monofluorosilane products, **52**, **53** and **54**, respectively. Addition of a further equivalent of HBF_4 yielded the corresponding di-fluorosilanes, **55**, **56** and **57**, respectively, as shown by ^{29}Si NMR (see Scheme 3-9). In a similar experiment, treatment of **42** and **43** with triflic acid yields the analogous silyl triflates, **58** and **59**, as in Scheme 3-8.

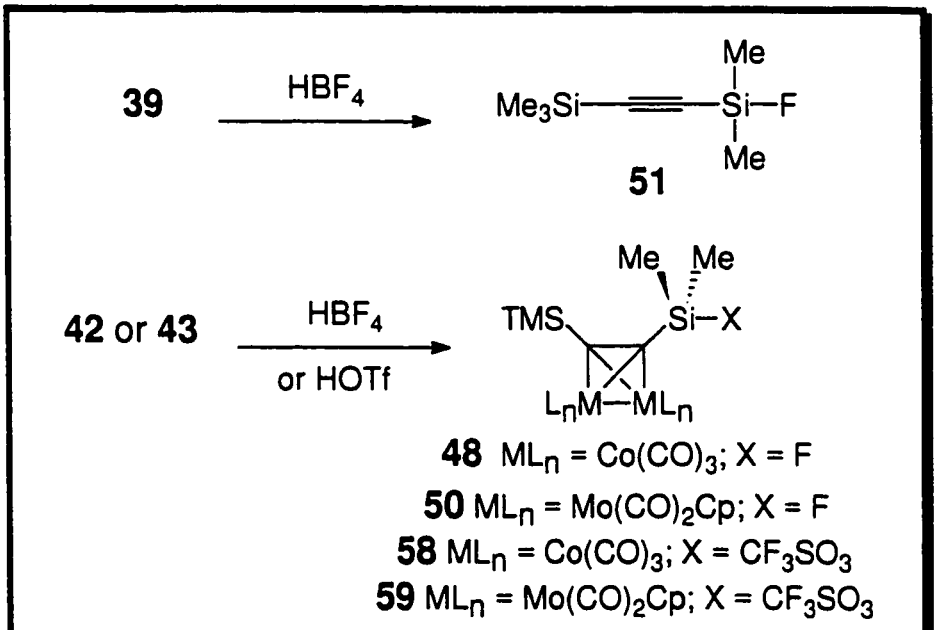

Scheme 3-8: Reactions of allyldisilaalkynes with HBF_4 or triflic acid.

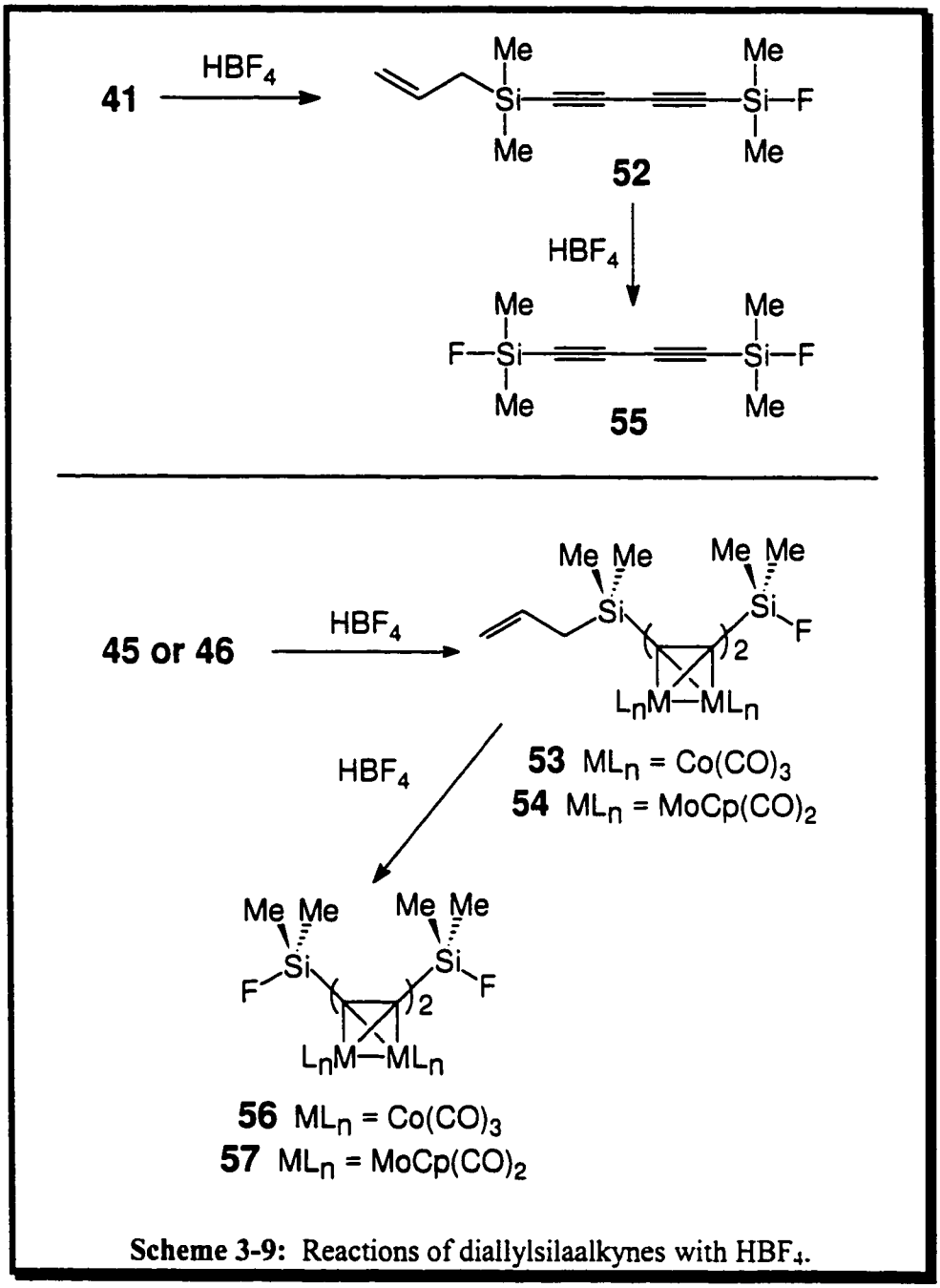

Scheme 3-9: Reactions of diallylsilaalkynes with HBF_4.

We have shown previously, by means of molecular orbital calculations at the extended Hückel level, that dimetallic clusters should provide some modest stabilization to alkynyl-silylium ions (see section 2.2). However, if the propene elimination process were to occur by the S_E2' mechanism depicted in Scheme 3-2, one would not necessarily expect enhanced reactivity for the Co or Mo clusters relative to the free ligands: the metal is too far removed from the intermediate β-silyl cation to participate in its stabilization. To examine this question, a series of competitive protonation experiments were run on an NMR-tube scale. Equimolar quantities of **39** versus **42**, **39** versus **43**, and **42** versus **43**, were each treated with less than one equivalent of HBF_4 at -80 °C, and the progress of the reaction was monitored by ^{19}F NMR. The NMR data (see Experimental Section) showed that, within the error limits, the free ligand and the Co or Mo complexes proved to be equally susceptible to protonation of the allyl substituents, with subsequent formation of the appropriate fluorosilane.

However, these experiments are open to the criticism that the free silyl-alkyne and its cluster complexes may not be equally soluble in the medium. To counter this argument, the mono-complexed diyne **47** was also allowed to react with HBF_4 at -80 °C; in this case, the ^{29}Si NMR spectrum of the product indicated that the major product, **60** was derived from attack on the allyl-silane at the uncomplexed triple bond, as seen in Scheme 3-10. It is apparent from the above studies that if free silylium ions are produced in these protiodesilylation reactions, they are insufficiently stabilized by the transition metals to have reasonable lifetimes. This may be a consequence of poor stabilization but may be more likely attributed to the facility with which triflate, and particularly fluoride, attack silicon centers.

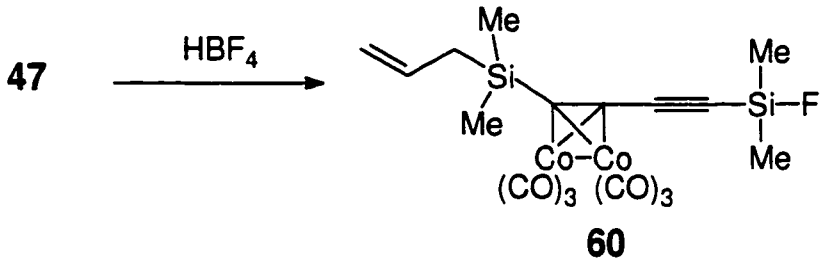

Scheme 3-10: Allylsilane competition for HBF_4.

3.5. Summary

The complexation of monoallyl- and diallyl-disilaalkynes and diallyl-disiladialkynes with $Co_2(CO)_6$ or $Mo_2(CO)_4Cp_2$ fragments readily occurs. It has been clearly demonstrated that protonation at the methylene terminus of an alkynylallylsilane (free or metal complexed alkyne) with either HBF_4 or triflic acid readily occurs with elimination of propene and formation of the corresponding silyl fluoride or triflate. There is, as yet, no evidence of an isolable metal-stabilized silyl cationic intermediate. It is evident that these electrophilic attacks on the allyl-silanes must avoid the use of any counter-ions that could form covalent bonds with silicon.

4. POSSIBLE INTRAMOLECULAR TRAPS FOR SILICON CATIONS.

4.1. Background

The ability of dimetallic tetrahedral clusters to stabilize a positive charge in a position α to the cluster is well known. This knowledge should be considered when seeking a synthetic route to stable silicon cations. Thus far two approaches have been discussed whereby Si-H and Si-$CH_2CH{=}CH_2$ fragments have been considered as silicon cation precursors. The incorporation of a CH_2 group, in the form of an alkyl chain, at the other terminus of the dimetallic cluster may be advantageous. Such a system might engender competition between the metal-stabilized silicon cation and a metal-stabilized carbocation produced *via* intramolecular hydride transfer. (see Scheme 4-1).

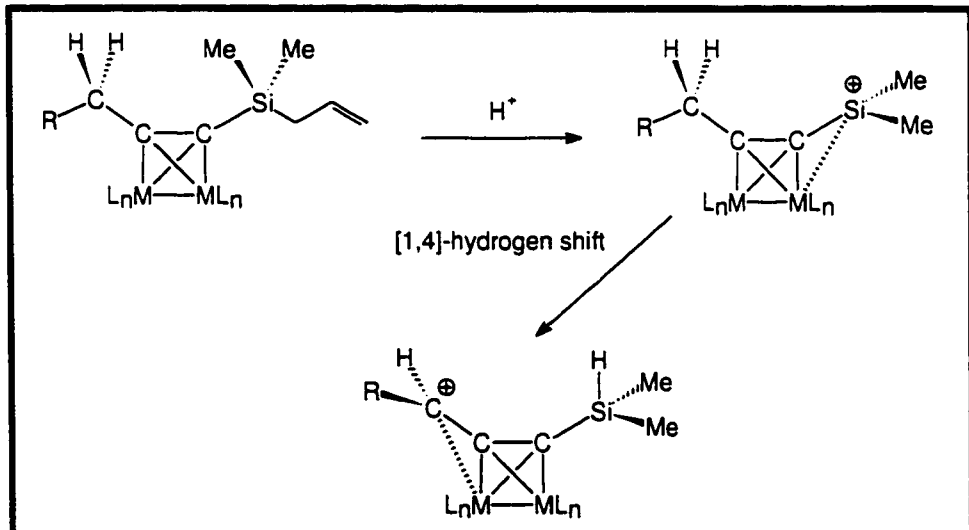

Scheme 4-1: Is a hydride transfer possible?

4.2. Possible hydride transfers.

Routes to the preparation of alkynes bearing an allylsilane and an alkyl chain with α protons as substituents were undertaken. 1-Hexyne was treated with butyllithium to give the corresponding lithio-alkyne which, when quenched with allyldimethylchlorosilane, gave **61** as depicted in Scheme 4-2. The ligand was easily metallated by the addition of $Co_2(CO)_8$ to afford the dicobalt cluster **62**.

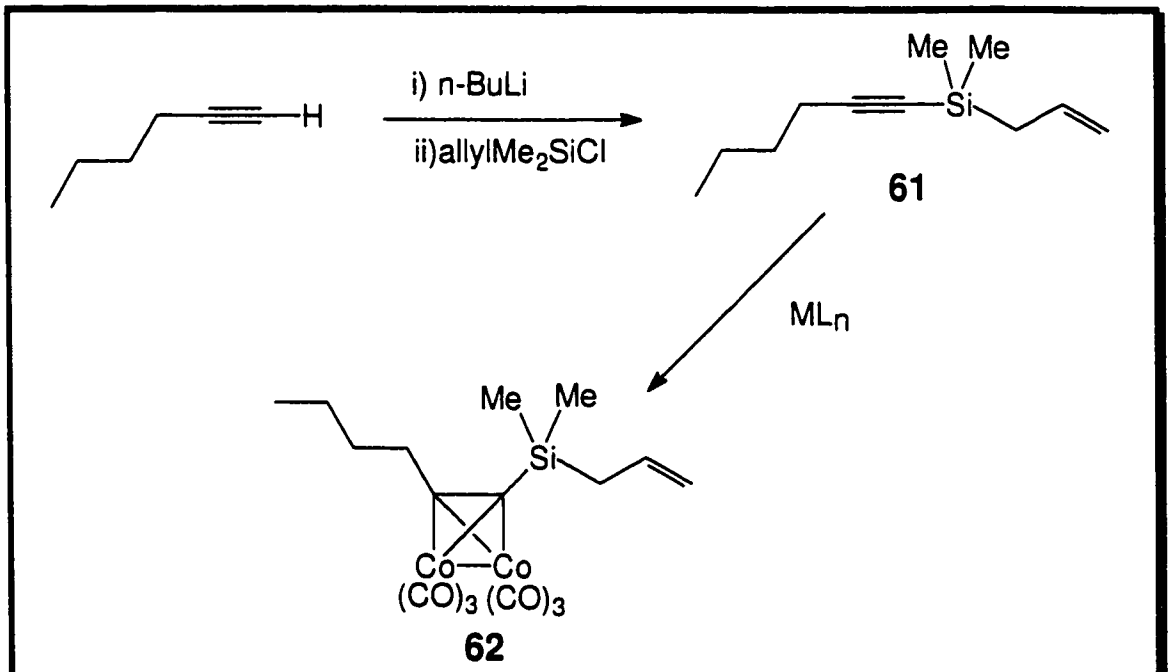

Scheme 4-2: Preparation of precursor allylsilanes.

The free ligand and the organometallic cluster were characterized by NMR and mass spectrometry. The 500 MHz ^1H and 125 MHz ^{13}C NMR spectra of both **61** and **62** have been completely assigned by means of ^1H-^1H COSY and ^1H-^{13}C NMR shift-correlated experiments, the spectra from which are shown in Figure 4-2 and Figure 4-3.

By identifying the terminal methyl proton resonance of the butyl chain, and the nearest neighbours, the entire butyl chain and the allyl groups can be assigned easily with the use of the ^{1}H-^{1}H COSY NMR spectrum (as seen in Figure 4-2). Subsequently the entire ^{13}C NMR spectrum can easily be assigned by with the ^{1}H-^{13}C NMR shift-correlated experiment (as seen in the Figure 4-3) as seen in the direct correlation.

The addition of tetrafluoroboric acid to **62** in an NMR tube at -80 °C was monitored by ^{29}Si-^{1}H HMBC NMR spectroscopy. The product generated in the reaction was the corresponding fluorosilane, **63**. There was no evidence of Si-H bond formation which could have arisen as a result of a hydride shift from the methylene group to the silicon cation site. Similarly, addition of triflic acid to **62** led to the formation of the analogous Si-triflate, **64**. The free ligand, **61**, reacts similarly with tetrafluoroboric acid and triflic acid to form the corresponding fluorosilane, **65**, or triflate compound, **66** (see Figure 4-1).

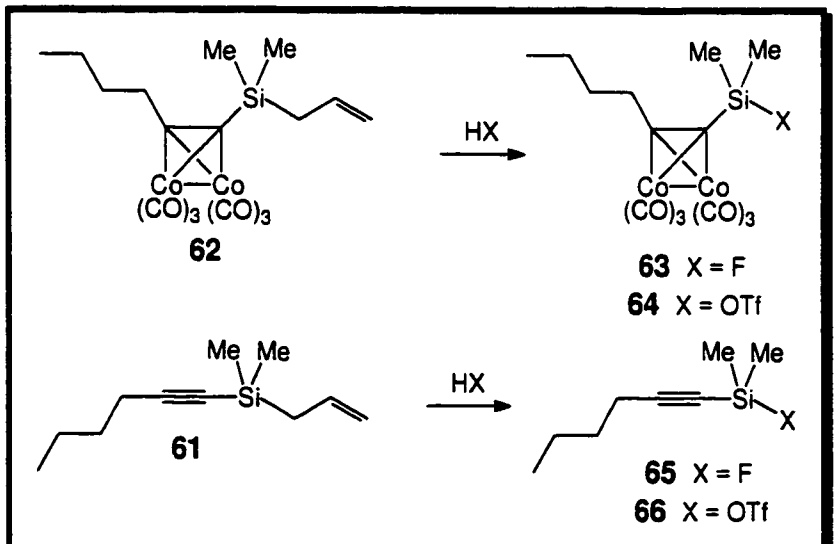

Figure 4-1: Reaction **61** and **62** with triflic acid and HBF_4.

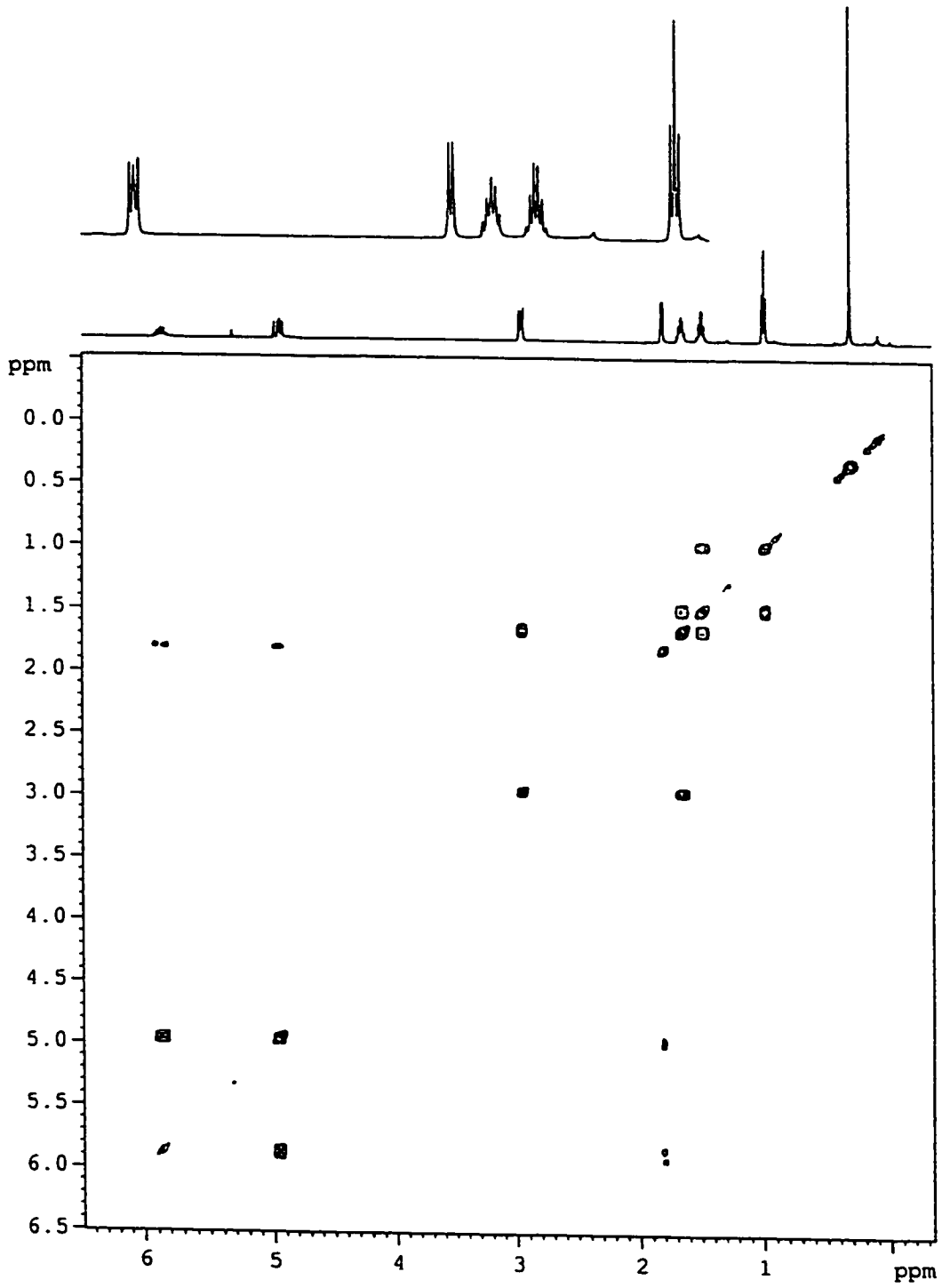

Figure 4-2: ^{1}H-^{1}H COSY for compound **62**.

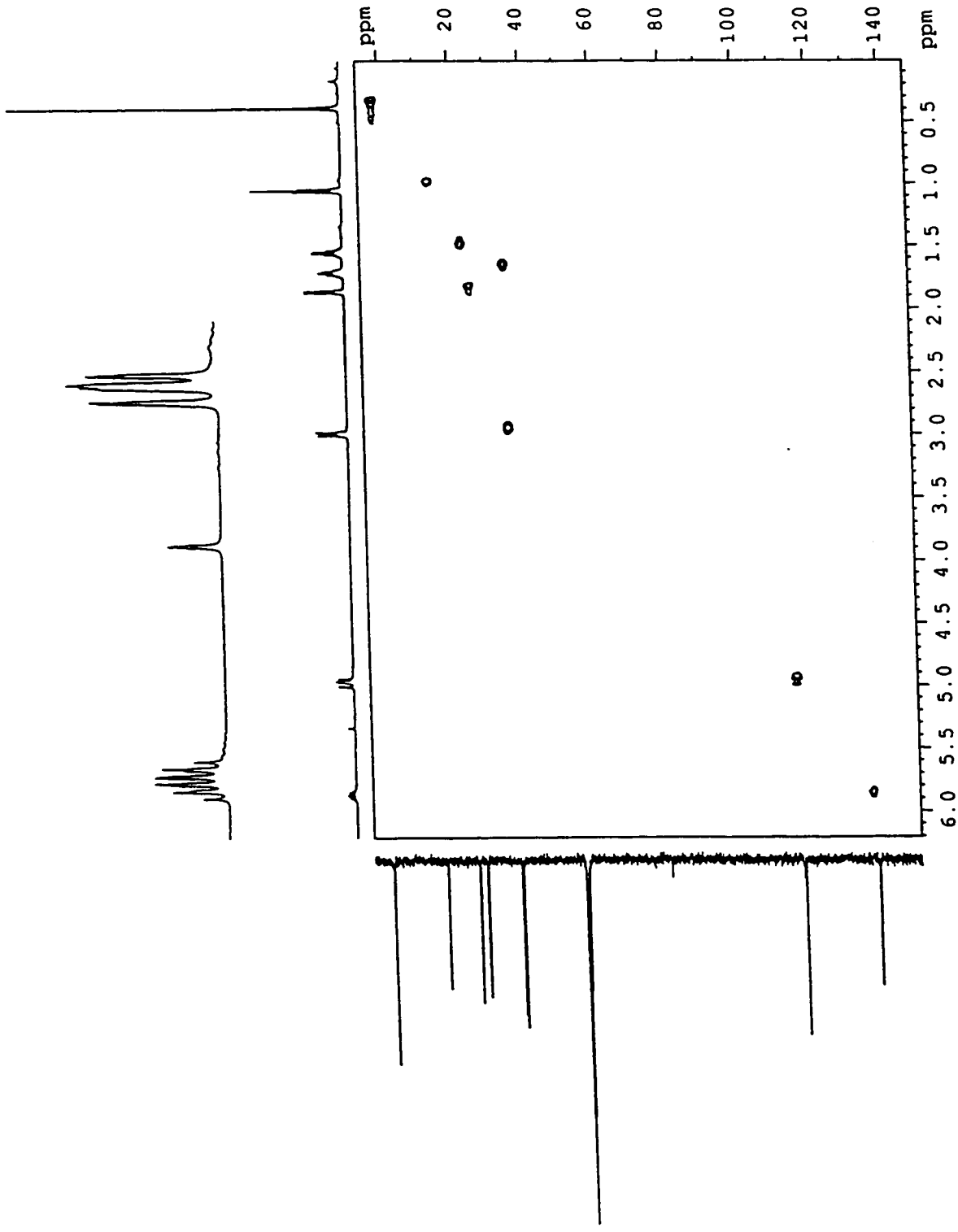

Figure 4-3: ^{1}H-^{13}C NMR single bond shift-correlated for **62**.

4.3. Carbocation versus Silicon cation: A Competitive Study

In continuation of our recent studies on the chemistry of allylsilane derivatives of transition metal clusters, we chose to incorporate potential precursors to silylium and carbenium centers in the same system. It is known that protonation of allylsilanes with HBF_4 leads to the loss of propene with concomitant formation of the corresponding fluorosilanes. Moreover, comparison of the free and complexed alkynyl-allylsilanes suggests that the process does not proceed *via* a discrete silylium ion, **34**, but rather *via* a β-silyl-stabilized carbocation, **49**, as in Scheme 3-7.

The examination of metal cluster stabilized cations was pioneered by Nicholas and has since been exploited by many groups.[85] In contrast to the normal linear arrangement of the C-C≡C-C linkage in free alkynes, complexation of the triple bond to a dimetallic fragment brings about a C-C≡C bend angle in the range 136° to 145° as also seen in the structure of **45**, and so forces the centers closer together, thus enhancing their ability to react. Thus, $Co_2(CO)_6$ moieties have been used not only as protecting groups,[86] but also to allow geometrically disfavoured cyclization reactions,[87] or to stabilize strained alkynes such as (hexafluorocyclohexa-3-ene-1-yne)$[Co_2(CO)_6]$.[88]

The synthesis of $(CH_2{=}CHCH_2)$-$SiMe_2$-C≡C-$CMe_2OH[Co_2(CO)_6]$, **67**, as outlined in Scheme 4-3 proceeds in an overall yield of 92%. The final product was identified by its mass and NMR spectra, which are analogous to those of related systems, such as $(CH_2{=}CHCH_2)$-$SiMe_2$-C≡C-$SiMe_3[Co_2(CO)_6]$.

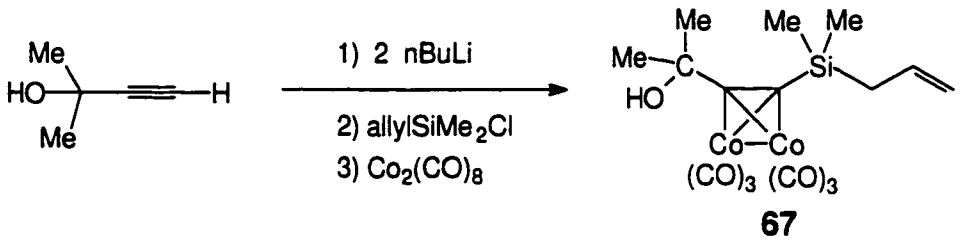

67

Scheme 4-3: Preparation of $(CH_2=CHCH_2)$-$SiMe_2$-C≡C-$CMe_2OH[Co_2(CO)_6]$, **67.**

We turned next to the treatment of **67** with HBF_4. We would expect that protonation could occur at either the allyl group (to yield ultimately a fluorosilane), or at the tertiary alcohol site (thus producing a carbocation). Addition of one equivalent of HBF_4 to **67** yielded, after chromatographic separation, the product, **68** (see page 66, Scheme 4-5), whose NMR spectra indicated loss of the alcohol functionality, retention of the allyl group, and formation of an $SiMe_2F$ moiety. The presence of this functionality was unambiguously revealed by the fluorine-coupled doublet, $^1J_{(Si\text{-}F)}$=251 Hz, in the ^{29}Si NMR spectrum. The ^{13}C NMR shows that the allyl peaks are shifted to lower field raising the possibility that the allyl group is bound to carbon rather than silicon (see Table 1).

The proposed structure of **68**, was confirmed, and the 500 MHz ^1H and 125 MHz ^{13}C NMR spectra were completely assigned by means of ^1H-^1H COSY, ^1H-^{13}C shift-correlated NMR experiments and a ^{13}C-DEPT experiment (as seen in Figure 4-4, and Figure 4-5). In the ^1H-^{13}C shift-correlated NMR experiments, the resonance attributable to the geminal methyl shows three strong correlations, one to its methyl partner, one to the quaternary carbon atom to which each methyl is attached and the last to the allylic

carbon resonance, clearly indicating that the allyl group is attached to the carbon and not the silicon. Further evidence for the migration of the allyl group to the carbon atom is provided from the two correlations between the quaternary carbon atom and the geminal methyl resonances to the allyl CH_2 resonance in the ^{1}H-^{13}C NMR shift-correlation spectrum.

The Lewis acid mediated version of the reaction described above was investigated next. The addition of BF_3•etherate to **67** should complex the alcohol and generate the propargylic ether complex (in effect the metal stabilized carbocation). This reagent has only one possible site of attack towards **67**, as opposed to an acid-type reagent which has two sites. The reaction was carried out by adding a 1:1 mixture of the organometallic complex and the Lewis acid. After chromatographic separation, the products revealed in ^{1}H and ^{13}C-NMR were identical to that described above, **68**. This provides supporting evidence that a metal-stabilized carbocation must be generated in order to ultimately form the product which was isolated in the from the reaction of **67** with HBF_4 or BF_3.

Another suitable precursor was synthesized in order to probe this competitive reaction further. An isopropenyl group was chosen as a carbocationic site for the study. This is an ideal group for the experiment since addition of HBF_4 can still attack to yield a carbocation and/or a silylium ion, without the formation of any water as a byproduct in the reaction (as is possible in the reaction of **67** and HBF_4). The desired precursor is easily prepared by silylating 2-methyl-1-buten-3-yne with chlorodimethylallylsilane to give **69**. The dimetallic cluster can easily be prepared by reacting **69** with $Co_2(CO)_8$ to

afford the dicobalt cluster **70**. The protonation of **70** with a limiting amount of acid gave the identical NMR spectra to the two reactions described above.

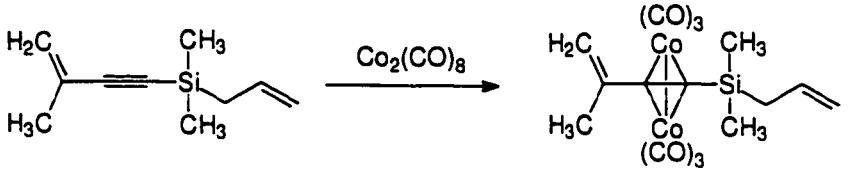

69 **70**

Scheme 4-4: Preparation of isopropenyl-cobalt cluster.

The fact that protonation of **67** or **70** generates the identical metal-stabilized carbocation, coupled with the fact that **68** can be generated from **67** with either HBF_4 or BF_3, provides supporting evidence for the mechanism described. We conjecture that the favored site of proton attack on **67** or **70** is at the alcohol or the isopropenyl groups respectively, to generate a cobalt-stabilized carbocation. Intramolecular electrophilic attack can then occur on the neighbouring allyl group to give a β-silyl stabilized carbocation. Subsequent nucleophilic attack by fluoride ion at the silicon center leads to cleavage of the Si-allyl linkage, to generate a fluorosilane as depicted in Scheme 4-5.

The results from both reactions of **67** and **70**, respectively, with HBF_4, imply that protonation occurs much more readily at the alcohol or the isopropenyl group to generate a metal-stabilized carbocation as opposed to the possible addition to the allylsilane. These results suggest that the dicobalt cluster provides greater stabilization to the carbocation as opposed to a β-silyl stabilized carbocation. It is probably this phenomenon, coupled with the formation of the silicon-fluoride bond, which provide the sources of the thermodynamic driving force of the reaction pathway described previously.

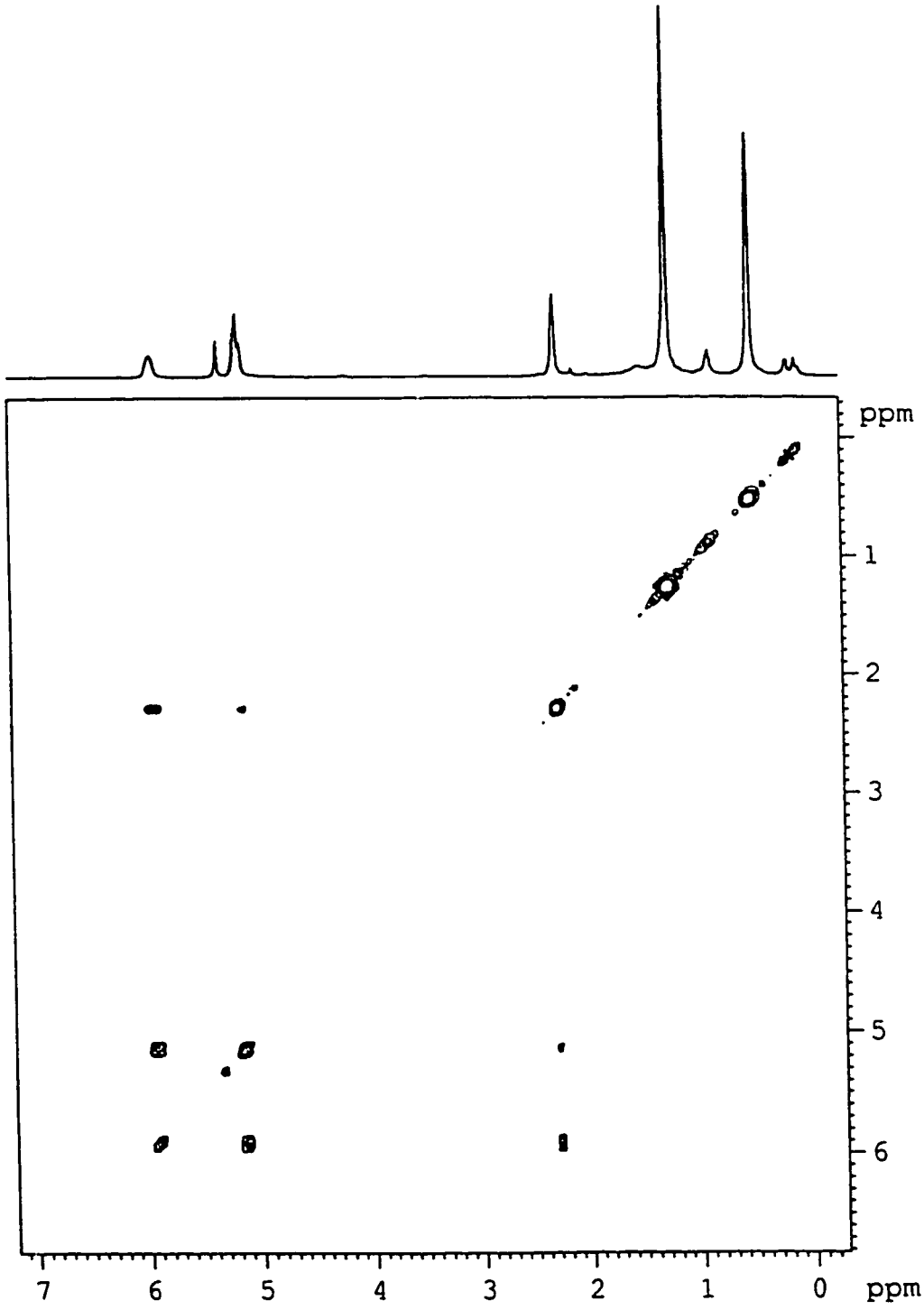

Figure 4-4: ^{1}H-^{1}H COSY for compound **68**.

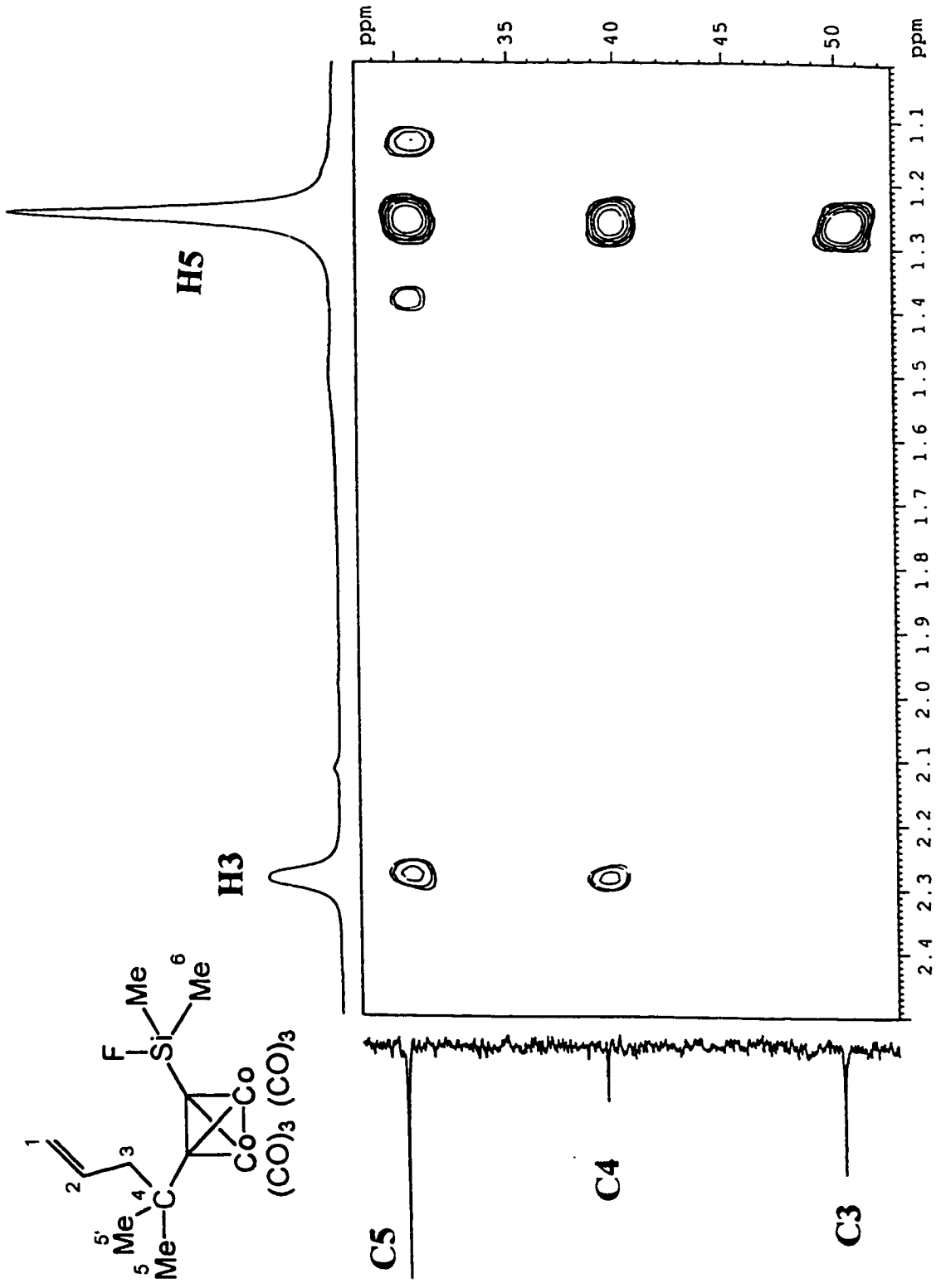

Figure 4-5: ^{1}H-^{13}C NMR multiple bond shift-correlated for compound **68**

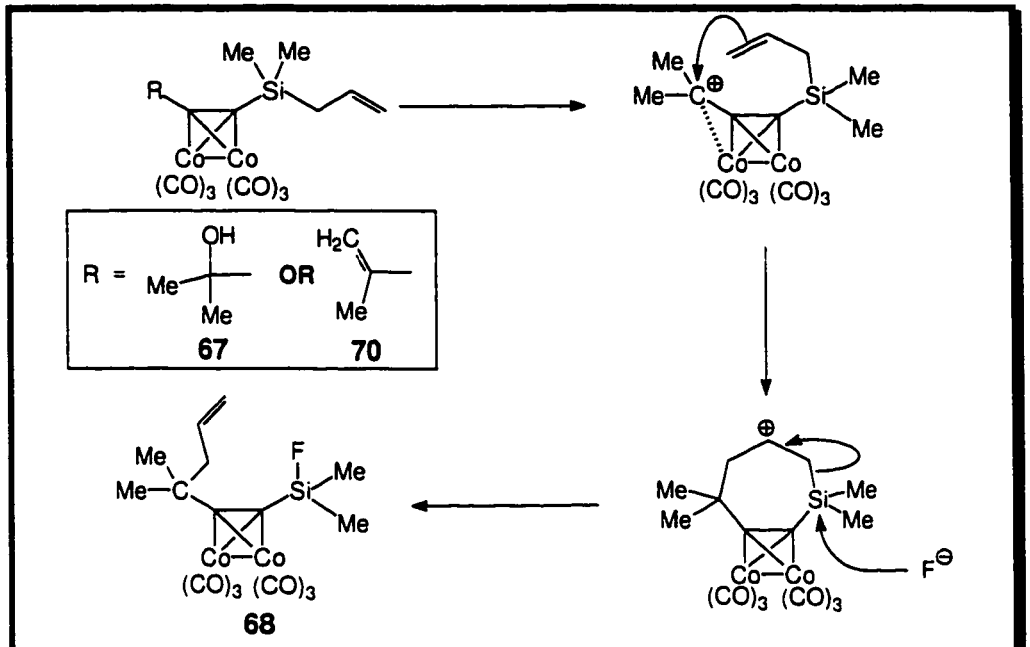

Scheme 4-5: Proposed mechanism showing allyl transfer from silicon to carbon.

Table 1: ^{1}H and ^{13}C NMR chemical shift comparison for compounds **67**, **68**, and **70**.

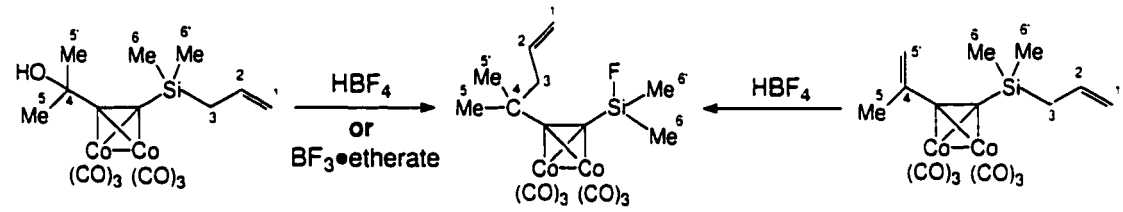

67 **68** **70**

	67		68		70	
	^{1}H : (ppm)	^{13}C: (ppm)	^{1}H: (ppm)	^{13}C: (ppm)	^{1}H: (ppm)	^{13}C: (ppm)
1	4.96	114.7	5.12	118.6	4.86	117.7
2	5.86	134.4	5.90	134.8	5.77	134.3
3	1.83	25.5	2.29	50.4	1.73	25.3
4	-	73.3	-	39.9	-	142.2
5	1.60	33.8	1.26	30.8	2.03	24.8
5'	1.60	33.8	1.26	30.8	5.24	114.5
6,6'	0.33	-1.0	0.53	0.7	0.25	-1.3
CO	-	200.7	-	200.6	-	200.9

In seeking a precedent for such an allyl transfer mechanism, we note that Schreiber used a cobalt-stabilized cation (Scheme 4-6) to induce cyclization and subsequent loss of the silyl fragment.[89] In contrast, in the current work, the silicon is a component of the cyclic cation and so is retained in the final structure.

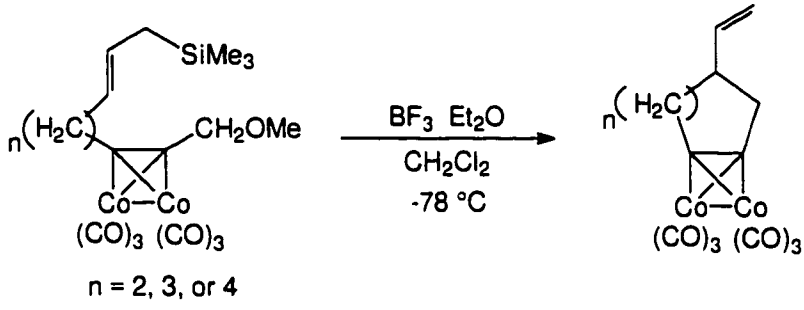

Scheme 4-6: Summary of Schreiber's cyclization reaction.

4.4. Compounds Containing Potential Silylium and Carbocationic Centers α to Dimetallic Clusters.

Thus far, the precursors that have been synthesized have all been homo-dimetallic cluster compounds, however, the preparation of mixed metal clusters would also be interesting. The introduction of a second metal might help in selectively stabilizing the silicon cation if formed as seen in section 1.2.2, for carbocations. The preparation of an iron-cobalt cluster is easily achieved by the dehydroxylation of **67** with iron pentacarbonyl. The concept of isolobality, whereby chemically different molecular fragments possess frontier orbitals of similar symmetry, energy, extension in space, and electron occupancy, has provided a simple theoretical framework with which to rationalize

much of cluster chemistry.[90] Isolobal substitution of a $Co(CO)_3^+$ vertex by an $Fe(CO)_3$ group should, in principle, yield a neutral cluster with the same electron count and, presumably, a similar structure. Indeed, EHMO calculations on the $(HC{\equiv}C\text{-}CH_2)FeCo(CO)_6$ cluster favor a structure in which the methylene moiety leans towards the $Fe(CO)_3$ vertex such that it makes an angle Θ of $\approx 55°$ (see Figure 4-6). Very recently, this proposal has received experimental support and the cluster $(MeC{\equiv}C\text{-}CH_2)FeCo(CO)_5PPh_3$ has been crystallographically characterized.[40]

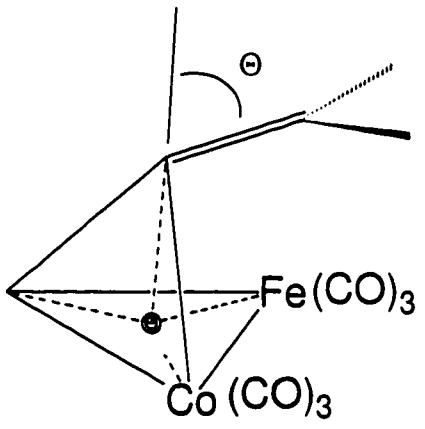

Figure 4-6: Coordinate system in iron-cobalt cluster.

The reaction of **67** with iron pentacarbonyl in acetone under reflux gave the corresponding iron-cobalt cluster **71** which was fully characterized by NMR and mass spectrometry. Interestingly, the addition of HBF_4 to **71** gave the fluorosilyl compound, **72**, which was characterized by ^{29}Si NMR spectroscopy, as well as by X-ray crystallography. Figure 4-7 shows the X-ray crystal structure of **72** and confirms its identity as a vinylidene complex.

The most relevant feature of the structure is the bending of the $C{=}CMe_2$ moiety towards the iron vertex, the $Fe{\bullet\bullet}CMe_2$ distance of 2.335 Å reflects its character as a model for a tertiary carbocation stabilized by an organometallic unit. In other iron-cobalt cluster systems that we have characterized, the Fe••C distances range from 2.29 Å for CH_2 groups to 2.7 Å for "tertiary cations" of the CR_2 type.[91] This pattern follows that established for the molybdenum-stabilized system $[Cp_2Mo_2(CO)_4(HC{\equiv}C\text{-}CR_2)]^+$ whereby the Mo••C distances range from 2.44 Å in primary cations ($Mo{\bullet\bullet}CH_2$), to 2.61 Å in secondary cations (Mo••CHR), and to 2.75 in tertiary cations ($Mo{\bullet\bullet}CR_2$).

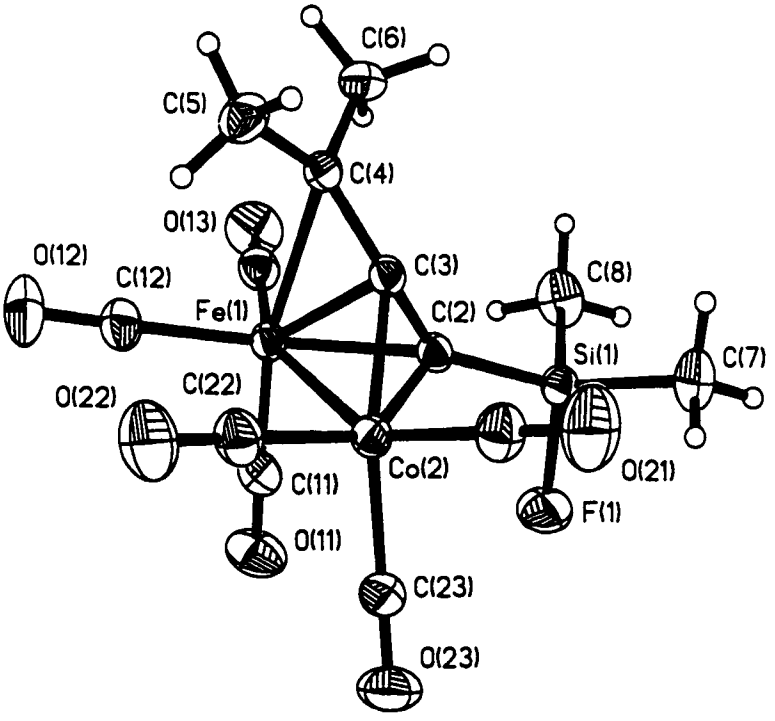

Figure 4-7: X-ray crystal structure of **72**, showing 30% thermal probability ellipsoids. *Salient bond lengths(Å)*: Fe(1)-Co(2) 2.5494(7), Co(2)-C(2) 2.015(3), Co(2)-C(3) 1.937(4), Fe(1)-C(2) 2.012(3), Fe(1)-C(3) 1.997(3), Fe(1)-C(4) 2.335(3), Si(1)-F(1) 1.601(3).

In an attempt to generate a metal-stabilized silicon cation, **71** was treated with $Ph_3C^+PF_6^-$, with the intention that the allyl would be removed by the triphenylmethyl cation. The only product observed in the reaction between **71** and triphenylmethyl hexafluorophosphate, as monitored by ^{29}Si-NMR, is the siloxane derivative of **73**. This may be rationalized as the trityl-initiated loss of the allyl group with concomitant formation of the fluoride **72**; subsequent hydrolysis during work up yielded the siloxane (see Scheme 4-7).

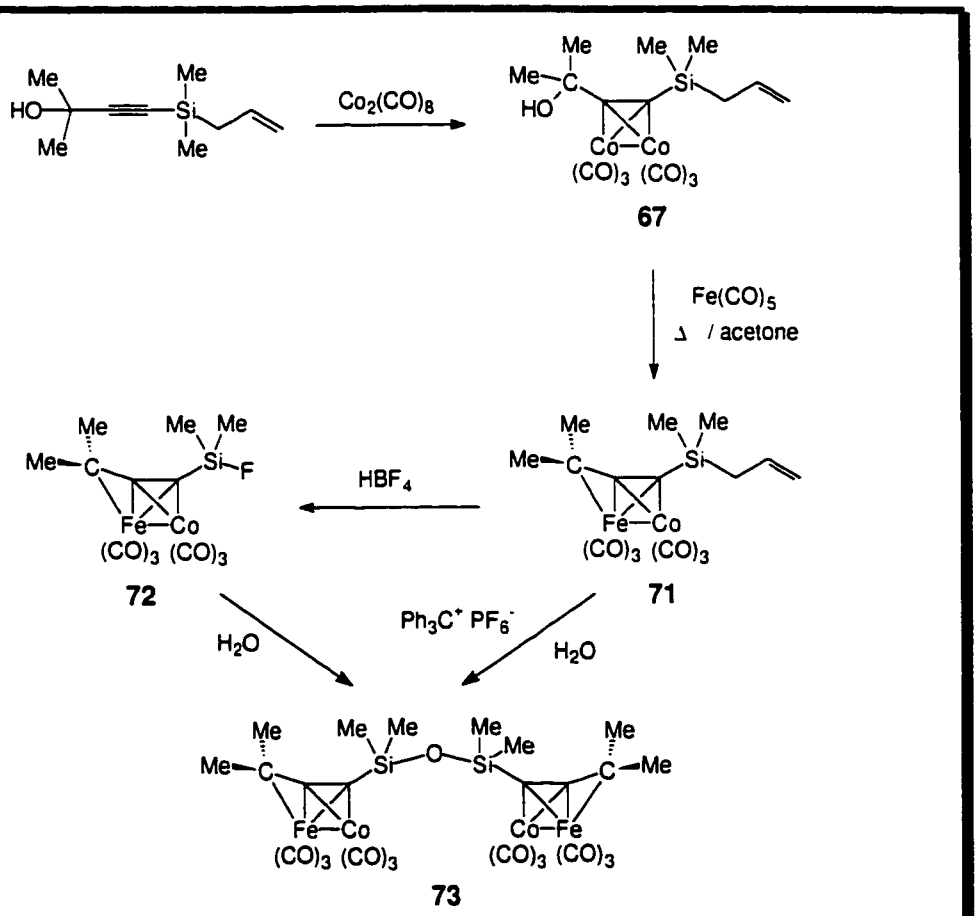

Scheme 4-7: Some chemistry of the iron-cobalt cluster, **71**.

4.5. Summary

It is evident from our results that HBF_4 reacts with allylsilanes, such as **62** and **71**, to give fluorosilanes. However, when an additional site for protonation is present, such as an alcohol or a site of unsaturation at the other terminus of the cluster, a different reaction pathway is seen. Protonation occurs to generate a metal-stabilized carbocation. The allyl group at the other terminus of the molecule behaves as the electrophile and adds to the cationic center at the γ-carbon generating a 7-membered ring with a β-silyl-stabilized cation. Fluoride can now attack at the silicon center and regenerate a new double bond; essentially, the allyl has migrated from the silicon atom to the carbon atom at the other terminus. (see Scheme 4-6).

5. FUTURE WORK.

5.1. Metal-Stabilized Silicon Cations: The Ongoing Challenge.

It has been clearly demonstrated that protonation at the methylene terminus of an alkynylallylsilane (free or metal complexed alkyne) with either HBF_4 or triflic acid readily occurs with elimination of propene and formation of the corresponding silyl fluoride or triflate. There is, as yet, no evidence of an isolable metal-stabilized silyl cationic intermediate. It is evident that these electrophilic attacks on the allyl-silanes must avoid the use of any counter-ions that could form covalent bonds with silicon.

We note that, in the recent report of Lambert and co-workers, the use of a least-coordinating anion does allow the preparation of a silylium salt **74** in solution by this procedure (see Scheme 5-1).[92]

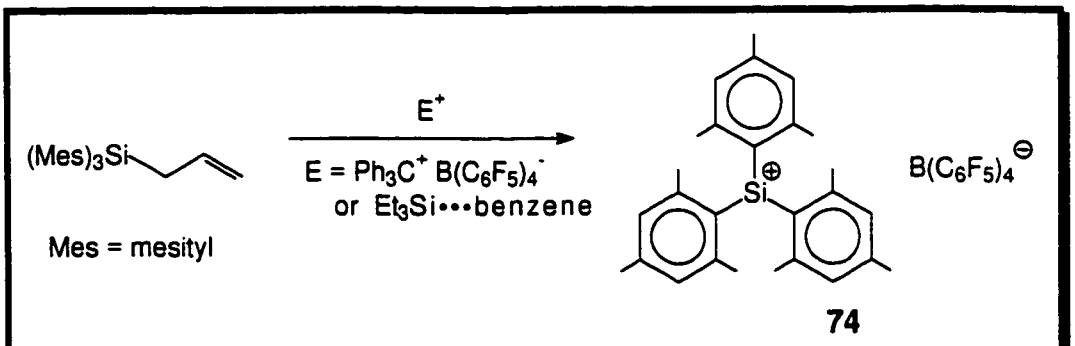

Scheme 5-1: Recent reports of $(Mes)_3Si^+$, by Lambert and co-workers.

It is clear that the next logical approach is to use electrophilic conditions to remove an allyl group in the appropriate alkynylallylsilane precursors. The use of triphenylmethyl perfluorinated tetraphenylborate as the electrophile to remove an allyl group from the appropriate precursor should lead to isolable metal-stabilized silicon cations (see Scheme 5-2).

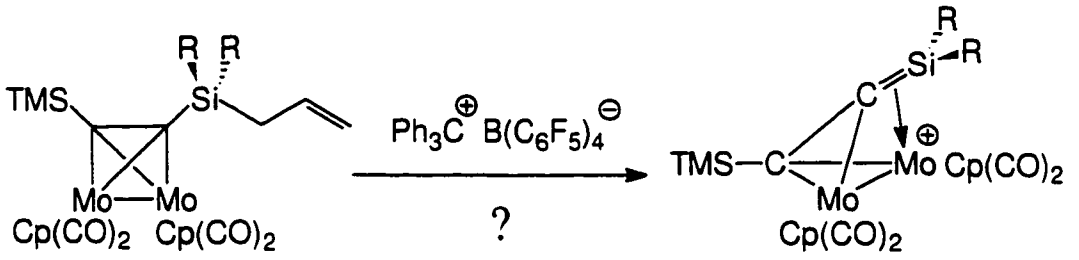

Scheme 5-2: Possiblity of deallylation of percursor with a least-coordinating anion?

5.2. Possible Isolobal Substitution.

The ideas promulgated by Wade, Mingos and Rudolph have allowed a convenient classification of structural types, and have demonstrated the relationships between molecular geometries and skeletal electron counts in clusters.[19, 20, 93] Nevertheless, isolobal substitution in a dicobalt cluster of a $Co(CO)_3^+$ vertex by an $Fe(CO)_3$ group should, in principle, yield a neutral cluster with the same electron count and, presumably, a similar structure to propargyl-dicobalt cations. Indeed, EHMO calculations on the $(HC{\equiv}C\text{-}CH_2)FeCo(CO)_6$ cluster favor a structure in which the methylene moiety leans towards the

$Fe(CO)_3$ vertex such that it makes an angle θ of 55° which is similar to that of **72**. The question that arises is "How general is the approach?"

The reaction of precursor compounds (which have silylalkoxy or silanol groups α to dicobalt clusters) with iron pentacarbonyl may lead to isolable products which will be structural models of silylium ions stabilized by dimetallic clusters (see Scheme 5-3).

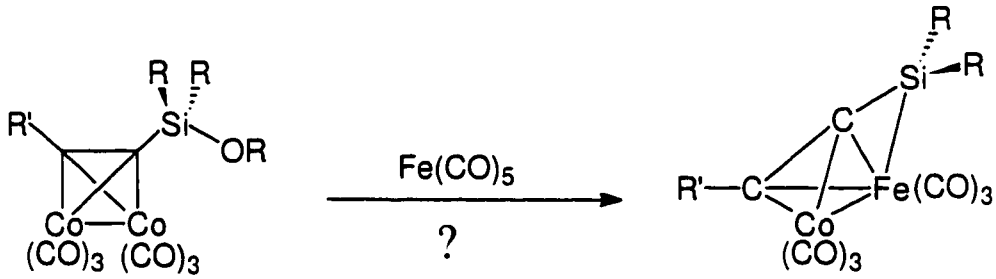

R = H or alkyl

Scheme 5-3: Isolobal substitution of $Co(CO)_3^+$ for $Fe(CO)_3$.

5.3. Allyl Transfer via 7-membered Ring.

We would like to trap the seven-membered ring intermediate in the allyl transfer reaction, described in section 4.3, so as to clarify the mechanism of this reaction. One method that would be used is to attempt to stabilize the cation that is being formed by simple alkyl group substitution at the β-allylic carbon.[94] A more interesting group to substitute at the β-allylic carbon would be a trimethylsilylmethyl group ($-CH_2SiMe_3$). The reaction of this compound with HBF_4 should generate a metal-stabilized carbocation, which is not only a stable tertiary cation but is also stabilized by two β silicon atoms. At this point either of two pathways could viably be followed: nucleophilic addition at

silicon, or elimination *via* three pathways. The cation center can eliminate by one of three ways to give different three products, or fluoride can attack to generate a product similar to **68**, namely **75**. Elimination can occur to give two structural isomers, **76** and **77**. The last and most interesting pathway is elimination to generate an exocyclic double bond with extrusion of fluorosilane, **78**, as seen Scheme 5-4, in a fashion similar to Schrieber's report. Hopefully, this simple experiment will provide some insight to the mechanism of the reaction, and the possible existence of the seven-membered ring intermediate.

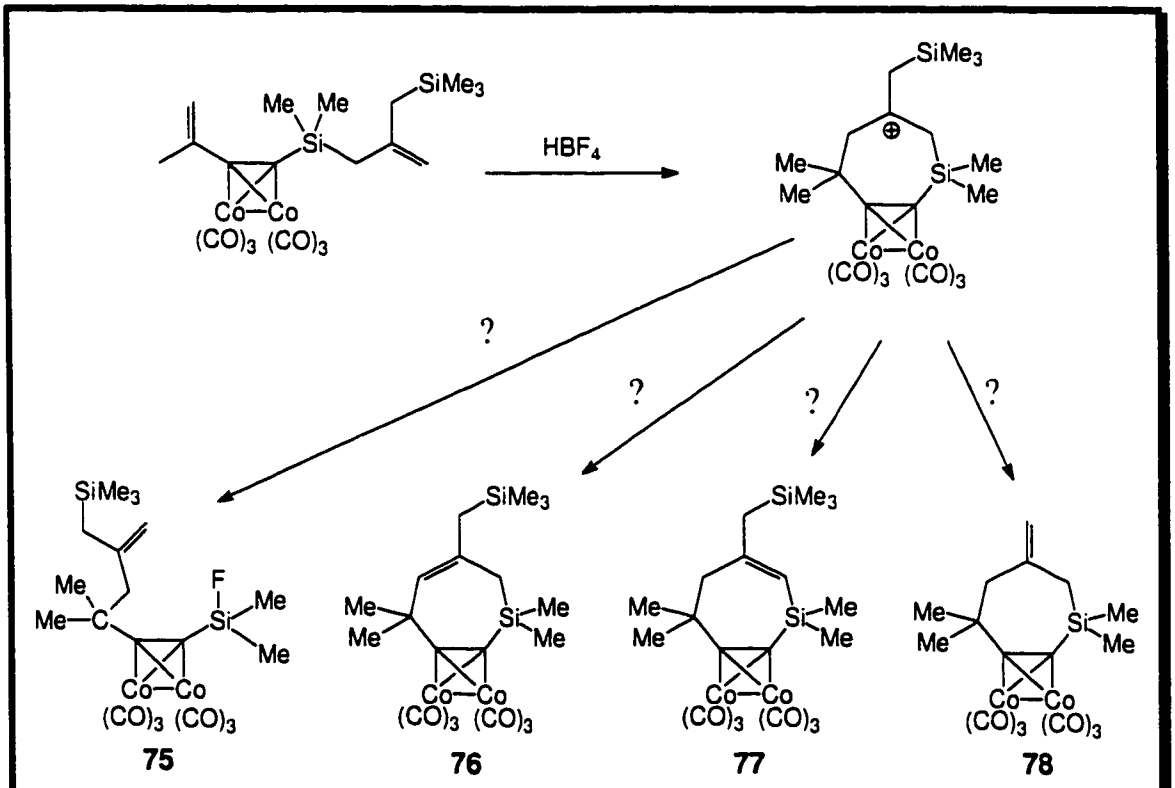

Scheme 5-4: Attempts to stabilize 7-memebered ring intermediate.

5.4. General Conclusions

We have presented evidence from molecular orbital calculations at the extended Hückel level that a silylium ion would be stabilized by interaction with a metal fragment; in this respect, a $(C_5H_5)Mo(CO)_2$ moiety is shown to be better able to alleviate the electron deficiency at silicon than is a $Co(CO)_3$ fragment.

Indeed, the X-ray crystal structure of TMS-C≡C-$Si(CH_3)_2(CH_2CH{=}CH_2)$ $[Mo_2(CO)_4Cp_2]$, **26**, suggests that steric hindrance precludes the approach of the bulky trityl cation to the Si-H bond in the attempted removal of hydride. It has been shown that the use of an allyl group is a viable approach to silicon cations, as corroborated by the recent reports of Lambert. In our studies, protonation of an alkynylallylsilane (free or metal complexed alkyne) with either HBF_4 or triflic acid readily occurs with elimination of propene and formation of the corresponding silyl fluoride or triflate. It is evident that these electrophilic attacks on the allyl-silanes must avoid the use of any counter-ions that could form covalent bonds with silicon.

When an additional site for protonation is present, such as an alcohol or a site of unsaturation at the other terminus of the cluster, the reaction seem to be selective and generates a metal-stabilized carbocation. The allyl group subsequently adds to the cationic center presumably *via* a 7-membered ring with a β-silyl-stabilized cation. Nucleophilic attack now occurs at the silicon center to generate a new double bond; essentially, the allyl group has migrated from the silicon atom to the carbon atom at the other terminus. (see Scheme 4-6).

6. EXPERIMENTAL

6.1. General Procedures

All syntheses were carried out under a dry nitrogen atmosphere utilizing conventional benchtop and glovebag techniques. Solvents were dried and distilled according to standard procedures.[95] $Mo_2Cp_2(CO)_4$ was prepared according to standard procedures.[96] Melting points were measured in open glass capillaries using a Thomas Hoover Unimelt capillary melting point apparatus. The melting points were not corrected. All glassware was flame dried prior to use.

6.2. NMR Spectra

All NMR spectra were recorded on a Bruker DRX-500, AC-300, or AC-200 NMR spectrometer.

Spectra used for characterization of molecules were recorded on a Bruker Avance DRX-500 spectrometer, with an 11.74 T superconducting magnet. These experiments included 1-D ^{1}H, ^{13}C and ^{29}Si NMR spectra as well as 2-D ^{1}H-^{1}H COSY, ^{1}H-^{13}C shift-correlated and long range ^{1}H-^{13}C shift-correlated spectra.

Following protonation of all organometallic complexes, spectra were acquired on the DRX-500 or AC-300.

The sample temperature was maintained by a Bruker Eurotherm variable temperature unit. Spectra were recorded on spinning samples (except during the acquisition of 2-D spectra), locked to a solvent signal. Peaks were referenced to a residual proton signal of the solvent, or to a ^{13}C solvent signal. Each temperature was

measured by placing a copper-constantan thermocouple, contained in an NMR tube, into the probe.

Proton spectra were acquired at 500.130 MHz with the use of a 5 mm broadband inverse probe with triple axis gradient capability. Typically, spectra were obtained with 8 scans in 32K data points over a 3.931 KHz spectral width (4.168 s acquisition time). The free induction decay (FID) was processed using exponential multiplication (line broadening: 0.15 Hz) and was zero-filled to 64K before Fourier transformation. Carbon-13 NMR spectra were recorded at 125.758 MHz using the 5 mm broadband inverse probe with triple axis gradient capability. The spectra were acquired over a 28.986 kHz spectral width in 32K data points (0.557 s acquisition time). The ^{13}C 90° pulse width was 4.4 μs (31° flip angle). Typically, relaxation delays of 1.0 s were used. The FIDs were processed using exponential multiplication (line broadening: 4.0 Hz) and zero-filled to 64K before Fourier transformation. ^{29}Si NMR spectra were acquired at 99.354 MHz.

Proton COSY 2-D NMR spectra were recorded in the absolute value mode using the pulse sequence: 90° - t_1 - 45° - ACQ and including pulsed field gradients for coherence selection. Typically, spectra were acquired in 2 scans for each of the 256 FIDs that contained 2K data points in F2 over a spectral width of 3930.82 Hz. The 90° ^1H pulse width was 6.6 μs. A 1.0 s relaxation delay was employed between acquisitions. Zero-filling in F1 produced a 1K x 1K data matrix with digital resolution of 3.84 Hz/point in both dimensions. During 2-D Fourier transformation a sine-bell squared window function was applied to both dimensions.

Inverse detected ^1H-^{13}C 2-D chemical shift correlation spectra were acquired in the phase sensitive mode using the pulsed field gradient version of the HSQC pulse sequence. Typically, the FIDs in the F2 (^1H) dimension were recorded over a 3.655 KHz spectral width in 1K data points. The 128 FIDs in the F1 (^{13}C) dimension were obtained

over a 21.368 kHz spectral width. Each FID was acquired in 2 scans. The fixed delays during the pulse sequence were a 1.0 s relaxation delay and a polarization transfer delay of 0.00178 s (corresponding to ¼[$^1J_{CH}$] = 140 Hz). The 90° ^{1}H pulse was 6.6 μs while the ^{13}C 90° pulse was also 11.6 μs. The data were processed using a sine-bell squared window function shifted by π/2 in both dimensions and linear prediction to 256 data points in F1 followed by zero-filling to 1K.

Inverse detected ^{1}H-^{13}C 2-D chemical shift correlation spectra through two- and three-bond coupling interactions were acquired in the absolute value mode using the pulsed field gradient version of the HMBC pulse sequence. Typically, the FIDs in the F2 (^{1}H) dimension were recorded over a 3.6558 KHz spectral width in 1K data points. The 128 FIDs in the F1 (^{13}C) dimension were obtained over a 21.368 KHz spectral width. Each FID was acquired in 2 scans. The fixed delays during the pulse sequence were a 1.0 s relaxation delay, a 0.0033 s delay for the low pass J-filter and 0.08 s delay to allow evolution of the long-range coupling. The 90° ^{1}H pulse was 6.6 μs while the ^{13}C 90° pulse was also 11.6 μs. The data were processed using a sine-bell squared window function shifted by π/2 in both dimensions and linear prediction to 256 data points in F1 followed by zero-filling to 1K.

Proton spectra which were acquired at 300.135 MHz with the use of a 5 mm QNP probe. Carbon-13 spectra were recorded at 75.469 MHz using the same probe. Proton spectra which were acquired at 200.135 MHz using a 5 mm QNP probe. Carbon-13 spectra were recorded at 50.033 MHz using the same probe.

6.3. Mass Spectra

Mass spectra were obtained on a VG Analytical ZAB-SE spectrometer with an accelerating potential of 8kV and a resolving power of 10,000.

6.4. IR Spectra

All infrared spectra were obtained on a Bio Rad FTS-40 FT-IR spectrometer and a SPC 3200 work station using NaCl 0.1 mm solution cells.

6.5. Microanalyses

Microanalyses were performed by Guelph Chemical Laboratories in Guelph, Ontario

6.6. X-ray Crystallography

X-ray crystallographic data for **26**, **32** and **43** were collected from single crystals which were mounted on a glass fibre and transferred to a P4 Siemens diffractometer, equipped with a rotating anode and graphite-monochromated Mo-Kα radiation (λ = 0.71073 Å). X-ray crystallographic data for **45** were collected from a single crystals which was mounted on a glass fibre and transferred to a P3 Siemens diffractometer, using an graphite-monochromated Ag-Kα radiation (λ = 0.56086 Å). Three standard reflections, that were measured after every 97 reflections, showed neither instrument instability nor crystal decay. Data were corrected for absorption using an empirical Ψ-scan method. The structures were solved by using the direct methods procedure in the Siemens SHELXTL program library,[97] and refined by full-matrix least-squares methods

with anisotropic thermal parameters for all non-hydrogen atoms except for the C(1) of structure **45** which was left isotropic.

X-ray crystallographic data for **72** were collected from a single crystal sample, which was mounted in a 0.2 mm sealed glass capillary. Data were collected using a P4 Siemens diffractometer, equipped with a Siemens SMART 1K Charge-Coupled Device (CCD) Area Detector (using the program SMART)[98] and a rotating anode using graphite-monochromated Mo-Kα radiation (λ = 0.71073 Å). The crystal-to-detector distance was 3.991 cm, and the data collection was carried out in 512 x 512 pixel mode, utilizing 2 x 2 pixel binning. The initial unit cell parameters were determined by a least-squares fit of the angular settings of the strong reflections, collected by a 4.5 degree scan in 15 frames over three different parts of reciprocal space (45 frames total). One complete hemisphere of data was collected, to better than 0.8 Å resolution. Upon completion of the data collection, the first 50 frames were recollected in order to improve the decay corrections analysis (if required). Processing was carried out by use of the program SAINT,[99] which applied Lorentz and polarization corrections to three-dimensionally integrated diffraction spots. The program SADABS[100] was utilized for the scaling of diffraction data, the application of a decay correction, and an empirical absorption correction based on redundant reflections. The structure was solved by using the direct methods procedure in the Siemens SHELXTL program library,[97] and refined by full-matrix least squares methods with anisotropic thermal parameters for all non-hydrogen atoms.

For **43**, the final refined structure was based on a disordered model in which the allyl could exist in one of two conformations. Based on the observed thermal

displacement ellipsoids, it was assumed that only the positions of the β carbon atoms of the ring were significantly affected by this disorder. The occupancy of the two conformations was allowed to refine as a free variable (the final ratio of approximately 71:29), and then hydrogen atoms for each unique component of the disorder were placed in calculated positions and allowed to refine based on the carbon atom to which they were attached.

Tables listing bond lengths, bond angles, positional parameters, and displacement coefficents for structures **26**, **32**, **43**, **45**, and **72**, can be located in Table 2 through Table 24.

6.7. Molecular Orbital Calculations

Molecular orbital calculations were performed *via* the extended Hückel method using H_{ij}'s,[101] orbital drawings were obtained by use of the program CACAO.[102]

6.8. Compound Preparation and Spectra Data

$Me_3SiC{\equiv}C\text{-}SiMe_2H$.

To a 250 mL round bottom flask containing a solution of trimethylsilylethyne (2.5 mL, 1.74 g, 17.72 mmol) in THF (30 mL) was added n-butyllithium (11.08 mL of a 1.6 M hexane solution, 17.72 mmol) dropwise at -78 °C *via* a syringe over a 30 minute period, and the solution was then allowed to warm to room temperature. After stirring for 2 h the solution was cooled to -78 °C and dimethylchlorosilane (2.3 mL, 1.94g, 17.72 mmol) in THF (5 mL) was added dropwise. The solution was allowed to warm to room

temperature and stirred for 24 h. The desired product was extracted by using a buffer solution ($NaH_2PO_4/KHPO_4$) of pH 6.8. After removal of hexane, the organic phase yielded $Me_3SiC{\equiv}C\text{-}SiMe_2H$ (2.66 g, 17.0 mmol; 96%) as an oil. ^1H NMR ($CDCl_3$, 200.13 MHz) δ 4.10 (septet, $^2J_{SiH}$ = 5.4 Hz, 1H, Si-H), 0.20 (d, $^2J_{Si\text{-}H}$ = 5.4 Hz, 6H, $SiMe_2$), 0.14 (s, 9H, Me_3Si); ^{13}C NMR ($CDCl_3$, 50.03 MHz) δ 115.8, 110.5 (C≡C), -0.2 (Me_3Si), -3.1 ($SiMe_2$); ^{29}Si-NMR (CH_2Cl_2, 59.63 MHz) δ -39.1 (doublet of septets, $^1J_{Si\text{-}H}$ = 200 Hz, Me_2SiH), -18.9 (decet, $^2J_{Si\text{-}H}$ = 6.7 Hz, Me_3Si). IR (neat liquid) ν_{SiH} at 2134 cm^{-1}. Mass spectrum: (DEI, m/z (%)): 156 (20) $[M]^+$, 141 (30) $[M\text{-}CH_3]^+$, 73 (100) $[Si(CH_3)_3]^+$.

$(Me_3SiC{\equiv}C\text{-}SiMe_2[Co_2(CO)_6])_2O$, (32).

To a 250 mL round bottom flask was transferred dicobalt octacarbonyl (3.40g, 10 mmol) under dry nitrogen which has been dissolved in THF (30 mL). A solution of $Me_3SiC{\equiv}C\text{-}SiMe_2H$ (1.56 mL, 1.08g, 10 mmol) in THF (30 mL) was next added dropwise over a 30 minute period. The solution was allowed to stir for 24 h at room temperature. After removal of solvent *in vacuo*, the residue was subjected to flash chromatography on silica gel. Elution with hexane gave dark red crystals of 32 (7.18 g, 8 mmol; 80%). ^1H NMR (CD_2Cl_2, 200.13 MHz) δ 0.38 (s, 6H, $SiMe_2$), 0.30 (s, 9H, Me_3Si); ^{13}C NMR (CD_2Cl_2, 125.03 MHz) δ 202.9 (Co-CO's), 93.2, 91.0 (*cluster* C's), 3.8 (Me_3Si), 1.9 (Me_2Si); ^{29}Si NMR (CH_2Cl_2, 59.63 MHz) δ -3.1 (septet, $^2J_{Si\text{-}H}$ = 6.8 Hz, Me_2Si), 0.79 (decet, $^2J_{Si\text{-}H}$ = 6.7 Hz, Me_3Si). IR (hexane) ν_{CO} at 2087, 2049, 2020 cm^{-1}. Mass spectrum: (DEI, m/z (%)): 814 (35) $[M\text{-}3(CO)]^+$, 758 (30) $[M\text{-}5(CO)]^+$, 702 (68) $[M\text{-}6(CO)]^+$, 674 (100) $[M\text{-}8(CO)]^+$, 646 (20) $[M\text{-}9(CO)]^+$, 618 (20) $[M\text{-}10(CO)]^+$.

$Me_3SiC{\equiv}C\text{-}SiPh_2H$.

Analogous to the synthesis of $Me_3SiC{\equiv}C\text{-}SiMe_2H$, trimethylsilylethyne (1.74 g, 2.5 mL, 17.72 mmol) in THF (30 mL), n-butyllithium (11.08 mL 1.6 M solution in hexane, 17.72 mmol) and diphenylchlorosilane (3.86 g, 17.72 mmol) in THF (5 mL) gave $Me_3SiC{\equiv}C\text{-}SiPh_2H$ (3.97 g, 14.18 mmol; 80 %). ^1H NMR (CD_2Cl_2, 200.13 MHz) δ 7.85 (m, 4H, aromatic), 7.58 (m, 6H, aromatic), 0.43 (s, 3H, Me_3Si); ^{13}C NMR (CD_2Cl_2, 50.03 MHz) δ 135.5, 128.6, (*meta and ortho C's*), 132.4 (*ipso*), 130.6 (*para*), 120.4, 106.2 (C≡C), -0.2 (Me_3Si); ^{29}Si NMR (CH_2Cl_2, 59.63 MHz) δ -42.1 (decet , $^1J_{Si\text{-}H}$ = 212 Hz, $SiPh_2H$), -18.7 ppm (doublet, $^2J_{Si\text{-}H}$ = 6.4 Hz, Me_3Si). IR (THF): ν_{SiH} at 2143 cm^{-1}.

$(Me_3SiC{\equiv}C\text{-}SiPh_2H)[Co_2(CO)_6]$, (25).

Analogous to the synthesis of **32**, $Me_3SiC{\equiv}C\text{-}SiPh_2H$ (0.475 g, 1.70 mmol) and dicobalt octacarbonyl (580 mg, 1.70 mmol) gave a mixture which was subjected to flash chromatography on silica gel using hexane as solvent. The first red-brown band was collected and the solvent removed by rotary evaporation to yielded **25** (0.796 g, 1.41 mmol; 83%). ^1H NMR (CD_2Cl_2, 200.13 MHz) δ 7.45 (m, 4H, aromatic), 7.14 (m, 6H, aromatic), 0.30 (s, 9H, Me_3Si); ^{13}C NMR (CD_2Cl_2, 50.03 MHz) δ 200.6 (Co CO's), 135.3, 128.5 (*meta and ortho C's*), 134.5 (*ipso*), 130.6 (*para*), 1.1 (Me_3Si); ^{29}Si NMR (CH_2Cl_2, 59.63) δ -17.9 (doublet, $^1J_{Si\text{-}H}$ = 252 Hz, Ph_2Si), 2.5 (decet, $^2J_{Si\text{-}H}$ = 6.7 Hz, Me_3Si). IR (hexane) : ν_{CO} at 2020, 2050, 2087 cm^{-1}; ν_{SiH} at 2145 cm^{-1}. Mass Spectrum (DEI, m/z (%)): 482 (5) $[M\text{-}3(CO)]^+$, 454 (35) $[M\text{-}4(CO)]^+$, 426 (80) $[M\text{-}5(CO)]^+$, 398 (100) $[M\text{-}6(CO)]^+$.

($Me_3SiC{\equiv}C\text{-}SiPh_2H$)[$Mo_2(CO)_4(C_5H_5)_2$], (26).

To a freshly prepared solution of $(C_5H_5)_2(CO)_4Mo_2$ (4.40g, 11 mmol) was added $Me_3SiC{\equiv}C\text{-}SiPh_2H$ (1.40 g, 10 mmol) in dry THF (30 mL) dropwise *via* a cannula over 45 min. The solution was allowed to stir at room temperature for 24 h. After removal of the solvent, the residue was recrystallized from THF/hexane (2:1) to yield red crystals of **26**, (5.57 g, 7.8 mmol; 78%). ^1H NMR (CD_2Cl_2, 200.13 MHz) δ 7.25 (m, 10H, aromatic), 4.78 (s, 11H, Cp-H's and Si-H), 0.07 (s, 9H, Me_3Si); ^{13}C NMR (CD_2Cl_2, 50.03 MHz) δ 229.0 (Mo-CO's), 137.2 (*ipso*), 135.7, 128.1 (*meta and ortho C's*), 129.9 (*para*), 90.2 (Cp-C's), 3.5 (Me_3Si); ^{29}Si NMR (CH_2Cl_2, 59.63 MHz) δ 6.6 (decet, Me_3Si), -10.8 (doublet, $^1J_{Si\text{-}H}$ = 211 Hz, $SiPh_2H$). IR (hexane) : ν_{CO} at 1883, 1950, 1981 cm^{-1}; ν_{SiH} at 2171 cm^{-1}.

$Me_3SiC{\equiv}C\text{-}SiMe_2$(allyl), (39)

Analogous to the synthesis of $Me_3SiC{\equiv}C\text{-}SiMe_2H$, trimethylsilylethyne (25g, 0.25 mol) in THF (100 mL), n-butyllithium (96 mL, 2.5 M in hexane, 0.25 mol) and allyldimethylchlorosilane (36 mL, 0.25 mol) in THF (10 mL) gave **39** as a clear oil (44.8g, 0.24 mol; 96%). ^1H NMR ($CDCl_3$, 500.13 MHz) δ 5.77 (m, 1H, $CH_2{=}CHCH_2$), 4.89 (m, 2H, $CH_2{=}CHCH_2$), 1.60 (m, 2H, $CH_2{=}CHCH_2$), 0.14 (s, 6H, $Si(CH_3)_2$), 0.12 (s, 9H, $Si(CH_3)_3$); ^{13}C NMR ($CDCl_3$, 125.03 MHz) δ 133.8 ($CH_2{=}CHCH_2$), 114.8 ($CH_2{=}CHCH_2$), 113.9, 112.0 ($C{\equiv}C$), 24.0 ($CH_2{=}CHCH_2$), -0.1 ($SiMe_2$), -2.3 ($SiMe_3$); ^{29}Si NMR (CH_2Cl_2, 99.36 MHz) δ -19.0, -19.2. Mass spectrum (DEI, m/z (%)): 181 (76) $[M\text{-}CH_3]^+$, 166 (87) $[M\text{-}2xCH_3]^+$, 155 (100) $[M\text{-}CH_2{=}CHCH_2]^+$, 73 (65) $[TMS]^+$;

(CI, NH_3, *m/z* (%)): 214 (78) $[M]^+$, 197 (41) $[M+1]^+$; (high resolution, DEI): calculated mass for $^{12}C_9H_{17}Si_2$ $[M-Me]^+$, 181.0869, observed, 181.0866 amu. Combustion analysis: calculated for $C_{10}H_{20}Si_2$: C 61.14, H 10.26 observed: C 61.40; H 10.95.

(allyl)Me_2Si-C≡C-SiMe_2(allyl), (40)

n-Butyllithium (99.5 mL of 1.6 M in hexane) was added dropwise to a solution of to dichloroethylene (6.9 g, 0.053 mol) in diethyl ether (30 mL) at -78 °C *via* cannula over a 30 min period. After stirring for 2 h, the solution was cooled to -78 °C and allyldimethylchlorosilane (16.6 mL, 14.8 g, 0.12 mol) in diethyl ether (5 mL) was added dropwise; the solution was allowed to warm to room temperature and stirred for 24 h. The product was extracted with water. After removal of volatile components by rotary evaporation, the organic phase yielded **40** (10.0 g, 0.0451 moles, 85%) as an oil. ^1H NMR ($CDCl_3$, 300.13 MHz) δ 5.75 (m, 1H, CH_2=C*H*CH_2), 4.84 (m, 2H, C*H*$_2$=CHCH_2), 1.59 (m, 2H, CH_2=CHC*H*$_2$), 0.13 (s, 6H, Si(C*H*$_3$)$_2$); ^{13}C NMR ($CDCl_3$, 50.03 MHz) δ 133.6 (*C*H_2=CHCH_2), 113.8 (CH_2=*C*HCH_2), 80.0 (*C*≡*C*), 23.9 (CH_2=CH*C*H_2), -2.4 (Si(*C*H_3)$_2$); ^{29}Si NMR (CH_2Cl_2, 59.63 MHz) δ -19.4. Mass spectrum (DEI, m/z (%)): 207 (16) $[M-CH_3]^+$, 181 (24) $[M-CH_2=CHCH_2]^+$, 99 (14)$[CH_2=CHCH_2SiMe_2]^+$; (CI, NH_3, *m/z* (%)): 240 (19) $[M+18]^+$, 223 (65) $[M+H]^+$; (high resolution, DEI): calculated mass for $^{12}C_{11}H_{19}Si_2$ $[M-Me]^+$, 207.1025, observed, 207.1016 amu.

(allyl)Me_2Si-C≡C-C≡C-SiMe_2(allyl), (41)

Analogous to the synthesis of **40**, hexachlorobutadiene (15.7 g, 61 mmol) in diethyl ether (75 mL), n-butyllithium (152.5 mL, 1.6 M in hexane) and allyldimethylchlorosilane (18

mL, 15.7g, 0.13 mol)) in diethyl ether (10 mL) gave **41** as a clear oil (12.01 g, 0.0488 mol; 80%).[103] ^{1}H NMR ($CDCl_3$, 500.13 MHz) δ 5.75 (m, 1H, CH_2=$CHCH_2$), 4.88 (m, 2H, (CH_2=$CHCH_2$), 1.61 (m, 2H, CH_2=$CHCH_2$), 0.15 (s, 6H, $Si(CH_3)_2$); ^{13}C NMR ($CDCl_3$, 125.03 MHz) δ 133.0 (CH_2=$CHCH_2$), 114.6 (CH_2=$CHCH_2$), 88.8, 84.3 (C≡C), 23.3 (CH_2=$CHCH_2$), -2.8 ($Si(CH_3)_2$); ^{29}Si NMR (CH_2Cl_2, 99.36 MHz) δ -16.5. Mass spectrum (DEI, *m/z* (%)): 231 (17) $[M\text{-}CH_3]^+$, 205 (100) $[M\text{-}CH_2{=}CHCH_2]^+$, 164 (51) [M-2 x ($CH_2$=$CHCH_2$)]$^+$; (CI, NH_3, *m/z* (%)): 264 (100) $[M+18]^+$, 247 (27) $[M+H]^+$; (high resolution, DEI): calculated mass for $^{12}C_{13}H_{19}Si_2$ $[M\text{-}Me]^+$, 231.1025, observed, 231.1023 amu.

(Me_3Si-C≡C$SiMe_2$(allyl))[$Co_2(CO)_6$], (42)

Analogous to the synthesis of **32, 39** (1.33 g, 6.8 mmol) and dicobalt octacarbonyl (2.33 g, 6.8 mmol) yielded **42** as a red oil (2.05 g, 5.8 mmol; 88 %). ^{1}H NMR (CD_2Cl_2, 200.13 MHz) δ 5.88 (m, 1H, CH_2CH=CH_2), 4.98 (m, 2H, CH_2CH=CH_2), 1.84 (m, 2H, CH_2CH=CH_2), 0.36 (s, 9H, $SiMe_3$), 0.37 (s, 6H, $SiMe_2$); ^{13}C NMR (CD_2Cl_2, 50.03 MHz) δ 203.3 (C≡O), 135.9 (CH_2CH=CH_2), 116.4 (CH_2CH=CH_2), 95.4, 92.9 (C≡C), 27.3 (CH_2CH=CH_2), 2.9 ($SiMe_3$), -0.49 ($SiMe_2$(allyl)); ^{29}Si NMR (CH_2Cl_2, 59.63 MHz) δ 0.64 (SiMe$_3$), -0.81 (SiMe$_2$(allyl)). IR (neat) ν_{CO} at 2048 and 2017 cm^{-1}. Mass spectrum (DEI, *m/z* (%)): 426 (40) $[M\text{-}2CO]^+$, 398 (30) $[M\text{-}3CO]^+$, 370 (75) $[M\text{-}4CO]^+$, 342 (70) $[M\text{-}5CO]^+$, 314 (100) $[M\text{-}6CO]^+$. Combustion analysis: calculated for $C_{16}H_{20}Si_2O_6$: C 42.26, H 3.69 observed: C 42.26; H 4.50.

(Me_3Si-C≡C$SiMe_2$(allyl))[$Mo_2(CO)_4Cp_2$], (43).

Analogous to the synthesis of **32, 39** (0.69 g, 3.5 mmol) and $Mo_2Cp_2(CO)_6$ (1.73 g, 3.5 mmol) yielded red powder **43** (1.8 g, 2.8 mmol; 80%). Crystals suitable for X-ray diffraction were grown by slow evaporation from CH_2Cl_2. ^{1}H NMR (CD_2Cl_2, 200.13 MHz) δ 5.78 (m, 1H, CH_2CH=CH_2), 5.19 (s, 10H, Cp-H's), 4.87 (m, 2H, CH_2CH=CH_2), 1.72 (m, 2H, CH_2CH=CH_2), 0.20 (s, 9H, SiMe_3), 0.12 (s, 6H, SiMe_2); ^{13}C NMR (CD_2Cl_2, 50.03 MHz) δ 229.6 (C≡O), 135.8 (CH_2CH=CH_2), 113.5 (CH_2CH=CH_2), 92.7, 92.5 (C≡C), 88.9 (Cp's), 27.3 (CH_2CH=CH_2), 3.5 (SiMe_3), 0.6 (SiMe_2(allyl)); ^{29}Si NMR (CH_2Cl_2, 59.63 MHz) δ -7.1 (SiMe_3), -10.9 (SiMe_2(allyl)). IR (neat) ν_{CO} at 2066 and 1998 cm^{-1}.

(allyl)Me_2 Si-C≡C-$SiMe_2$(allyl))[$Co_2(CO)_6$], (44).

Analogous to the synthesis of **32, 40** (1.11 g, 5.0 mmol) and dicobalt octacarbonyl (1.71 g, 5.0 mmol) yielded **44** as a red oil (2.2 g, 4.4 mmol; 87%). ^{1}H NMR (CD_2Cl_2, 500.13 MHz) δ 5.78 (m, 1H, CH_2CH=CH_2), 4.95 (m, 2H, CH_2CH=CH_2), 1.63 (m, 2H, CH_2CH=CH_2), 0.29 (s, 6H, SiMe_2); ^{13}C NMR (CD_2Cl_2, 75.03 MHz) δ 201.6 (C≡O), 133.6 (CH_2CH=CH_2), 114.6 (CH_2CH=CH_2), 25.2 (CH_2CH=CH_2), -1.0 (SiMe_2); ^{29}Si NMR (CH_2Cl_2, 99.36 MHz) δ -0.8 (SiMe_2). IR (neat) ν_{CO} at 2018, 2046, and 2085 cm^{-1}. Mass spectrum: (DEI, *m/z* (%)): 467 (15) [M-(CH_2CH=CH_2)]$^+$, 424 (60) [M-3(CO)]$^+$, 396 (50) [M - 4(CO)]$^+$, 368 (45) [M - 5(CO)]$^+$, 340 (100) [M - 6(CO)]$^+$.

(allyl)Me_2 Si-C≡C-C≡C-SiMe_2(allyl))[$Co_2(CO)_6]_2$, (45).

Analogous to the synthesis of **32, 41** (1.2 g, 4.9 mmol) and dicobalt octacarbonyl (4.2 g, 12.3 mmol) yielded **45** (2.7 g, 3.3 mmol; 67 %).. Crystals suitable for X-ray diffraction were grown by slow evaporation from hexanes. ^{1}H NMR (CD_2Cl_2, 200.13 MHz) δ 5.87 (m, 1H, CH_2CH=CH_2), 4.93 (m, 2H, CH_2CH=CH_2), 1.91 (m, 2H, CH_2CH=CH_2), 0.32 (s, 6H, $SiMe_2$); ^{13}C NMR (CD_2Cl_2, 50.03 MHz) δ 200.0 (C≡O), 134.0 (CH_2CH=CH_2), 114.7 (CH_2CH=CH_2), 25.0 (CH_2CH=CH_2), -1.4 (SiMe_2(allyl)); ^{29}Si NMR (CH_2Cl_2, 59.63 MHz) δ -0.9. IR (neat) ν_{CO} at 2077, 2057 and 2029 cm^{-1}.

(allyl)Me_2 Si-C≡C-C≡C-SiMe_2(allyl))[$Mo_2(CO)_4Cp_2]_2$, (46).

Analogous to the synthesis of **32, 41** (1.5 g, 6.1 mmol) and $Mo_2Cp_2(CO)_6$ (7.4 g, 15.2 mmol) yielded **46** as a red oil (4.9 g, 4.4 mmol; 72 %). ^{1}H NMR (CD_2Cl_2, 200.13 MHz) δ 5.79 (m, 2H, CH_2CH=CH_2), 5.37 (s, 20H, Cp-H's), 5.00 (m, 4H, CH_2CH=CH_2), 1.69 (s, 2H, CH_2CH=CH_2), 0.14 (s, 12H, SiMe_2); ^{13}C NMR (CD_2Cl_2, 50.03 MHz) δ 135.3 (CH_2CH=CH_2), 113.4 (CH_2CH=CH_2), 92.7 (Cp's), 25.3 (CH_2CH=CH_2), -1.2 (SiMe_2(allyl)); ^{29}Si NMR (CH_2Cl_2, 59.63 MHz) δ -22.2. IR (neat) ν_{CO} at 1998, 1957 and 1935 cm^{-1}.

(allyl)Me_2 Si-C≡C-C≡C-SiMe_2(allyl))[$Co_2(CO)_6$], (47).

Analogous to the synthesis of **32, 41** (1.5 g, 6.1 mmol) and dicobalt octacarbonyl (1.9 g, 5.5 mmol) yielded **47** as a dark red oil (1.81 g, 3.4 mmol; 62 %). ^{1}H NMR (CD_2Cl_2, 200.13 MHz) δ 5.79 (m, 2H, CH_2CH=CH_2), 4.89 (m, 4H, CH_2CH=CH_2), 1.65 (m, 4H, CH_2CH=CH_2), 0.30, 0.19 (s, 12H, SiMe_2). ^{13}C NMR (CD_2Cl_2, 50.03 MHz) δ 199.8

(*C*≡O), 134.3, 133.7 (CH_2*C*H=CH_2), 114.6, 114.0 (CH_2CH=*C*H_2), 103.8, 102.1 (cluster carbons), 89.0, 85.2 (*C*≡*C*), 24.2, 23.7 (*C*H_2CH=CH_2), -1.5, -2.3 (Si*Me*$_2$(allyl)); ^{29}Si NMR (CH_2Cl_2, 59.63 MHz) δ 0.9, -15.4. IR (hexane) ν_{CO} at 2092, 2058 and 2032 cm^{-1}.

$H_3C(CH_2)_3$-C≡C-$SiMe_2CH_2CH$=CH_2, (61)

n-Butyllithium (38.0 mL, 1.6 M in hexane) was added dropwise to a solution of 1-hexyne (7.0 mL, 5.0 g, 0.0609 mol) in diethyl ether (30 mL) at -78 °C *via* syringe over 30 minutes, after which the solution was allowed to warm to room temperature. After stirring for 2 h the solution was cooled to -78 °C and allyldimethylchlorosilane (9.0 mL, 8.30 g, 0.0617 mol) in diethyl ether (15 mL) was added dropwise. The solution was allowed to warm to room temperature and stirred for 24 h. The crude mixture was extracted with water and the separated organic phase was dried over $MgSO_4$. Removal of the solvent and other volatile organic components by rotary evaporation yielded **61** as a clear oil (10.04 g, 0.0554 mol, 91%). ^{1}H NMR ($CDCl_3$, 500.13 MHz) δ 5.79 (m, 1H, CH_2=C*H*CH_2), 4.85 (m, 2H, C*H*$_2$=$CHCH_2$), 2.19 (m, 2H, $H_3C(CH_2)_2$C*H*$_2$-C≡C), 1.57 (m, 2H, C*H*$_2$=$CHCH_2$), 1.47 (m, 2H, H_3CCH_2C*H*$_2CH_2$-C≡C), 1.37 (m, 2H, H_3CC*H*$_2CH_2CH_2$-C≡C), 0.88 (m, 3H, *H*$_3C(CH_2)_3$-C≡C), 0.04 (s, 6H, Si(C*H*$_3)_2$). ^{13}C NMR ($CDCl_3$, 125.03 MHz) δ 134.2 (CH_2=*C*HCH_2), 113.4 (*C*H_2=$CHCH_2$), 108.6, 82.7 (C≡C), 30.7 (H_3CCH_2*C*H_2CH_2-C≡C), 24.2 (CH_2=CH*C*H_2), 21.8 (H_3C*C*$H_2(CH_2)_2$-C≡C), 19.5 ($H_3C(CH_2)_2$*C*H_2-C≡C), 13.5 (H_3*C*$(CH_2)_2$-C≡C), -2.1 (Si(*C*$H_3)_2$). ^{29}Si NMR (CH_2Cl_2, 99.36 MHz) δ -19.3. Mass spectrum (DEI, *m/z* (%)): 180 (60) ([M]$^+$), 165 (100) ([M-

$CH_3]^+$), 139 (100) ([M-$CH_2CH{=}CH_2]^+$); Mass spectrum (high resolution, (DEI)): calculated for mass $^{12}C_{11}H_{20}Si$ ([M]$^+$), 180.1334 amu; observed, 180.1337 amu.

$H_3C(CH_2)_3$-C≡C-$SiMe_2CH_2CH{=}CH_2[Co_2(CO)_6]$, (62)

Analogous to the synthesis of **32, 61** (1.0 g, 5.56 mmol) and dicobalt octacarbonyl (1.90 g, 5.56 mmol) yielded **62** as a dark red oil (2.39 g, 5.12 mmol; 92 %). ^{1}H NMR ($CDCl_3$, 500.13 MHz) δ 5.87 (m, 1H, $CH_2{=}C\mathit{H}CH_2$), 4.94 (m, 2H, $C\mathit{H}_2{=}CHCH_2$), 2.95 (m, 2H, $H_3C(CH_2)_2C\mathit{H}_2$-), 1.80 (m, 2H, $C\mathit{H}_2{=}CHCH_2$), 1.65 (m, 2H, $H_3CCH_2C\mathit{H}_2CH_2$-), 1.49 (m, 2H, $H_3CC\mathit{H}_2CH_2CH_2$-), 0.98 (m, 3H, $\mathit{H}_3C(CH_2)_3$-), 0.31 (s, 6H, $Si(C\mathit{H}_3)_2$). ^{13}C NMR ($CDCl_3$, 125.03 MHz) δ 201.2 (C≡O), 134.4 ($CH_2{=}\mathit{C}HCH_2$), 113.4 ($\mathit{C}H_2{=}CHCH_2$), 77.6 (C≡C), 35.5 ($H_3CCH_2CH_2\mathit{C}H_2$-), 35.2($H_3CCH_2\mathit{C}H_2CH_2$-), 25.3 ($CH_2{=}CH\mathit{C}H_2$), 23.2 ($H_3C\mathit{C}H_2(CH_2)_2$-), 14.0 ($H_3\mathit{C}(CH_2)_2CH_2$-), 13.5 ($H_3\mathit{C}(CH_2)_2$-), -1.2 ($Si(\mathit{C}H_3)_2$). ^{29}Si NMR ($CH_2Cl_2$, 99.36 MHz) δ -0.81. IR (hexane) ν_{CO} at 2087, 2046 and 2019 cm^{-1}. Mass spectrum (DEI, *m/z* (%)): 410 (30) ([M-2CO]$^+$), 382 (28) ([M-3CO]$^+$), 354 (45) ([M-4CO]$^+$), 326 (100) ([M-5CO]$^+$).

$CH_2{=}CHCH_2SiMe_2$-C≡C-$C(CH_3)_2OH$ [104]

n-Butyllithium (125 mL, 1.6 M in hexane) was added dropwise to a solution of 2-methyl-3-butyn-2-ol (10 mL, 8.68 g, 0.10 mol) in diethyl ether/THF (30 mL) at -50 °C *via* syringe over 30 minutes. After stirring for 2 h at -50 °C a solution of allyldimethylchlorosilane (14.6 mL, 13.46 g, 0.10 mol) in diethyl ether (15 mL) was added dropwise. The solution was allowed to warm to room temperature slowly and stirred for 24 h. The crude mixture was extracted with water and the separated organic

phase was dried over $MgSO_4$. Removal of the solvent and other volatile organic components by rotary evaporation yielded CH_2=$CHCH_2SiMe_2$-C≡C-$C(CH_3)_2OH$ as a clear oil (16.7 g, 0.092 mol, 92%). ^1H NMR ($CDCl_3$, 500.13 MHz) δ 5.70 (m, 1H, CH_2=C*H*CH_2), 4.88 (m, 2H, C*H*$_2$=$CHCH_2$), 2.31 (s, 1H, O*H*), 1.62 (m, 2H, CH_2=$CHCH_2$), 1.48 (s, 6H, $HO(CH_3)_2C$), 0.15 (s, 6H, $Si(CH_3)_2$). ^{13}C NMR ($CDCl_3$, 125.03 MHz) δ 134.5 (CH_2=*C*HCH_2), 113.7 (*C*H_2=$CHCH_2$), 112.3, 84.5 (C≡C), 63.0 ($HO(CH_3)_2C$), 31.3 ($HO(CH_3)_2C$), 24.8 (CH_2=$CHCH_2$), -2.3 ($Si(CH_3)_2$). ^{29}Si NMR (CH_2Cl_2, 99.36 MHz) δ -17.9. IR (hexane) ν_{OH} at 3354, $\nu_{C\equiv C}$ at 2170 cm^{-1}. Mass spectrum (DEI, m/z (%)): 165 (15) ($[M\text{-}OH]^+$), 99 (100) ($[CH_2=CHCH_2Si(CH_3)_2]^+$); (CI, m/z (%)): 200 (30) ($[M\text{-}18]^+$), 182 (100) ($[M]^+$), 165 (35) ($[M\text{-}OH]^+$); Mass spectrum (high resolution, (DEI)): calculated for mass $^{12}C_9H_{15}SiO$ ($[M]^+$), 167.0892 amu; observed, 167.0898 amu.

CH_2=$CHCH_2SiMe_2$-C≡C-$C(CH_3)_2OH$ [$Co_2(CO)_6$], (67)

Analogous to the synthesis of **32,** CH_2=$CHCH_2SiMe_2$-C≡C-$C(CH_3)_2OH$ (1.0 g, 5.56 mmol) and dicobalt octacarbonyl (1.90 g, 5.56 mmol) yielded **67** as a dark red oil (2.39 g, 5.12 mmol; 92 %). ^1H NMR ($CDCl_3$, 500.13 MHz) δ 5.86 (m, 1H, CH_2=C*H*CH_2), 4.96 (m, 2H, C*H*$_2$=$CHCH_2$), 1.83 (m, 2H, CH_2=$CHCH_2$), 1.60 (s, 6H, $C(CH_3)_2OH$), 0.33 (s, 6H, $Si(CH_3)_2$). ^{13}C NMR ($CDCl_3$, 125.03 MHz) δ 200.7 (*C*≡O), 134.4 (CH_2=*C*HCH_2), 114.7 (*C*H_2=$CHCH_2$), 73.3 ($C(CH_3)_2OH$), 33.8 ($C(CH_3)_2OH$), 25.5 (CH_2=$CHCH_2$), -1.0 ($Si(CH_3)_2$). ^{29}Si NMR (CH_2Cl_2, 99.36 MHz) δ -1.1. IR (hexane) ν_{OH} at 3615, ν_{CO} at 2090, 2051 and 2025 cm^{-1}. Mass spectrum (DEI, m/z (%)): 412 (50) ($[M\text{-}2CO]^+$), 384

(70) ([M-3CO]$^+$), 356 (80) ([M-4CO]$^+$), 328 (70) ([M-5CO]$^+$), 300 (100) ([M-4CO]$^+$); (CI, NH_3, *m/z* (%)): 356 (100) ([M-4CO]$^+$), 300 (20) ([M-6CO]$^+$), 182 (80) ([CH_2=$CHCH_2SiMe_2$-C≡C-$C(CH_3)_2OH$]$^+$).

H_2C=CCH_3-C≡C-$SiMe_2CH_2CH$=CH_2, (69)

n-Butyllithium (49.3 mL, 1.6 M in hexane) was added dropwise to a solution of 2-methyl-2-buten-3-yne (7.5 mL, 5.2 g, 78.86 mmol) in diethyl ether (30 mL) at -78 °C *via* syringe over 30 minutes, after which the solution was allowed to warm to room temperature. After stirring for 2 h the solution was cooled to -78 °C and allyldimethylchlorosilane (11.5 mL, 10.6 g , 78.86 mol) in diethyl ether (15 mL) was added dropwise. The solution was allowed to warm to room temperature and stirred for 24 h. The crude mixture was extracted with water and the separated organic phase was dried over $MgSO_4$. Removal of the solvent and other volatile organic components by rotary evaporation yielded **69** as a clear oil (12.1 g, 73.34 mmol, 93%). ^{1}H NMR ($CDCl_3$, 200.13 MHz) δ 5.78 (m, 1H, CH_2=C*H*CH_2), 5.28 (m, 2H, *H*$_2$C=), 4.90 (m, 2H, C*H*$_2$=$CHCH_2$), 1.86 (m, 3H, CH_3), 1.62 (m, 2H, C*H*$_2$=$CHCH_2$), 0.15 (s, 6H, Si(C*H*$_3$)$_2$). ^{13}C NMR ($CDCl_3$, 125.03 MHz) δ 134.0 (CH_2=*C*HCH_2), 126.7 (H_2C=), 123.0 (H_2C=*C*CH_3), 113.8 (*C*H_2=$CHCH_2$), 107.2, 91.31 (C≡C), 23.9 (CH_2=CH*C*H_2), 23.3 (H_3C), -2.3 (Si(*C*H_3)$_2$). ^{29}Si NMR (CH_2Cl_2, 99.36 MHz) δ -18.5. Mass spectrum (DEI, m/z (%)): 164 (10) ([M]$^+$), 149 (20) ([M-CH_3]$^+$), 123 (100) ([M-CH_2CH=CH_2]$^+$); Mass spectrum (CI, m/z (%)): 165 (10) ([M+1]$^+$).

CH_2=CCH_3-C≡C-$Si(Me)_2CH_2CH$=CH_2 [$Co_2(CO)_6$], (70)

Analogous to the synthesis of **32,** CH_2=$CHCH_2SiMe_2$-C≡C-CH_2=CCH_3 (1.0 g, 6.06 mmol), and dicobalt octacarbonyl (2.07 g, 6.06 mmol), yielded **70** as a dark red oil (2.46 g, 5.45 mmol; 90 %). ^{1}H NMR ($CDCl_3$, 200.13 MHz) δ 5.77 (m, 1H, CH_2=C*H*CH_2), 5.24 (m, 2H, *H*$_2$C=CCH_3), 4.86 (m, 2H, C*H*$_2$=$CHCH_2$), 2.03 (m, 3H, H_2C=CC*H*$_3$), 1.73 (m, 2H, CH_2=CHC*H*$_2$) 0.25 (s, 6H, Si(C*H*$_3$)$_2$). ^{13}C NMR ($CDCl_3$, 125.03 MHz) δ 200.9 (*C*≡O), 142.2 (H_2C=*C*CH_3), 134.3 (CH_2=*C*HCH_2), 117.7 (*C*H_2=$CHCH_2$), 114.5 (H_2*C*=CCH_3), 25.3 (CH_2=CH*C*H_2), 24.8 (H_2C=C*C*H_3), -1.3 (Si(*C*H_3)$_2$). ^{29}Si NMR (CH_2Cl_2, 99.36 MHz) δ -0.9. IR (hexane) ν_{CO} at 2088, 2050 and 2021 cm^{-1}. Mass spectrum (DEI, m/z (%)): 394 (60) ([M-(CO)]$^+$), 366 (35) ([M-2(CO)]$^+$), 338 (35) ([M-3(CO)]$^+$), 310 (40) ([M-4(CO)]$^+$), 282 (70) ([M-5(CO)]$^+$), 123 (100) ([CH_2=$CHCH_2SiMe_2$-C≡C]$^+$); (CI, m/z (%)): 451 (30) ([M+1]$^+$).

CH_2=$CHCH_2SiMe_2$-C≡C-$C(CH_3)_2$ [$CoFe(CO)_6$], (71)

A one neck 250 mL round bottom flask fitted with a reflux condenser was charged with **67** (5.0 g, 10.29 mmol), freshly distilled iron pentacarbonyl (10.15 mL, 15.12 g, 77.16 mmol) and acetone (75 mL) and allowed to reflux for 48 hours. Subsequently the solvent was removed from the mixture under vacuum. The mixture was subjected to flash silica gel chromatography with petroleum ether / hexanes solvent (5:1). The first orange band was collected and the solvent removed by rotary evaporation yielding **71** as a orange oil (1.05 g, 2.26 mol, 22%). ^{1}H NMR ($CDCl_3$, 500.13 MHz) δ 5.86 (m, 1H, CH_2=C*H*CH_2), 4.94 (m, 2H, C*H*$_2$=$CHCH_2$), 2.02 (s, 3H, (CH_3)C(C*H*$_3$)OH), 1.88 (s, 3H,

$(CH_3)C(CH_3)OH$), 1.81 (m, 2H, CH_2=$CHCH_2$), 0.37 (s, 3H, $Si(CH_3)$), 0.32 (s, 3H, $Si(CH_3)$). ^{13}C NMR ($CDCl_3$, 125.03 MHz) δ 211.0. (C≡O), 134.3 (CH_2=$CHCH_2$), 114.3 (CH_2=$CHCH_2$), 109.4 (cluster carbons), 34.3 ($C(CH_3)_2OH$), 30.1 ($C(CH_3)_2OH$), 25.5 (CH_2=$CHCH_2$), -0.8 ($Si(CH_3)_2$). ^{29}Si NMR (CH_2Cl_2, 99.36 MHz) δ 1.3. IR (hexane) ν $_{CO}$ at 2088, 2086, 2049, 2020 and 1973 cm^{-1}. Mass spectrum (DEI, m/z (%)): 392 (20) ($[M-2CO]^+$), 364 (15) ($[M-3CO]^+$), 336 (20) ($[M-4CO]^+$), 308 (10) ($[M-5CO]^+$), 280 (100), ($[M-6CO]^+$), 123 (35) ($[CH_2=CHCH_2Si(CH_3)_2-C≡C]^+$); Mass spectrum (CI, m/z (%)): 449 (80) ($[M-1]^+$), 420 (70) ($[M-1CO]^+$); Mass spectrum (high resolution, (DEI)): calculated for mass $^{12}C_{14}H_{17}SiCoFeO_4$ ($[M]^+$), 391.9578 amu; observed, 391.9588 amu

Reaction of Me_3Si-C≡C-$SiMe_2$(allyl)$[ML_n]_2$ with HBF_4.

To a solution of the compound in CH_2Cl_2 (0.5 mL of a 0.05 M solution) in a 5 mm NMR tube was added HBF_4-etherate (0.9 equiv.) at -80°C. The 282.42 MHz ^{19}F spectra were acquired at this temperature.

39 gave **51**: δ -156.8 (septet, $^1J_{Si-F}$ = 269 Hz; $^3J_{F-H}$ = 7 Hz).

42 gave **48**: δ -152.8 (septet, $^1J_{Si-F}$ = 279 Hz; $^3J_{F-H}$ = 6 Hz).

43 gave **50**: δ -132.2 (septet, $^1J_{Si-F}$ = 269 Hz; $^3J_{F-H}$ = 7 Hz).

Reaction of (allyl)Me_2Si-C≡C-C≡C-$SiMe_2$(allyl)$[ML_n]_m$ (m = 2 or 4) with HBF_4.

To a solution of the compound in CH_2Cl_2 (1.5 mL of a 0.05 M solution) in a 10 mm NMR tube was added HBF_4 etherate complex (0.9 equiv.) at -80 °C. The 59.6 MHz ^{29}Si NMR spectra were acquired at this temperature. The sample was then removed

from the probe and kept at -80 °C in a dry ice/isopropanol bath where a second equivalent of HBF_4 was added, and the ^{29}Si NMR spectrum was obtained at -80 °C.

41 gave **52**: δ -6.1 (d, $^1J_{Si-F}$ = 278 Hz), -15.7 (s); and then **55**: δ 4.1 (d, $^1J_{Si-F}$ = 271 Hz).

45 gave **53**: δ 17.1 (d, $^1J_{Si-F}$ = 278 Hz), 5.9 (s); and then **56**: δ 17.1 (d, $^1J_{Si-F}$ = 278 Hz).

46 gave **54**: δ 3.6 (d, $^1J_{Si-F}$ = 270 Hz), -15.8 (s); and then **57**: δ 3.9 (d, $^1J_{Si-F}$ = 271 Hz).

61 gave **65**: δ 3.3 (d, $^1J_{Si-F}$ = 289 Hz).

62 gave **63**: δ 18.0 (d, $^1J_{Si-F}$ = 276 Hz).

71 gave **72**: δ 20.7 (d, $^1J_{Si-F}$ = 276 Hz). Crystals suitable for X-ray diffraction of **72**, were grown by slow evaporation from CH_2Cl_2.

Reaction of Me_3Si-C≡C-$SiMe_2$(allyl)[ML_n]$_2$ with HOTf.

To a solution of the compound in acetonitrile (1.5 mL of a 0.05 M solution) in a 10 mm NMR tube was added triflic acid (0.9 equiv.) at -80 °C. The 59.6 MHz ^{29}Si spectra were acquired at this temperature.

42 gave **58**: δ -0.3 ($SiMe_3$), -4.9 ($SiMe_2$).

43 gave **59**: δ -6.2 ($SiMe_3$), -11.2 ($SiMe_2$).

61 gave **66**: δ -17.1 ($SiMe_2$).

62 gave **64**: δ 25.1 ($SiMe_2$).

Competitive reactions

HBF_4•etherate (0.9 equiv.) was added at -80 °C a 10 mm NMR tube containing equimolar amounts of the two compounds in CH_2Cl_2 (1.5 mL of a 0.05 M solution of

each). The 282.42 MHz ^{19}F spectra were acquired at this temperature, and the 59.6 MHz ^{29}Si spectrum of **47** was also acquired at this temperature.

39 *versus* **42** : gave **48** (47%) and **51** (53%).

39 *versus* **43** : gave **50** (48%) and **51** (52%).

42 *versus* **43** : gave **48** (52%) and **50** (48%).

47 gave **53** : δ 4.1 (doublet, $^{1}J_{Si\text{-}F}$ = 271 Hz), 0.8 (s). $[Co_2(CO)_8](CH_2{=}CHCH_2\text{-}SiMe_2\text{-}C{\equiv}C\text{-}C{\equiv}C\text{-}SiMe_2F)$

Reaction of $CH_2{=}CHCH_2SiMe_2\text{-}C{\equiv}C\text{-}C(CH_3)_2$ $[CoFe(CO)_6]$, (71) with Ph_3C^+ PF_6^-

A 100 mL round bottom flask was charged with **71** (0.354g, 0.79 mmol) and Ph_3C^+ PF_6^- (0.61 g, 1.58 mmol) and 50 mL of CH_2Cl_2 and allowed to stir at room temperature under nitrogen for 48 hours. Subsequently the solvent was removed by rotary evaporation. Hexanes was next added to the mixture and the resulting red solution was gravity filtered and the solvent was remove by rotary evaporation to yield 73 (0.40 g, 0.49 mmol, 62%) as a red solid. ^{29}Si NMR (CH_2Cl_2, 99.36 MHz): δ -21.990.

Reaction of $CH_2{=}CCH_3\text{-}C{\equiv}C\text{-}Si(Me)_2CH_2{=}CHCH_2$ $[Co_2(CO)_6]$, (70) with HBF_4 or the Preparation of 68.

A 100 mL round bottom flask was charged with **70** (0.254 g, 0.56 mmol) in 50 mL of CH_2Cl_2 and cooled to -78 °C. HBF_4•etherate (0.083 mL, 0.56 mmol) was next added and allowed to stir at -78 °C for 2 hour. The reaction mixture was allowed to warm-up slowly to 10 °C and was stirred for an additional 24 hours. The reaction mixture was quenched with 5 mL of a 0.1M solution of bicarbonate and then extracted with three 15 mL

portions of pentane. The organic layers were combined and dried over $MgSO_4$ filtered and the solvent removed by rotary evaporation. The resulting solid was subjected to flash silica gel chromatography with hexane as the solvent the second brown band yielded **68** as a brown solid (0.15 g, 0.31 mmol, 55%). ^1H NMR ($CDCl_3$, 500.13 MHz) δ 5.90 (m, 1H, CH_2=C*H*$CH_2C(CH_3)_2$-), 5.12 (m, 2H, C*H*$_2$=$CHCH_2C(CH_3)_2$-), 2.29 (m, 2H, CH_2=$CHCH_2C(CH_3)_2$-), 1.26 (m, 6H, $C(CH_3)_2$-), 0.53 (s, 6H, $Si(CH_3)_2$). ^{13}C NMR ($CDCl_3$, 125.03 MHz) δ 200.6 (*C*≡O), 134.8 (CH_2=*C*$HCH_2C(CH_3)_2$-), 118.6 (*C*H_2=$CHCH_2C(CH_3)_2$-), 50.4 (CH_2=$CHCH_2C(CH_3)_2$-), 39.9 (CH_2=$CHCH_2C(CH_3)_2$-), 30.8 ($C(CH_3)_2$-), 0.7 ($Si(CH_3)_2$). ^{29}Si NMR (CH_2Cl_2, 99.36 MHz) δ 19.4 (d, $^1J_{Si\text{-}F}$ = 251 Hz). IR (hexane) ν_{CO} at 2091, 2051 and 2025 cm^{-1}. Mass spectrum (DEI, m/z (%)): 442 (5) ($[M\text{-}(CO)]^+$), 414 (45) ($[M\text{-}2(CO)]^+$), 386 (65) ($[M\text{-}3(CO)]^+$), 358 (70) ($[M\text{-}4(CO)]^+$), 330 (100) ($[M\text{-}5(CO)]^+$).

Reaction of $HOC(CH_3)_2$-C≡C-$Si(Me)_2CH_2$=$CHCH_2$ [$Co_2(CO)_6$] + HBF_4 or the Preparation of 68.

Analogous to the synthesis of **68, 67** (0.212 g, 0.45 mmol) and HBF_4•etherate (0.067 mL, 0.45 mmol) yielded **68** as a dark red oil (0.10 g, 0.22 mmol; 49 %). Spectral data identical to those described above for preparation of **68**.

Reaction of $HOC(CH_3)_2$-C≡C-$Si(Me)_2CH_2$=$CHCH_2$ [$Co_2(CO)_6$] + BF_3•etherate or the Preparation of 68.

Analogous to the synthesis of **68,** however 4Å molecular sieves were also added to the round bottom flask and were filter off prior to the extraction procedure descibed , **67**

(0.265 g, 0.57 mmol) and BF_3•etherate (0.070 mL, 0.57 mmol) yielded **68** as a dark red oil (0.14 g, 0.29 mmol; 52 %). Spectral data identical to those described above for preparation of **68**.

REFERENCES

1 G. Raabe and J. Michl, in *The Chemistry of Organic Silicon Compounds*, S. Patai and Z. Rappoport (eds.), Wiley, Chichester, 1989, page 1015 - 1142.

2 *CRC Handbook of Chemistry and Physics, 75th Edition*, ed. D. R. Lide, CRC Press, Boca Raton, 1996.

3 B. F. G. Johnson, R. D. Johnston, and J. Lewis, *J. Chem. Soc. (A)*, (1968) 2865.

4 H.H. Freeman, in *Carbonium Ions*, G.A. Olah and P.v.R. Schleyer (eds.), Wiley Interscience, New York, 1973, Vol. 4, chapter 28.

5 R. T. Morrison and R. N. Boyd, *Organic Chemistry*, 4th Edition, Allyn and Bacon, Boston, 1983, pp. 495-496.

6 (a) E. A. Hill and R. Wiesner, *J. Am. Chem. Soc.*, *91* (1969) 510. (b) R. Gleiter, R. Seeger, H. Binder, E. Fluck and M. Cais, *Angew. Chem., Int. Ed. Engl.*, *11* (1972) 1028. (c) J. J. Dannenberg, M. K. Levenberg and J. H. Richards, *Tetrahedron*, *29*, (1973) 1575.

7 R. E. Davis, H. D. Simpson, N. Conte and R. Pettit, *J. Am. Chem. Soc.*, *93* (1971) 6688.

8 D. Seyferth and J. S. Merola, *J. Organomet. Chem.*, *160* (1978) 275.

9 M. D. Rausch, E. A. Mintz and D. W. Macomber, *J. Org. Chem.*, *45* (1980) 689.

10 (a) M. Cais, *Organomet. Chem. Rev.*, *1* (1966) 435. (b) L. W. Haynes and R. Pettit, in *Carbonium Ions*, G. A. Olah and P. v. R. Schleyer (eds.), Wiley, Interscience, New York, 1976, Vol. 5, pp. 2049-2133.

11 J. D. Holmes, D. A. K. Jones and R. Pettit, *J. Organomet. Chem.*, *4* (1965) 324.

12 (a) M. Acampora, A. Ceccon, M. Dal Farra, G. Giacometti and G. Rigatti, *J. Chem Soc. Perkin Trans. 2*, (1977) 483. (b) A. Ceccon, A. Gobbo and A. Venzo, *J. Organomet. Chem.*, *162* (1978) 311.

13 D. Seyferth, J. S. Merola and J. S. Eschbach, *J. Am. Chem. Soc.*, *100* (1978) 4124.

14 P. A. Downton, B. G. Sayer and M. J. McGlinchey, *Organometallics*, *11* (1992) 3281.

15 K. L. Malisza, L. C. F. Chao, J. F. Britten, B. G. Sayer, G. Jaouen, S. Top, A. Decken and M. J. McGlinchey, *Organometallics*, *12* (1993) 2462.

16 S. Lupon, M. Kapon, M. Cais and F. H. Herbstein, *Angew. Chem., Int. Ed. Engl.*, *11* (1972) 1025.

17 U. Behrens, *J. Organomet. Chem.*, *182* (1979) 89.

18 T. A. Albright, R. Hoffmann and P. Hoffmann, *Chem. Ber.*, *111* (1978) 1591.

19 K. Wade, in *Transition Metal Clusters*, B. F. G. Johnson (ed.), Wiley-Interscience, New York, 1980, pp. 193-264.

20 D. M. P. Mingos, *Acc. Chem. Res.*, *17* (1984) 331.

21 M. J. McGlinchey, M. Mlekuz, P. Bougeard, B. G. Sayer, A. Marinetti, J-Y. Saillard and G. Jaouen, *Can. J. Chem.*, *61* (1983) 1319.

22 B. E. R. Schilling and R. Hoffmann, *J. Am. Chem. Soc.*, *101* (1979) 3456.

23 M. Elian and R. Hoffmann, *Inorg. Chem.*, *14* (1975) 1058.

24 M. F. D'Agostino, C. S. Frampton and M. J. McGlinchey, *J. Organomet. Chem.*, *394* (1990) 145.

25 S. Padmanabhan and K. M. Nicholas, *J. Organomet. Chem.*, *212* (1984) C23.

26 S. L. Schreiber, M. T. Klimas and S. Sammakia, *J. Am. Chem. Soc.*, *109* (1987) 5749.

27 C. Cordier, M. Gruselle, G. Jaouen, V. I. Bakhmutov, M. V. Galakhov, L. L. Troitskaya and V. I. Sokolov, *Organometallics*, *10* (1991) 2303.

28 M. V. Galakhov, V. I. Bakhmutov, I. V. Barinov and O. A. Reutov, *J. Organomet. Chem.*, *421* (1991) 65.

29 A. Meyer, D. J. McCabe and M. D. Curtis, *Organometallics*, *6* (1987) 1491.

30 H. El-Amouri, J. Vaissermann, Y. Besace, K. P. C. Vollhardt and G. E. Ball, *Organometallics*, *12* (1993) 605.

31 H. El-Amouri, Y. Besace, J. Vaissermann, G. Jaouen and M. J. McGlinchey, *Organometallics*, *13* (1994) 4426.

32 M. V. Galakhov, V. I. Bakhmutov and I. V. Barinov, *Magn. Res. Chem. 29* (1991) 506.

33 D. H. Bradley, M. A. Khan and K. M. Nicholas, *Organometallics*, *8* (1989) 554.

34 D. H. Bradley, M. A. Khan and K. M. Nicholas, *Organometallics*, *11* (1992) 2598.

35 H. El Hafa, C. Cordier, M. Gruselle, Y. Besace, G. Jaouen and M. J. McGlinchey, *Organometallics*, *13* (1994) 5149.

36 S. Top, G. Jaouen and M. J. McGlinchey, *J. Chem. Soc., Chem. Commun.*, (1980) 1110.

37 N. M. Loim, I. A. Mamedyarova, M. N. Nefedova, G. S. Natzke and V. I. Sokolov, *Tetrahedron Lett.*, (1992) 3611.

38 D. Seyferth, *Adv. Organomet. Chem.*, *14* (1976) 97.

39 M. F. D'Agostino, M. Mlekuz, J. W. Kolis, B. G. Sayer, C. A. Rodger, J.-F. Halet, J.-Y. Saillard and M. J. McGlinchey, *Organometallics*, *5* (1986) 2345.

40 D. Osella, G. Dutto, G. Jaouen, A. VessiPres, P. R. Raithby, L. De Benedetto and M. J. McGlinchey, *Organometallics*, *12* (1993) 4545.

41 L. L. Troitskaya, V. I. Sokolov, V. I. Bakhmutov, O. A. Reutov, M. Gruselle, C. Cordier and G. Jaouen, *J. Organomet. Chem.*, *364* (1989) 195.

42 A. A. Koridze, N. M. Astakhova and P. V. Petrovskii, *J. Organomet. Chem.*, *254* (1983) 345.

43 G. H. Young, M. V. Raphael, A. Wojcicki, M. Calligaris, G. Nardin and N. Bresciani-Pahor, *Organometallics*, *10* (1991) 1934.

44 W.J. Pietro and W.J. Hehre, *J. Am. Chem. Soc.*, *104* (1982) 4329.

45 L. Szepes and T. Baer, *J. Am. Chem. Soc.*, *106* (1984) 273.

46 G.W. Goodloe, E.R. Austin, and F.W. Lampe, *J. Am. Chem. Soc.*, *101* (1979) 3472.

47 Y. Apeloig and P.V.R. Schelyer, *Tetrahedron Lett.*, (1977) 4647.

48 A.C. Hopkinson and M.H. Lien, *J. Mol. Struct., 104* (1983) 303.

49 R.J. Corriu and M. Henner, *J. Organomet. Chem., 174* (1974) 1.

50 G.A. Olah and L.D. Field, *Organometallics, 1* (1982) 1485.

51 (a) P.D. Lickiss, *Chem. Soc. Rev.*, (1992) 271. (b) L. Pauling, *Science, 263* (1994) 983. (c) G. A. Olah, G. Rasul, X. Li, H. A. Buchholz, G. Sandford and G. K. S. Prakash, *Science, 263* (1994) 983. (d) C. A. Reed and Z. Xie, *Science, 263* (1994) 983. (e) J. B. Lambert and S. Zhang, *Science, 263* (1994) 984.

52 (a) V. D. Nefedov, T. A. Kochina and E. N. Sinotova, *Russian Chem. Rev., 55* (1986) 426. (b) H. Schwarz, in *The Chemistry of Organic Silicon Compounds*, S. Patai, Z. Rappoport (eds.), Wiley, Chichester, 1989, Part 2, Chapter 7.

53 (a) J. B. Lambert, S. Zhang, *Science, 263* (1993) 1917. (b) J. B. Lambert , S. Zhang, S. M. Ciro, *Organometallics, 13* (1994) 2430.

54 C. A. Reed, Z. Xie, R. Rau, A. Benesi, *Science, 262* (1993) 984.

55 (a) P. D. Bartlett, F. E. Condon and A. Schneider, *J. Am. Chem. Soc., 66* (1944) 1531. (b) N. C. Deno, H. J. Peterson and G. S. Gaines, *Chem. Rev., 60* (1960) 7

56 (a) R. Walsh in *The Chemistry of Orgaonsilicon Comounds;* S. Patai and Z. Rappoport (eds.), Wiley, Chichester, 1989, Part 1, pp 371. (b) E. A. Brinkman, K. Salomon, W. Tumas and J. I. Brauman, *J. Am. Chem. Soc., 117* (1995) 4905.

57 R. T. Edidin, J. R. Norton, K. Mislow, *Organometallics, 1* (1982) 561.

58 L. Girard, P. E. Lock, H. El-Amouri and M. J. McGlinchey, *J. Organomet. Chem.*, *478* (1994) 189.

59 H. B. Bürgi and J. D. Dunitz, *Acc. Chem. Res.*, *16* (1983) 153.

60 These distance and angle parameters are derived from the x-ray crystal structure of $[(fulvalene)Mo_2(CO)_4(Me\text{-}C{\equiv}C\text{-}CH_2)]^+$.

61 M. Gruselle, H. El Hafa, M. Nikolski, G. Jaouen, J. Vaissermann, L. Li and M. J. McGlinchey, *Organometallics*, *12* (1993) 4917.

62 B. K Campion, R. H. Heyn and T. D. Tilley, *J. Am. Chem. Soc.*, *110* (1988) 7558.

63 R. J. P. Corriu, J. J. E. Moreau and H. Praet, *Organometallics*, *8* (1989) 2779.

64 U. Lay and H. Lang, *J. Organomet. Chem.*, *418* (1991) 79.

65 H. Lang, U. Lay and L. Zsolnai, *J. Organomet. Chem.*, *417* (1991) 377.

66 R. Davis and L. A. P. Kane-Maguire in *Comprehensive Organometallic Chemistry*; G. Wilkinson, F. G. A. Stone and E. W. Abel (eds.), Pergamon Press, New York, 1982, Vol. 3, pp. 1240-1241 and references therein.

67 W. I. Bailey, Jr., M. H. Chisholm, F. A. Cotton and L. A. Rankin, *J. Am. Chem. Soc.*, *100* (1978) 5764.

68 J. A. Beck, S. A. R. Knox, R. F. D. Stone, M. J. Winter and P. Woodward, *J. Chem. Soc., Dalton Trans.*, (1982) 195.

69 R. J. P. Corriu, J. J. E. Moreau and H. Praet, *Organometallics*, *9* (1990) 2086.

70 E. Kloster-Jensen and C. Rømming, *Acta. Chem. Scand.*, *B40* (1986) 604.

71 R. D. W. Kemmit and D. R. Russell, in *Comprehensive Organometallic Chemistry;* G. Wilkinson, F. G. A. Stone and E. W. Abel (eds.), Pergamon Press, New York, 1982, Vol. 5, pp. 195 and references therein.

72 R. J. Gillespie and I. Hargittai, *The VSEPR Model of Molecular Geometry*; Allyn and Bacon, Needham Heights, MA, 1991, pp. 90-91 and references therein.

73 (a) J. B. Lambert and Y. Zhao, *J. Am. Chem. Soc., 118* (1996) 7867. (b) H. -U. Siehl, F. -P. Kaufmann, Y. Apeloig, V. Braude, D. Danovich, A. Berndt and N. Stamatis, *Angew. Chem., Int. Ed. Engl., 30* (1991) 1479.

74 (a) A. Hosomi and H. Sakurai, *Tetrahedron Lett.* (1976) 1295. (b) I. Fleming, J. Dunoguès and R. Smithers, *Org. React., 37* (1989) 57.

75 M. D. McClain, M. S. Hay, M. D. Curtis and J. W. Kampf, *Organometallics, 13* (1994) 4377.

76 G. A. Olah, *Angew. Chem., Int. Ed. Engl., 34* (1995) 1393.

77 M. Kondratenko, H. El Hafa, M. Gruselle, J. Vaissermann, G. Jaouen and M.J. McGlinchey, *J. Am. Chem. Soc., 117* (1995) 6907.

78 (a) H. Lang, S. Blau, G. Rheinwald and G. Wildermuth, *J. Organomet. Chem., 489* (1995) C17. (b) H. Lang, S. Blau and G. Rheinwald, *J. Organomet. Chem., 492* (1995) 81. (c) H. Lang, S. Blau, G. Rheinwald and L. Zsolnai, *J. Organomet. Chem., 494* (1995) 65.

79 (a) M. Maekawa, M. Munakata, T. Kuroda-Sowa and K. Hachiya, *Inorg. Chim. Acta, 236* (1995) 181. (b) M. Maekawa, M. Munakata, T. Kuroda-Sowa and K. Hachiya, *Polyhedron, 14* (1995) 2879.

80 (a) P. Magnus and D. P. Becker, *J. Chem. Soc., Chem. Commun.*, (1985) 640. (b) H. Lang, M. Weinmann and L. Zsohai, *J. Organomet. Chem., 522* (1996) 277.

81 J. Lewis, B. Lin, M. S. Khan, M. R. A. Al-Mandhary and P. R. Raithby, *J. Organomet. Chem., 484* (1994) 161.

82 Y. Rubin, C. B. Knobler and F. Diederich, *J. Am. Chem. Soc., 112* (1990) 4966.

83 (a) T. Kuhnen, R. Ruffolo, M. Stradiotto, D. Ulbrich, M. A. Brook and M. J. McGlinchey, (b). T. Kuhnen, M. Stradiotto, R. Ruffolo, D. Ulbrich, M. A. Brook and M. J. McGlinchey, accepted for publication.

84 E. Pretsch, T. Clerc, J. Seibl and W. Simon, *Tables of Spectral data for Structure Determination of Organic Compounds, 2nd Edition*, Springer-Verlag, Berlin, 1989.

85 K. M. Nicholas, *Acc. Chem. Res., 20* (1986) 207.

86 K. M. Nicholas and R. Pettit, *Tetrahedron Lett., 37* (1971) 3475.

87 (a) D. D. Grove, F. Miskevich, C. C. Smith and J. R. Corte, *Tetrahedron Lett.*, (1990) 6277. (b) D. D. Grove, J. R. Corte, R. P. Spencer, M. E. Pauly and N. P. Rath, *J. Chem. Soc., Chem. Commun.*, (1994) 49. (c) K. L. Malisza, L. Girard, D. W. Hughes, J. F. Britten and M. J. McGlinchey, *Organometallics, 14* (1995) 4676.

88 N. A. Bailey and R. Mason, *J. Chem. Soc. (A),* (1968) 1293.

89 S. L. Schreiber, T. Sammakia and W. E. Crowe, *J. Am. Chem. Soc.*, *108* (1986) 3128.

90 R. Hoffmann, R., *Angew. Chem., Int. Ed. Engl., 21* (1982) 711. and references therein

91 J. Dunn, unpublished result from this laboratory.

92 J. B. Lambert and Y. Zhao, *Angew. Chem. Int. Ed. Engl., 36* (1997) 400.

93 R. W. Rudolph, *Acc. Chem. Res., 9* (1976) 446.

94 H. Mayr and M. Patz, *Angew. Chem. Int. Ed. Engl., 33* (1994) 938.

95 D. D. Perrin, W. L. F. Armarego and D. R. Perrin, *Purification of Laboratory Chemicals, 2nd Edition*, Pergamon Press, Elmsford, New York, 1980.

96 M. D. Curtis, N. A. Fotinos, L. Messerle, A. P. Sattelberger, *Inorg. Chem., 22* (1983) 1559.

97 (a) G. M. Sheldrick, *SHELXTLPC*, Release 4.1; Siemens Crystallographic Research System: Madison, WI 1990. Shelxl library. (b) V. Schomaker and K. N. Trueblood, *Acta. Crstallogr., B24* (1968) 63.

98 SMART (1996), Release 4.05; Siemens Energy And Automation Inc., Madison, WI 53719.

99 SAINT (1996), Release 4.05; Siemens Energy And Automation Inc., Madison, WI 53719.

100 Sheldrick, G. M. SADABS (Siemens Area Detector Absorption Corrections) (1996).

101 (a) R. Hoffmann, *J. Chem. Phys., 39* (1963) 1397. (b) R. Hoffmann, W. N. Lipscomb, *J. Chem. Phys., 36* (1962) 2179. (c) R. Hoffmann, W. N. Lipscomb, *J. Chem. Phys., 36* (1962) 3489. (d) J. H. Ammeter, H. -B. Bürgi, J. C. Thibeault, R. J. Hoffmann, *J. Am. Chem. Soc., 100* (1978) 3686.

102 C. Mealli, D. M. Proserpio, *J. Chem. Educ., 67* (1990) 3399.

103 C. Tretner, B. Zobel, R. Hummeltenberg and W. Uhlig, *J. Organomet. Chem., 468* (1994) 63.

104 D. L. Trumbo, C. S. Marvel, *J. Polymer Sci. Part A, 24* (1986) 2231.

APPENDIX

Table 2: Crystal data and structure refinement for **26** and **32.**

	26	**32**
Empirical formula	$C_{31}H_{30}Mo_2O_4Si_2$	$C_{26}H_{30}Co_4O_{13}Si_4$
Molecular Weight	714.6	898.58
Description	red parallelepiped	black parallelepiped
Dimensions, mm	0.3 x 0.3 x 0.2	0.36 x 0.34 x 0.27
Temperature, K	300	293(2) K
Wavelength, Å	MoKα (λ = 0.71073 Å)	MoKα (λ = 0.71073 Å)
Crystal system	Monoclinic	Monoclinic
Space group	$P2_1/c$	C2/c
Z	4	4
a, Å	17.061(2)	14.093(2)
b, Å	9.756(2)	10.285(1)
c, Å	17.922(3)	27.689(3)
β, deg	96.64(3)	92.153(9)
Volume, $Å^3$	2963.1(8)	4010.6(7)
Calcd Density, g/cm^3	1.602	1.488
Abs coeff, mm^{-1}	0.962	1.797
F(000)	1440	1816
θ-range for collection, deg.	5.0 to 60.0°	2.45 to 30.00
Index ranges	$-1 \le h \le 23$,	$-1 \le< h \le 19$,
	$-1 \le k \le 13$,	$-1 \le k \le 14$,
	$-25 \le l \le 25$	$-38 \le l \le 38$
No. Reflections collected	10440	7179
No. Independent reflection	8627	5848
Rint (%)	3.01	3.78)
Refinement method	Full-matrix least-squares on F^2	
Data / parameter	8625 / 357	5837 / 213
Goodness-of-fit on F^2	1.10	1.074
Final R indices ($I>2\sigma(I)$)*	R1 = 0.0405	R1 = 0.0385,
	wR2 = 0.0824	wR2 = 0.0828
R indices (all data)*	R1 = 0.0674	R1 = 0.0626,
	wR2 = 0.0937	wR2 = 0.0965
Largest diff. Peak, $e/Å^3$	0.427	0.364
Largest diff. Hole, $e/Å^3$	-0.494	-0.287

$*R_1 = \Sigma| |Fo| - |Fc| | / \Sigma|Fo|$; $wR_2 = (\Sigma[w(F_o^2 - F_c^2)^2] / \Sigma[wF_o^4])^{1/2}$

Table 3: Crystal data and structure refinement for **43** and **45**.

	43	**45**
Empirical formula	$C_{24}H_{30}Mo_2O_4Si_2$	$C_{26}H_{22}Co_4O_{12}Si_2$
Molecular Weight	630.54	818.34
Description	parallelepiped	plate
Dimensions, mm	0.3 x 0.2 x 0.2	0.3 x 0.2 x 0.35
Temperature, K	293(2)	293(2)
Wavelength, Å	0.71073	0.56086
Crystal system	Monoclinic	Monoclinic
Space group	C2/c	C2/c
Z	8	4
a, Å	15.058(3)	12.604(3)
b, Å	12.474(2)	15.447(3)
c, Å	29.128(6)	18.382(4)
β, deg	100.12(3)	107.20(3)
Volume, $Å^3$	5386(2)	3418.8(12)
Calcd Density, g/cm^3	1.555	1.590
Abs coeff, mm^{-1}	1.046	1.055
F(000)	2544	1640
θ-range for collection, deg.	2.13 to 29.98	1.69 to 16.05
Index ranges	$-19 \le h \le 19$, $ú \le k \le 17$, $0 \le l \le 40$	$-1 \le h \le 12$, $-1 \le k \le 15$, $-18 \le l \le 17$
No. Reflections collected	6630	2212
No. Independent reflection	6630	1708
R(int)	0.0470	0.0665
Refinement method	Full-matrix least-squares on F^2	
Data / restraints / parameter	6595 / 0 / 289	1708 / 0 / 199
Goodness-of-fit on F^2	1.059	0.594
Final R indices ($I>2\sigma(I)$)*	$R_1 = 0.0433$	$R_1 = 0.0387$
	$wR_2 = 0.0932$	$wR_2 = 0.0460$
R indices (all data)*	$R_1 = 0.0751$	$R_1 = 0.1713$
	$wR_2 = 0.1250$	$wR_2 = 0.0673$
Largest diff. Peak, $e/Å^3$	0.722	0.257
Largest diff. Hole, $e/Å^3$	-0.390	-0.258

$$*R_1 = \Sigma| |Fo| - |Fc| | / \Sigma|Fo| ; \quad wR_2 = (\Sigma[w(F_o^2 - F_c^2)^2] / \Sigma[wF_o^4])^{1/2}$$

Table 4: Crystal data and structure refinement for **72**.

	72
Empirical formula	$C_{13}H_{12}SiFO_6CoFe$
Molecular Weight	426.10
Description	parallelepiped
Dimensions, mm	0.2 x 0.25 x 0.15
Temperature, K	300(2) K
Wavelength, Å	0.71073 A
Crystal system	Monoclinic
Space group	P21/n
Z	4
a, Å	8.2492(2)
b, Å	15.4888(2)
c, Å	13.6408(3)
β, deg	94.7430(10)
Volume, $Å^3$	1736.92(6)
Calcd Density, g/cm^3	1.629
Abs coeff, mm^{-1}	1.892
F(000)	856
θ-range for collection, deg.	1.99 to 26.58
Index ranges	$-10 \le h \le 10$,
	$-19 \le k \le 19$,
	$-16 \le l \le 16$
No. Reflections collected	14037
No. Independent reflection	3375
R(int)	0.0470
Refinement method	Full-matrix least-squares on F^2
Data / restraints / parameter	3375 / 0 / 209
Goodness-of-fit on F^2	1.059
Final R indices ($I>2\sigma(I)$)*	R1 = 0.0396,
	wR2 = 0.0890
R indices (all data)*	R1 = 0.0622,
	wR2 = 0.1016
Largest diff. Peak, $e/Å^3$	0.479
Largest diff. Hole, $e/Å^3$	-0.360

$$*R_1 = \Sigma| |Fo| - |Fc| | / \Sigma|Fo| ; \quad wR_2 = (\Sigma[w(F_o^2 - F_c^2)^2] / \Sigma[wF_o^4])^{1/2}$$

Table 5: Atomic coordinates (x 10^4) and equivalent isotropic displacement parameters (A^2 x 10^3) for **26**.

U(eq) is defined as one third of the trace of the orthogonalized Uij tensor.

	x	y	z	U(eq)
Mo(1)	1671(1)	1971(1)	115(1)	30(1)
Mo(2)	3307(1)	2136(1)	188(1)	29(1)
Si(1)	2664(1)	-1070(1)	-771(1)	40(1)
Si(4)	2527(1)	-108(1)	1685(1)	31(1)
C(2)	2562(2)	393(3)	-88(2)	30(1)
C(3)	2532(2)	626(3)	690(2)	27(1)
C(5)	2377(5)	-615(8)	-1827(4)	91(2)
C(6)	2085(4)	-2573(5)	-549(4)	66(2)
C(7)	3662(3)	-1648(7)	-636(5)	88(3)
C(8)	1634(2)	-1040(3)	1829(2)	35(1)
C(9)	1428(2)	-2297(4)	1498(3)	57(2)
C(10)	783(3)	-2966(5)	1664(3)	69(2)
C(11)	324(3)	-2386(5)	2142(3)	72(2)
C(12)	507(3)	-1170(6)	2469(4)	99(3)
C(13)	1158(3)	-494(5)	2316(4)	79(2)
C(14)	3369(2)	-1227(3)	1972(2)	34(1)
C(15)	3913(2)	-782(5)	2561(3)	48(1)
C(16)	4554(2)	-1536(6)	2774(3)	62(2)
C(17)	4661(3)	-2745(6)	2409(3)	65(2)
C(18)	4139(3)	-3205(5)	1834(4)	73(2)
C(19)	3503(3)	-2454(5)	1616(3)	58(2)
C(20)	3684(3)	4286(4)	-194(3)	56(2)
C(21)	4303(3)	3401(5)	-170(3)	60(2)
C(22)	4131(3)	2416(5)	-760(3)	57(2)
C(23)	3426(3)	2694(4)	-1151(3)	47(1)
C(24)	3143(2)	3856(4)	-798(3)	48(1)
C(25)	1128(3)	4132(4)	132(3)	57(2)
C(26)	580(2)	3140(5)	255(3)	58(2)
C(27)	802(2)	2511(5)	981(3)	54(2)
C(28)	1479(2)	3111(4)	1305(3)	49(1)
C(29)	1674(3)	4099(4)	778(3)	54(2)
C(30)	3293(2)	2880(4)	1253(2)	40(1)
C(31)	4089(2)	850(4)	667(2)	39(1)
C(32)	1034(2)	357(4)	-188(3)	50(1)
C(33)	1670(2)	2201(4)	-1019(2)	46(1)
O(30)	3333(2)	3384(3)	1866(2)	64(1)
O(31)	4586(1)	189(3)	922(2)	62(1)
O(32)	645(2)	-535(4)	-389(2)	93(2)
O(33)	1618(2)	2401(4)	-1690(2)	68(1)

* Equivalent isotropic U defined as one third of the atoms

Table 6: Selected bond lengths [Å] and angles [deg] for **26**.

Mo(1)-Mo(2)	2.783 (1)	C(9)-C(10)	1.342 (7)
Mo(1)-C(2)	2.223 (3)	C(9)-H(9)	1.041 (49)
Mo(1)-C(3)	2.142 (3)	C(10)-C(11)	1.350 (8)
Mo(1)-C(25)	2.306 (4)	C(10)-H(10)	0.858 (46)
Mo(1)-C(26)	2.222 (4)	C(11)-C(12)	1.344 (8)
Mo(1)-C(27)	2.329 (5)	C(11)-H(11)	0.961 (44)
Mo(1)-C(28)	2.460 (5)	C(12)-C(13)	1.347 (8)
Mo(1)-C(29)	2.393 (5)	C(12)-H(12)	0.827 (49)
Mo(1)-C(32)	1.954 (4)	C(13)-H(13)	0.701 (45)
Mo(1)-C(33)	2.044 (4)	C(14)-C(15)	1.393 (5)
Mo(2)-C(2)	2.146 (3)	C(14)-C(19)	1.388 (6)
Mo(2)-C(3)	2.237 (3)	C(15)-C(16)	1.336 (6)
Mo(2)-C(20)	2.321 (4)	C(15)-H(15)	0.816 (41)
Mo(2)-C(21)	2.253 (5)	C(16)-C(17)	1.372 (8)
Mo(2)-C(22)	2.345 (5)	C(16)-H(16)	0.843 (40)
Mo(2)-C(23)	2.493 (4)	C(17)-C(18)	1.357 (7)
Mo(2)-C(24)	2.430 (4)	C(17)-H(17)	0.781 (48)
Mo(2)-C(30)	2.045 (4)	C(18)-C(19)	1.331 (7)
Mo(2)-C(31)	1.957 (3)	C(18)-H(18)	0.864 (44)
Si(1)-C(2)	1.901 (3)	C(19)-H(19)	0.807 (45)
Si(1)-C(5)	1.951 (7)	C(20)-C(21)	1.361 (7)
Si(1)-C(6)	1.838 (6)	C(20)-C(24)	1.403 (6)
Si(1)-C(7)	1.784 (6)	C(20)-H(20)	0.804 (36)
Si(4)-C(3)	1.923 (3)	C(21)-C(22)	1.435 (7)
Si(4)-C(8)	1.818 (3)	C(21)-H(21)	0.876 (48)
Si(4)-C(14)	1.830 (3)	C(22)-C(23)	1.348 (6)
Si(4)-H(2)	1.521 (37)	C(22)-H(22)	0.762 (40)
C(2)-C(3)	1.420 (5)	C(23)-C(24)	1.411 (6)
C(5)-H(5A)	1.085 (81)	C(23)-H(23)	0.851 (42)
C(5)-H(5B)	0.793 (29)	C(24)-H(24)	0.824 (34)
C(5)-H(5C)	0.790 (33)	C(25)-C(26)	1.381 (6)
C(6)-H(6A)	0.857 (64)	C(25)-C(29)	1.401 (7)
C(6)-H(6B)	0.865 (52)	C(25)-H(25)	0.836 (38)
C(6)-H(6C)	0.981 (61)	C(26)-C(27)	1.450 (7)
C(7)-H(7A)	0.835 (44)	C(26)-H(26)	0.840 (39)
C(7)-H(7B)	0.665 (59)	C(27)-C(28)	1.363 (6)
C(8)-C(9)	1.390 (6)	C(27)-H(27)	0.854 (40)
C(8)-C(13)	1.366 (8)	C(28)-C(29)	1.416 (7)

C(28)-H(28)	0.870 (41)	C(32)-O(32)	1.128 (5)
C(29)-H(29)	0.726 (36)	C(33)-O(33)	1.212 (5)
C(30)-O(30)	1.198 (5)	H(5A)-H(5B)	1.106 (83)
C(31)-O(31)	1.120 (4)		

Mo(2)-Mo(1)-C(2)	49.2(1)	C(25)-Mo(1)-C(33)	87.6(2)
Mo(2)-Mo(1)-C(3)	52.0(1)	C(26)-Mo(1)-C(33)	98.7(2)
C(2)-Mo(1)-C(3)	37.9(1)	C(27)-Mo(1)-C(33)	135.3(1)
Mo(2)-Mo(1)-C(25)	110.4(1)	C(28)-Mo(1)-C(33)	145.8(2)
C(2)-Mo(1)-C(25)	156.8(1)	C(29)-Mo(1)-C(33)	113.5(2)
C(3)-Mo(1)-C(25)	143.9(1)	C(32)-Mo(1)-C(33)	82.9(2)
Mo(2)-Mo(1)-C(26)	144.4(1)	Mo(1)-Mo(2)-C(2)	51.6(1)
C(2)-Mo(1)-C(26)	166.3(1)	Mo(1)-Mo(2)-C(3)	49.1(1)
C(3)-Mo(1)-C(26)	142.8(2)	C(2)-Mo(2)-C(3)	37.7(1)
C(25)-Mo(1)-C(26)	35.5(2)	Mo(1)-Mo(2)-C(20)	110.4(1)
Mo(2)-Mo(1)-C(27)	131.9(1)	C(2)-Mo(2)-C(20)	145.6(1)
C(2)-Mo(1)-C(27)	140.0(1)	C(3)-Mo(2)-C(20)	155.7(1)
C(3)-Mo(1)-C(27)	105.8(1)	Mo(1)-Mo(2)-C(21)	143.5(1)
C(25)-Mo(1)-C(27)	59.7(2)	C(2)-Mo(2)-C(21)	144.5(2)
C(26)-Mo(1)-C(27)	37.1(2)	C(3)-Mo(2)-C(21)	167.4(1)
Mo(2)-Mo(1)-C(28)	99.6(1)	C(20)-Mo(2)-C(21)	34.6(2)
C(2)-Mo(1)-C(28)	128.1(1)	Mo(1)-Mo(2)-C(22)	130.9(1)
C(3)-Mo(1)-C(28)	90.7(1)	C(2)-Mo(2)-C(22)	108.3(1)
C(25)-Mo(1)-C(28)	58.7(2)	C(3)-Mo(2)-C(22)	143.2(1)
C(26)-Mo(1)-C(28)	58.2(2)	C(20)-Mo(2)-C(22)	58.0(2)
C(27)-Mo(1)-C(28)	32.9(1)	C(21)-Mo(2)-C(22)	36.3(2)
Mo(2)-Mo(1)-C(29)	88.9(1)	Mo(1)-Mo(2)-C(23)	99.2(1)
C(2)-Mo(1)-C(29)	136.1(1)	C(2)-Mo(2)-C(23)	93.6(1)
C(3)-Mo(1)-C(29)	109.3(1)	C(3)-Mo(2)-C(23)	130.4(1)
C(25)-Mo(1)-C(29)	34.6(2)	C(20)-Mo(2)-C(23)	57.4(2)
C(26)-Mo(1)-C(29)	56.8(2)	C(21)-Mo(2)-C(23)	57.2(2)
C(27)-Mo(1)-C(29)	55.7(2)	C(22)-Mo(2)-C(23)	32.2(1)
C(28)-Mo(1)-C(29)	33.9(2)	Mo(1)-Mo(2)-C(24)	88.6(1)
Mo(2)-Mo(1)-C(32)	125.6(1)	C(2)-Mo(2)-C(24)	111.3(1)
C(2)-Mo(1)-C(32)	76.4(1)	C(3)-Mo(2)-C(24)	136.4(1)
C(3)-Mo(1)-C(32)	88.2(1)	C(20)-Mo(2)-C(24)	34.3(2)
C(25)-Mo(1)-C(32)	121.9(2)	C(21)-Mo(2)-C(24)	56.1(2)
C(26)-Mo(1)-C(32)	89.9(2)	C(22)-Mo(2)-C(24)	54.6(2)
C(27)-Mo(1)-C(32)	89.5(2)	C(23)-Mo(2)-C(24)	33.3(1)
C(28)-Mo(1)-C(32)	118.7(2)	Mo(1)-Mo(2)-C(30)	86.9(1)
C(29)-Mo(1)-C(32)	143.8(2)	C(2)-Mo(2)-C(30)	115.3(1)
Mo(2)-Mo(1)-C(33)	85.8(1)	C(3)-Mo(2)-C(30)	77.7(1)
C(2)-Mo(1)-C(33)	80.5(1)	C(20)-Mo(2)-C(30)	89.3(2)
C(3)-Mo(1)-C(33)	117.8(1)	C(21)-Mo(2)-C(30)	99.3(2)

C(22)-Mo(2)-C(30)	135.1(1)	H(6A)-C(6)-H(6B)	125.4(59)
C(23)-Mo(2)-C(30)	146.4(1)	Si(1)-C(6)-H(6C)	101.4(34)
C(24)-Mo(2)-C(30)	114.9(1)	H(6A)-C(6)-H(6C)	124.0(54)
Mo(1)-Mo(2)-C(31)	127.8(1)	H(6B)-C(6)-H(6C)	87.7(49)
C(2)-Mo(2)-C(31)	87.1(1)	Si(1)-C(7)-H(7A)	114.2(34)
C(3)-Mo(2)-C(31)	78.8(1)	Si(1)-C(7)-H(7B)	109.0(45)
C(20)-Mo(2)-C(31)	120.7(2)	H(7A)-C(7)-H(7B)	123.0(56)
C(21)-Mo(2)-C(31)	88.7(2)	Si(4)-C(8)-C(9)	123.7(3)
C(22)-Mo(2)-C(31)	87.5(2)	Si(4)-C(8)-C(13)	117.7(3)
C(23)-Mo(2)-C(31)	115.8(1)	C(9)-C(8)-C(13)	118.5(4)
C(24)-Mo(2)-C(31)	141.0(1)	C(8)-C(9)-C(10)	120.5(4)
C(30)-Mo(2)-C(31)	84.2(1)	C(8)-C(9)-H(9)	117.3(24)
C(2)-Si(1)-C(5)	115.0(2)	C(10)-C(9)-H(9)	122.0(24)
C(2)-Si(1)-C(6)	111.6(3)	C(9)-C(10)-C(11)	119.2(5)
C(5)-Si(1)-C(6)	108.1(3)	C(9)-C(10)-H(10)	118.0(32)
C(2)-Si(1)-C(7)	107.9(3)	C(11)-C(10)-H(10)	122.8(32)
C(5)-Si(1)-C(7)	109.4(4)	C(10)-C(11)-C(12)	121.6(5)
C(6)-Si(1)-C(7)	104.3(3)	C(10)-C(11)-H(11)	114.6(27)
C(3)-Si(4)-C(8)	114.3(1)	C(12)-C(11)-H(11)	123.6(27)
C(3)-Si(4)-C(14)	113.2(1)	C(11)-C(12)-C(13)	119.9(6)
C(8)-Si(4)-C(14)	107.8(2)	C(11)-C(12)-H(12)	132.1(35)
C(3)-Si(4)-H(2)	106.3(14)	C(13)-C(12)-H(12)	107.6(33)
C(8)-Si(4)-H(2)	106.3(13)	C(8)-C(13)-C(12)	120.3(5)
C(14)-Si(4)-H(2)	108.5(12)	C(8)-C(13)-H(13)	122.5(41)
Mo(1)-C(2)-Mo(2)	79.1(1)	C(12)-C(13)-H(13)	114.9(42)
Mo(1)-C(2)-Si(1)	137.8(2)	Si(4)-C(14)-C(15)	117.4(3)
Mo(2)-C(2)-Si(1)	130.4(2)	Si(4)-C(14)-C(19)	123.5(3)
Mo(1)-C(2)-C(3)	68.0(2)	C(15)-C(14)-C(19)	119.1(3)
Mo(2)-C(2)-C(3)	74.6(2)	C(14)-C(15)-C(16)	119.8(4)
Si(1)-C(2)-C(3)	140.2(2)	C(14)-C(15)-H(15)	118.3(27)
Mo(1)-C(3)-Mo(2)	78.9(1)	C(16)-C(15)-H(15)	121.9(26)
Mo(1)-C(3)-Si(4)	126.7(2)	C(15)-C(16)-C(17)	119.2(4)
Mo(2)-C(3)-Si(4)	133.2(1)	C(15)-C(16)-H(16)	114.9(31)
Mo(1)-C(3)-C(2)	74.1(2)	C(17)-C(16)-H(16)	125.8(31)
Mo(2)-C(3)-C(2)	67.7(2)	C(16)-C(17)-C(18)	122.3(4)
Si(4)-C(3)-C(2)	148.9(2)	C(16)-C(17)-H(17)	121.6(37)
Si(1)-C(5)-H(5A)	103.3(39)	C(18)-C(17)-H(17)	116.1(38)
Si(1)-C(5)-H(5B)	83.3(20)	C(17)-C(18)-C(19)	118.9(5)
H(5A)-C(5)-H(5B)	70.2(44)	C(17)-C(18)-H(18)	125.1(26)
Si(1)-C(5)-H(5C)	102.1(24)	C(19)-C(18)-H(18)	115.9(27)
H(5A)-C(5)-H(5C)	128.4(46)	C(14)-C(19)-C(18)	120.8(4)
H(5B)-C(5)-H(5C)	157.2(33)	C(14)-C(19)-H(19)	121.7(32)
Si(1)-C(6)-H(6A)	109.4(42)	C(18)-C(19)-H(19)	117.5(32)
Si(1)-C(6)-H(6B)	104.9(37)	Mo(2)-C(20)-C(21)	70.0(3)

Mo(2)-C(20)-C(24)	77.2(3)	C(26)-C(25)-H(25)	121.1(25)
C(21)-C(20)-C(24)	105.9(4)	C(29)-C(25)-H(25)	133.5(25)
Mo(2)-C(20)-H(20)	115.4(27)	Mo(1)-C(26)-C(25)	75.6(3)
C(21)-C(20)-H(20)	127.5(24)	Mo(1)-C(26)-C(27)	75.5(2)
C(24)-C(20)-H(20)	126.6(24)	C(25)-C(26)-C(27)	109.2(4)
Mo(2)-C(21)-C(20)	75.4(3)	Mo(1)-C(26)-H(26)	115.2(29)
Mo(2)-C(21)-C(22)	75.3(3)	C(25)-C(26)-H(26)	120.7(29)
C(20)-C(21)-C(22)	108.0(4)	C(27)-C(26)-H(26)	130.1(29)
Mo(2)-C(21)-H(21)	111.3(38)	Mo(1)-C(27)-C(26)	67.4(3)
C(20)-C(21)-H(21)	123.6(37)	Mo(1)-C(27)-C(28)	78.8(3)
C(22)-C(21)-H(21)	128.1(37)	C(26)-C(27)-C(28)	108.7(4)
Mo(2)-C(22)-C(21)	68.4(3)	Mo(1)-C(27)-H(27)	123.5(26)
Mo(2)-C(22)-C(23)	80.0(3)	C(26)-C(27)-H(27)	131.0(25)
C(21)-C(22)-C(23)	110.0(4)	C(28)-C(27)-H(27)	120.2(25)
Mo(2)-C(22)-H(22)	118.9(31)	Mo(1)-C(28)-C(27)	68.2(3)
C(21)-C(22)-H(22)	123.3(28)	Mo(1)-C(28)-C(29)	70.4(3)
C(23)-C(22)-H(22)	126.6(29)	C(27)-C(28)-C(29)	105.2(4)
Mo(2)-C(23)-C(22)	67.8(3)	Mo(1)-C(28)-H(28)	126.3(28)
Mo(2)-C(23)-C(24)	70.9(3)	C(27)-C(28)-H(28)	120.2(27)
C(22)-C(23)-C(24)	105.1(4)	C(29)-C(28)-H(28)	134.5(27)
Mo(2)-C(23)-H(23)	127.0(29)	Mo(1)-C(29)-C(25)	69.3(3)
C(22)-C(23)-H(23)	128.6(28)	Mo(1)-C(29)-C(28)	75.7(3)
C(24)-C(23)-H(23)	126.3(28)	C(25)-C(29)-C(28)	112.4(4)
Mo(2)-C(24)-C(20)	68.6(2)	Mo(1)-C(29)-H(29)	121.1(32)
Mo(2)-C(24)-C(23)	75.8(2)	C(25)-C(29)-H(29)	119.9(31)
C(20)-C(24)-C(23)	111.0(4)	C(28)-C(29)-H(29)	127.6(31)
Mo(2)-C(24)-H(24)	125.5(26)	Mo(2)-C(30)-O(30)	174.9(3)
C(20)-C(24)-H(24)	129.2(25)	Mo(2)-C(31)-O(31)	173.9(3)
C(23)-C(24)-H(24)	119.7(26)	Mo(1)-C(32)-O(32)	176.6(4)
Mo(1)-C(25)-C(26)	69.0(3)	Mo(1)-C(33)-O(33)	174.9(3)
Mo(1)-C(25)-C(29)	76.1(3)	C(5)-H(5A)-H(5B)	42.4(33)
C(26)-C(25)-C(29)	104.5(4)	C(5)-H(5B)-H(5A)	67.4(43)
Mo(1)-C(25)-H(25)	110.5(27)		

Table 7: Anisotropic displacement parameters ($Å^2$ x 10^3) for **26**.

The anisotropic displacement factor exponent takes the form:
$-2p^2$ [$h^2 a^{*2}$ U11 + ... + 2 h k a* b* U12]

	U11	U22	U33	U12	U13	U23
Mo(1)	24(1)	31(1)	33(1)	2(1)	2(1)	3(1)
Mo(2)	25(1)	27(1)	34(1)	-2(1)	4(1)	1(1)
Si(1)	48(1)	33(1)	42(1)	-3(1)	11(1)	-9(1)
Si(4)	31(1)	32(1)	31(1)	0(1)	4(1)	4(1)
C(2)	25(1)	29(2)	36(2)	0(1)	3(1)	2(1)
C(3)	19(1)	26(1)	37(2)	-1(1)	1(1)	4(1)
C(6)	65(3)	44(2)	90(5)	-10(2)	9(3)	-12(3)
C(7)	53(3)	82(4)	132(7)	12(3)	22(4)	-59(5)
C(8)	30(2)	38(2)	39(2)	2(1)	5(1)	10(2)
C(9)	50(2)	58(3)	67(3)	-17(2)	21(2)	-14(2)
C(10)	57(3)	63(3)	89(4)	-22(3)	14(3)	-9(3)
C(11)	37(2)	65(3)	115(5)	-8(2)	19(3)	17(3)
C(12)	71(3)	72(4)	171(7)	-8(3)	79(4)	-15(4)
C(13)	70(3)	51(3)	127(6)	-12(2)	54(4)	-20(3)
C(14)	29(2)	38(2)	34(2)	-2(1)	3(1)	10(2)
C(15)	38(2)	54(3)	51(3)	2(2)	0(2)	0(2)
C(16)	38(2)	81(3)	62(3)	2(2)	-10(2)	4(3)
C(17)	42(2)	71(3)	80(4)	16(2)	4(2)	24(3)
C(18)	59(3)	47(3)	108(5)	18(2)	-2(3)	-11(3)
C(19)	44(2)	48(2)	77(4)	5(2)	-12(2)	-11(2)
C(20)	70(3)	33(2)	67(3)	-16(2)	14(3)	1(2)
C(21)	38(2)	63(3)	80(4)	-20(2)	10(2)	22(3)
C(22)	46(2)	54(3)	79(3)	7(2)	35(2)	20(2)
C(23)	55(2)	47(2)	41(2)	-10(2)	13(2)	6(2)
C(24)	44(2)	41(2)	59(3)	2(2)	8(2)	20(2)
C(25)	60(3)	42(2)	69(3)	22(2)	10(2)	10(2)
C(26)	30(2)	68(3)	74(3)	16(2)	4(2)	-4(3)
C(27)	40(2)	61(3)	63(3)	9(2)	22(2)	-1(2)
C(28)	49(2)	54(2)	44(2)	16(2)	6(2)	-12(2)
C(29)	44(2)	34(2)	84(4)	4(2)	8(2)	-10(2)
C(30)	31(2)	40(2)	49(2)	-10(2)	5(1)	-8(2)
C(31)	26(2)	45(2)	47(2)	-3(1)	7(2)	7(2)
C(32)	26(2)	51(2)	73(3)	2(2)	3(2)	-10(2)
C(33)	33(2)	57(2)	47(2)	7(2)	1(2)	11(2)
O(30)	66(2)	70(2)	55(2)	-17(2)	8(2)	-23(2)
O(31)	33(1)	68(2)	85(2)	10(1)	3(1)	21(2)
O(32)	39(2)	73(2)	167(4)	-21(2)	10(2)	-36(2)
O(33)	60(2)	100(3)	42(2)	10(2)	1(1)	18(2)

The anisotropic displacement exponent takes the form: $-2p^2(h^2a^{*2}U_{11} + ... + 2hka^*b^*U_{12})$

Table 8: Hydrogen coordinates (x 10^4) and isotropic displacement parameters ($Å^2$ x 10^3) for **26**.

	x	y	z	U
H(2)	2565(19)	1116(38)	2214(20)	60(12)
H(5A)	2634(43)	-1446(81)	-2120(43)	204(35)
H(5B)	2838(16)	-496(28)	-1821(15)	8(7)
H(5C)	1928(19)	-414(33)	-1836(18)	28(9)
H(6A)	2232(37)	-2831(66)	-98(37)	132(29)
H(6B)	1605(31)	-2385(55)	-731(33)	97(21)
H(6C)	2119(32)	-3149(60)	-993(34)	113(21)
H(7A)	3833(27)	-1809(52)	-189(25)	64(19)
H(7B)	3726(31)	-2063(56)	-917(32)	87(21)
H(9)	1764(25)	-2646(46)	1087(27)	84(15)
H(10)	688(26)	-3759(47)	1469(26)	75(16)
H(11)	-110(24)	-2946(45)	2257(25)	73(14)
H(12)	322(27)	-749(51)	2809(27)	82(17)
H(13)	1286(27)	26(47)	2571(27)	63(17)
H(15)	3833(23)	-52(42)	2761(23)	56(13)
H(16)	4846(24)	-1229(47)	3148(25)	68(15)
H(17)	5033(27)	-3201(53)	2515(30)	93(19)
H(18)	4199(24)	-3934(44)	1573(24)	64(14)
H(19)	3210(26)	-2725(47)	1261(26)	75(16)
H(20)	3625(20)	4904(37)	92(20)	36(11)
H(21)	4707(29)	3418(57)	180(31)	109(21)
H(22)	4411(22)	1837(41)	-836(23)	50(13)
H(23)	3199(24)	2288(44)	-1538(24)	62(14)
H(24)	2721(20)	4207(38)	-970(20)	42(11)
H(25)	1124(21)	4509(39)	-288(21)	44(12)
H(26)	194(22)	2980(43)	-69(23)	58(13)
H(27)	568(22)	1909(39)	1222(22)	50(12)
H(28)	1684(23)	2863(43)	1751(24)	61(14)
H(29)	2016(21)	4548(39)	808(22)	43(12)

Table 9: Atomic coordinates (x 10^4) and equivalent isotropic displacement parameters (A^2 x 10^3) for **32**.

U(eq) is defined as one third of the trace of the orthogonalized Uij tensor.

	x	y	z	U(eq)
Co(1)	-873(1)	1177(1)	3815(1)	40(1)
Co(2)	754(1)	1535(1)	4174(1)	39(1)
O(1)	0	2270(3)	2500	49(1)
Si(1)	793(1)	1881(1)	2918(1)	40(1)
Si(4)	-415(1)	4523(1)	3956(1)	49(1)
C(2)	240(2)	1994(2)	3512(1)	36(1)
C(3)	-106(2)	2807(2)	3835(1)	36(1)
C(11)	-758(2)	-497(3)	3626(1)	60(1)
O(11)	-686(2)	-1530(2)	3502(1)	101(1)
C(12)	-1490(2)	1120(3)	4377(1)	62(1)
O(12)	-1878(2)	1067(3)	4722(1)	103(1)
C(13)	-1865(2)	1657(3)	3437(1)	53(1)
O(13)	-2500(2)	1969(3)	3202(1)	86(1)
C(21)	1859(2)	2394(3)	4212(1)	59(1)
O(21)	2555(2)	2934(3)	4245(1)	99(1)
C(22)	455(2)	1683(3)	4801(1)	51(1)
O(22)	284(2)	1779(3)	5194(1)	83(1)
C(23)	1198(2)	-106(3)	4105(1)	53(1)
O(23)	1481(2)	-1123(2)	4063(1)	78(1)
C(31)	1759(2)	3104(4)	2915(1)	75(1)
C(32)	1232(2)	209(3)	2811(1)	67(1)
C(41)	-1164(3)	5091(3)	3434(1)	91(1)
C(42)	707(2)	5483(3)	4011(1)	76(1)
C(43)	-1077(2)	4629(4)	4523(1)	76(1)

Table 10: Selected bond lengths [Å] and angles [deg] for **32**.

Co(1)-C(13)	1.784(3)	Si(1)-C(31)	1.854(3)
Co(1)-C(11)	1.808(3)	Si(1)-C(32)	1.855(3)
Co(1)-C(12)	1.812(3)	Si(4)-C(3)	1.852(2)
Co(1)-C(2)	1.992(2)	Si(4)-C(41)	1.853(3)
Co(1)-C(3)	1.994(2)	Si(4)-C(43)	1.859(3)
Co(1)-Co(2)	2.4914(5)	Si(4)-C(42)	1.865(3)
Co(2)-C(21)	1.790(3)	C(2)-C(3)	1.330(3)
Co(2)-C(22)	1.807(3)	C(11)-O(11)	1.122(4)
Co(2)-C(23)	1.813(3)	C(12)-O(12)	1.121(3)
Co(2)-C(3)	1.994(2)	C(13)-O(13)	1.133(3)
Co(2)-C(2)	2.002(2)	C(21)-O(21)	1.128(3)
O(1)-Si(1)	1.6284(9)	C(22)-O(22)	1.130(3)
O(1)-Si(1a)	1.6284(9)	C(23)-O(23)	1.126(3)
Si(1)-C(2)	1.849(2)		

C(13)-Co(1)-C(11)	99.80(14)	C(21)-Co(2)-C(2)	102.81(11)
C(13)-Co(1)-C(12)	96.92(13)	C(22)-Co(2)-C(2)	140.35(11)
C(11)-Co(1)-C(12)	105.6(2)	C(23)-Co(2)-C(2)	103.79(11)
C(13)-Co(1)-C(2)	104.39(11)	C(3)-Co(2)-C(2)	38.88(9)
C(11)-Co(1)-C(2)	101.51(12)	C(21)-Co(2)-Co(1)	151.88(10)
C(12)-Co(1)-C(2)	141.85(12)	C(22)-Co(2)-Co(1)	98.71(9)
C(13)-Co(1)-C(3)	101.28(11)	C(23)-Co(2)-Co(1)	97.84(9)
C(11)-Co(1)-C(3)	138.95(12)	C(3)-Co(2)-Co(1)	51.34(6)
C(12)-Co(1)-C(3)	106.30(12)	C(2)-Co(2)-Co(1)	51.23(6)
C(2)-Co(1)-C(3)	38.98(9)	Si(1)-O(1)-Si(1a)	151.5(2)
C(13)-Co(1)-Co(2)	151.90(9)	O(1)-Si(1)-C(2)	108.39(7)
C(11)-Co(1)-Co(2)	99.55(10)	O(1)-Si(1)-C(31)	108.34(14)
C(12)-Co(1)-Co(2)	97.28(9)	C(2)-Si(1)-C(31)	107.13(12)
C(2)-Co(1)-Co(2)	51.59(6)	O(1)-Si(1)-C(32)	109.82(13)
C(3)-Co(1)-Co(2)	51.32(6)	C(2)-Si(1)-C(32)	110.77(13)
C(21)-Co(2)-C(22)	97.78(14)	C(31)-Si(1)-C(32)	112.3(2)
C(21)-Co(2)-C(23)	99.37(14)	C(3)-Si(4)-C(41)	106.87(14)
C(22)-Co(2)-C(23)	105.81(13)	C(3)-Si(4)-C(43)	109.72(14)
C(21)-Co(2)-C(3)	102.50(12)	C(41)-Si(4)-C(43)	110.5(2)
C(22)-Co(2)-C(3)	103.74(11)	C(3)-Si(4)-C(42)	108.35(13)
C(23)-Co(2)-C(3)	140.14(11)	C(41)-Si(4)-C(42)	110.7(2)

C(43)-Si(4)-C(42)	110.6(2)	C(2)-C(3)-Co(1)	70.44(13)
C(3)-C(2)-Si(1)	144.6(2)	Si(4)-C(3)-Co(1)	132.51(12)
C(3)-C(2)-Co(1)	70.58(13)	Co(2)-C(3)-Co(1)	77.34(8)
Si(1)-C(2)-Co(1)	135.44(12)	O(11)-C(11)-Co(1)	179.1(3)
C(3)-C(2)-Co(2)	70.21(13)	O(12)-C(12)-Co(1)	178.9(3)
Si(1)-C(2)-Co(2)	130.47(12)	O(13)-C(13)-Co(1)	179.2(3)
Co(1)-C(2)-Co(2)	77.18(8)	O(21)-C(21)-Co(2)	178.7(3)
C(2)-C(3)-Si(4)	144.6(2)	O(22)-C(22)-Co(2)	178.8(3)
C(2)-C(3)-Co(2)	70.91(13)	O(23)-C(23)-Co(2)	179.5(3)
Si(4)-C(3)-Co(2)	133.06(12)		

Table 11: Anisotropic displacement parameters ($Å^2$ x 10^3) for **32**.

The anisotropic displacement factor exponent takes the form:
$-2p^2$ [h^2 a^{*2} U11 + ... + 2 h k a* b* U12]

	U11	U22	U33	U23	U13	U12
Co(1)	37(1)	42(1)	41(1)	3(1)	3(1)	-10(1)
Co(2)	39(1)	41(1)	37(1)	5(1)	-2(1)	-3(1)
O(1)	59(2)	53(2)	36(1)	0	-8(1)	0
Si(1)	36(1)	51(1)	33(1)	-1(1)	3(1)	-4(1)
Si(4)	51(1)	39(1)	57(1)	-6(1)	-4(1)	1(1)
C(2)	33(1)	40(1)	35(1)	3(1)	0(1)	-6(1)
C(3)	36(1)	37(1)	37(1)	4(1)	0(1)	-3(1)
C(11)	57(2)	50(2)	74(2)	-1(1)	2(1)	-15(1)
O(11)	103(2)	51(1)	148(3)	-19(2)	4(2)	-15(1)
C(12)	51(2)	88(2)	49(2)	6(2)	6(1)	-19(2)
O(12)	85(2)	164(3)	60(2)	9(2)	28(1)	-29(2)
C(13)	42(1)	68(2)	51(1)	3(1)	4(1)	-9(1)
O(13)	54(1)	124(2)	79(2)	18(2)	-12(1)	0(1)
C(21)	51(2)	62(2)	64(2)	8(1)	-8(1)	-8(1)
O(21)	58(1)	105(2)	132(2)	12(2)	-15(2)	-32(1)
C(22)	54(1)	57(2)	43(1)	5(1)	-4(1)	-4(1)
O(22)	102(2)	105(2)	42(1)	1(1)	8(1)	-4(2)
C(23)	48(1)	55(2)	54(2)	8(1)	-1(1)	-1(1)
O(23)	84(2)	53(1)	97(2)	2(1)	1(1)	15(1)
C(31)	62(2)	107(3)	58(2)	-6(2)	15(1)	-37(2)
C(32)	65(2)	72(2)	62(2)	-7(2)	7(2)	24(2)
C(41)	113(3)	57(2)	99(3)	9(2)	-39(2)	16(2)
C(42)	77(2)	50(2)	100(3)	-13(2)	10(2)	-18(2)
C(43)	69(2)	82(2)	79(2)	-27(2)	13(2)	8(2)

Table 12: Hydrogen coordinates (x 10^4) and isotropic displacement parameters ($Å^2$ x 10^3) for **32**.

	x	y	z	U(eq)
H(31A)	2064(2)	3073(4)	2611(1)	113
H(31B)	2215(2)	2917(4)	3172(1)	113
H(31C)	1498(2)	3955(4)	2962(1)	113
H(32A)	1516(2)	170(3)	2502(1)	100
H(32B)	711(2)	-391(3)	2817(1)	100
H(32C)	1697(2)	-18(3)	3059(1)	100
H(41A)	-1340(3)	5982(3)	3483(1)	136
H(41B)	-1726(3)	4565(3)	3404(1)	136
H(41C)	-815(3)	5021(3)	3144(1)	136
H(42A)	560(2)	6377(3)	4073(1)	113
H(42B)	1038(2)	5421(3)	3715(1)	113
H(42C)	1101(2)	5145(3)	4272(1)	113
H(43A)	-1236(2)	5520(4)	4584(1)	114
H(43B)	-689(2)	4298(4)	4787(1)	114
H(43C)	-1649(2)	4124(4)	4489(1)	114

Table 13: Atomic coordinates (x 10^4) and equivalent isotropic displacement parameters (A^2 x 10^3) for **43**.

U(eq) is defined as one third of the trace of the orthogonalized Uij tensor.

	x	y	z	U(eq)
Mo(1)	2597(1)	3594(1)	1870(1)	43(1)
Mo(2)	1916(1)	2688(1)	948(1)	43(1)
Si(3)	70(1)	3960(1)	1404(1)	47(1)
Si(2)	2100(1)	5765(1)	1032(1)	52(1)
C(1)	1942(3)	4376(3)	1234(1)	39(1)
C(2)	1279(3)	3793(3)	1373(1)	38(1)
C(3)	3893(4)	2764(5)	2260(2)	81(2)
C(4)	3762(4)	3704(6)	2497(2)	84(2)
C(5)	3874(3)	4572(5)	2199(2)	74(2)
C(6)	4071(3)	4142(4)	1789(2)	62(1)
C(7)	4083(3)	3026(5)	1829(2)	68(2)
C(8)	1686(5)	1200(4)	478(2)	81(2)
C(9)	2375(5)	934(4)	845(2)	79(2)
C(10)	2012(4)	926(4)	1249(2)	77(2)
C(11)	1090(4)	1184(4)	1139(2)	73(2)
C(12)	883(4)	1355(4)	659(2)	82(2)
C(13)	3098(3)	3121(5)	819(2)	64(1)
C(14)	1429(3)	3476(4)	372(2)	55(1)
C(15)	1951(3)	4510(4)	2256(2)	55(1)
C(16)	1916(4)	2427(4)	2089(2)	63(1)
C(17)	-335(4)	2970(5)	1792(2)	83(2)
C(18)	-143(4)	5318(5)	1633(2)	81(2)
C(19)	-604(3)	3840(5)	808(2)	67(1)
O(13)	3788(3)	3299(4)	721(2)	95(2)
O(14)	1180(3)	3873(4)	19(1)	87(1)
O(15)	1630(3)	4999(4)	2517(1)	87(1)
O(16)	1562(3)	1728(4)	2245(1)	90(1)
C(20)	2202(4)	6696(4)	1536(2)	76(2)
C(21)	3116(4)	5885(5)	752(2)	92(2)
C(22)	1101(4)	6232(4)	592(2)	78(2)
C(23A)	932(17)	7400(19)	596(9)	80(2)
C(23B)	1311(7)	7323(8)	395(4)	80(2)
C(24)	1020(7)	8194(7)	478(4)	153(4)

Table 14: Selected bond lengths [Å] and angles [deg] for **43**.

Mo(1)-C(16)	1.952(6)	Si(2)-C(1)	1.858(4)
Mo(1)-C(15)	1.974(5)	Si(2)-C(21)	1.863(6)
Mo(1)-C(1)	2.172(4)	Si(2)-C(22)	1.889(6)
Mo(1)-C(2)	2.257(4)	C(1)-C(2)	1.353(5)
Mo(1)-C(4)	2.302(5)	C(3)-C(7)	1.375(8)
Mo(1)-C(3)	2.322(5)	C(3)-C(4)	1.393(9)
Mo(1)-C(5)	2.334(5)	C(4)-C(5)	1.417(9)
Mo(1)-C(7)	2.370(5)	C(5)-C(6)	1.388(8)
Mo(1)-C(6)	2.373(5)	C(6)-C(7)	1.397(8)
Mo(1)-Mo(2)	2.9290(8)	C(8)-C(9)	1.393(8)
Mo(2)-C(13)	1.959(5)	C(8)-C(12)	1.415(9)
Mo(2)-C(14)	1.972(5)	C(9)-C(10)	1.383(8)
Mo(2)-C(2)	2.183(4)	C(10)-C(11)	1.406(8)
Mo(2)-C(1)	2.262(4)	C(11)-C(12)	1.394(8)
Mo(2)-C(8)	2.296(5)	C(13)-O(13)	1.147(6)
Mo(2)-C(9)	2.330(5)	C(14)-O(14)	1.143(6)
Mo(2)-C(12)	2.330(5)	C(15)-O(15)	1.145(6)
Mo(2)-C(10)	2.361(5)	C(16)-O(16)	1.155(6)
Mo(2)-C(11)	2.370(5)	C(22)-C(23A)	1.48(2)
Si(3)-C(17)	1.849(6)	C(22)-C(23B)	1.531(11)
Si(3)-C(2)	1.850(4)	C(23A)-C(23B)	0.89(2)
Si(3)-C(19)	1.855(5)	C(23A)-C(24)	1.06(2)
Si(3)-C(18)	1.870(5)	C(23B)-C(24)	1.212(13)
Si(2)-C(20)	1.857(5)		
C(16)-Mo(1)-C(15)	84.6(2)	C(15)-Mo(1)-C(3)	115.9(2)
C(16)-Mo(1)-C(1)	115.3(2)	C(1)-Mo(1)-C(3)	146.5(2)
C(15)-Mo(1)-C(1)	91.7(2)	C(2)-Mo(1)-C(3)	158.7(2)
C(16)-Mo(1)-C(2)	80.7(2)	C(4)-Mo(1)-C(3)	35.1(2)
C(15)-Mo(1)-C(2)	80.6(2)	C(16)-Mo(1)-C(5)	134.3(2)
C(1)-Mo(1)-C(2)	35.51(14)	C(15)-Mo(1)-C(5)	85.3(2)
C(16)-Mo(1)-C(4)	99.0(2)	C(1)-Mo(1)-C(5)	109.5(2)
C(15)-Mo(1)-C(4)	84.1(2)	C(2)-Mo(1)-C(5)	140.7(2)
C(1)-Mo(1)-C(4)	144.9(2)	C(4)-Mo(1)-C(5)	35.6(2)
C(2)-Mo(1)-C(4)	164.6(2)	C(3)-Mo(1)-C(5)	58.1(2)
C(16)-Mo(1)-C(3)	87.3(2)	C(16)-Mo(1)-C(7)	110.4(2)

C(15)-Mo(1)-C(7)	140.0(2)	C(2)-Mo(2)-C(12)	108.9(2)
C(1)-Mo(1)-C(7)	112.5(2)	C(1)-Mo(2)-C(12)	139.9(2)
C(2)-Mo(1)-C(7)	137.1(2)	C(8)-Mo(2)-C(12)	35.6(2)
C(4)-Mo(1)-C(7)	57.6(2)	C(9)-Mo(2)-C(12)	58.5(2)
C(3)-Mo(1)-C(7)	34.1(2)	C(13)-Mo(2)-C(10)	109.2(2)
C(5)-Mo(1)-C(7)	57.3(2)	C(14)-Mo(2)-C(10)	140.3(2)
C(16)-Mo(1)-C(6)	143.3(2)	C(2)-Mo(2)-C(10)	112.4(2)
C(15)-Mo(1)-C(6)	117.0(2)	C(1)-Mo(2)-C(10)	137.2(2)
C(1)-Mo(1)-C(6)	94.5(2)	C(8)-Mo(2)-C(10)	57.5(2)
C(2)-Mo(1)-C(6)	129.5(2)	C(9)-Mo(2)-C(10)	34.3(2)
C(4)-Mo(1)-C(6)	57.8(2)	C(12)-Mo(2)-C(10)	57.5(2)
C(3)-Mo(1)-C(6)	57.1(2)	C(13)-Mo(2)-C(11)	142.7(2)
C(5)-Mo(1)-C(6)	34.3(2)	C(14)-Mo(2)-C(11)	117.6(2)
C(7)-Mo(1)-C(6)	34.3(2)	C(2)-Mo(2)-C(11)	93.8(2)
C(16)-Mo(1)-Mo(2)	83.8(2)	C(1)-Mo(2)-C(11)	128.7(2)
C(15)-Mo(1)-Mo(2)	128.08(14)	C(8)-Mo(2)-C(11)	58.0(2)
C(1)-Mo(1)-Mo(2)	49.99(10)	C(9)-Mo(2)-C(11)	57.8(2)
C(2)-Mo(1)-Mo(2)	47.64(10)	C(12)-Mo(2)-C(11)	34.5(2)
C(4)-Mo(1)-Mo(2)	147.7(2)	C(10)-Mo(2)-C(11)	34.6(2)
C(3)-Mo(1)-Mo(2)	113.9(2)	C(13)-Mo(2)-Mo(1)	83.5(2)
C(5)-Mo(1)-Mo(2)	135.1(2)	C(14)-Mo(2)-Mo(1)	127.32(14)
C(7)-Mo(1)-Mo(2)	91.14(14)	C(2)-Mo(2)-Mo(1)	49.82(10)
C(6)-Mo(1)-Mo(2)	101.67(14)	C(1)-Mo(2)-Mo(1)	47.35(10)
C(13)-Mo(2)-C(14)	85.0(2)	C(8)-Mo(2)-Mo(1)	148.3(2)
C(13)-Mo(2)-C(2)	116.1(2)	C(9)-Mo(2)-Mo(1)	114.6(2)
C(14)-Mo(2)-C(2)	91.9(2)	C(12)-Mo(2)-Mo(1)	135.3(2)
C(13)-Mo(2)-C(1)	81.8(2)	C(10)-Mo(2)-Mo(1)	91.7(2)
C(14)-Mo(2)-C(1)	80.2(2)	C(11)-Mo(2)-Mo(1)	101.7(2)
C(2)-Mo(2)-C(1)	35.39(14)	C(17)-Si(3)-C(2)	112.8(2)
C(13)-Mo(2)-C(8)	98.9(2)	C(17)-Si(3)-C(19)	109.5(3)
C(14)-Mo(2)-C(8)	84.3(2)	C(2)-Si(3)-C(19)	109.0(2)
C(2)-Mo(2)-C(8)	144.4(2)	C(17)-Si(3)-C(18)	106.9(3)
C(1)-Mo(2)-C(8)	164.3(2)	C(2)-Si(3)-C(18)	110.6(2)
C(13)-Mo(2)-C(9)	86.2(2)	C(19)-Si(3)-C(18)	107.9(3)
C(14)-Mo(2)-C(9)	115.6(2)	C(20)-Si(2)-C(1)	109.3(2)
C(2)-Mo(2)-C(9)	146.7(2)	C(20)-Si(2)-C(21)	109.6(3)
C(1)-Mo(2)-C(9)	159.3(2)	C(1)-Si(2)-C(21)	112.0(3)
C(8)-Mo(2)-C(9)	35.0(2)	C(20)-Si(2)-C(22)	106.8(3)
C(13)-Mo(2)-C(12)	134.3(2)	C(1)-Si(2)-C(22)	111.8(2)
C(14)-Mo(2)-C(12)	85.7(2)	C(21)-Si(2)-C(22)	107.2(3)

C(2)-C(1)-Si(2)	137.6(3)	C(9)-C(8)-Mo(2)	73.8(3)
C(2)-C(1)-Mo(1)	75.7(2)	C(12)-C(8)-Mo(2)	73.5(3)
Si(2)-C(1)-Mo(1)	128.6(2)	C(10)-C(9)-C(8)	107.6(6)
C(2)-C(1)-Mo(2)	69.1(2)	C(10)-C(9)-Mo(2)	74.1(3)
Si(2)-C(1)-Mo(2)	138.2(2)	C(8)-C(9)-Mo(2)	71.2(3)
Mo(1)-C(1)-Mo(2)	82.65(14)	C(9)-C(10)-C(11)	109.1(6)
C(1)-C(2)-Si(3)	137.6(3)	C(9)-C(10)-Mo(2)	71.6(3)
C(1)-C(2)-Mo(2)	75.5(2)	C(11)-C(10)-Mo(2)	73.1(3)
Si(3)-C(2)-Mo(2)	129.3(2)	C(12)-C(11)-C(10)	107.5(6)
C(1)-C(2)-Mo(1)	68.8(2)	C(12)-C(11)-Mo(2)	71.2(3)
Si(3)-C(2)-Mo(1)	138.0(2)	C(10)-C(11)-Mo(2)	72.4(3)
Mo(2)-C(2)-Mo(1)	82.54(13)	C(11)-C(12)-C(8)	107.4(6)
C(7)-C(3)-C(4)	108.8(6)	C(11)-C(12)-Mo(2)	74.3(3)
C(7)-C(3)-Mo(1)	74.9(3)	C(8)-C(12)-Mo(2)	70.9(3)
C(4)-C(3)-Mo(1)	71.7(3)	O(13)-C(13)-Mo(2)	174.3(5)
C(3)-C(4)-C(5)	107.2(5)	O(14)-C(14)-Mo(2)	174.5(4)
C(3)-C(4)-Mo(1)	73.2(3)	O(15)-C(15)-Mo(1)	173.3(4)
C(5)-C(4)-Mo(1)	73.4(3)	O(16)-C(16)-Mo(1)	175.2(4)
C(6)-C(5)-C(4)	107.5(5)	C(23A)-C(22)-C(23B)	34.5(10)
C(6)-C(5)-Mo(1)	74.4(3)	C(23A)-C(22)-Si(2)	114.6(9)
C(4)-C(5)-Mo(1)	71.0(3)	C(23B)-C(22)-Si(2)	109.7(5)
C(5)-C(6)-C(7)	108.3(6)	C(23B)-C(23A)-C(24)	76(2)
C(5)-C(6)-Mo(1)	71.3(3)	C(23B)-C(23A)-C(22)	76(2)
C(7)-C(6)-Mo(1)	72.8(3)	C(24)-C(23A)-C(22)	152(3)
C(3)-C(7)-C(6)	108.2(5)	C(23A)-C(23B)-C(24)	58(2)
C(3)-C(7)-Mo(1)	71.0(3)	C(23A)-C(23B)-C(22)	70(2)
C(6)-C(7)-Mo(1)	73.0(3)	C(24)-C(23B)-C(22)	128.0(11)
C(9)-C(8)-C(12)	108.4(6)	C(23A)-C(24)-C(23B)	45.6(14)

Table 15: Anisotropic displacement parameters ($Å^2$ x 10^3) for **43**.

The anisotropic displacement factor exponent takes the form:
$-2p^2$ [h^2 a^{*2} U11 + ... + 2 h k a* b* U12]

	U11	U22	U33	U23	U13	U12
Mo(1)	40(1)	46(1)	39(1)	-1(1)	-1(1)	3(1)
Mo(2)	43(1)	42(1)	41(1)	-6(1)	4(1)	5(1)
Si(3)	36(1)	53(1)	53(1)	-5(1)	10(1)	0(1)
Si(2)	56(1)	44(1)	55(1)	6(1)	6(1)	-10(1)
C(1)	41(2)	38(2)	39(2)	-1(2)	6(2)	-1(2)
C(2)	40(2)	34(2)	38(2)	-1(2)	2(2)	3(2)
C(3)	58(3)	81(4)	90(4)	17(4)	-23(3)	19(3)
C(4)	54(3)	135(6)	54(3)	-15(4)	-17(2)	6(4)
C(5)	49(3)	74(4)	90(4)	-28(3)	-12(3)	4(3)
C(6)	35(2)	70(3)	78(4)	-5(3)	1(2)	-3(2)
C(7)	43(3)	73(4)	83(4)	-19(3)	-7(2)	16(2)
C(8)	116(5)	57(3)	65(4)	-26(3)	7(3)	8(3)
C(9)	92(4)	54(3)	92(5)	-14(3)	19(4)	21(3)
C(10)	97(5)	45(3)	83(4)	3(3)	1(3)	15(3)
C(11)	93(4)	43(3)	86(4)	-10(3)	23(3)	-9(3)
C(12)	83(4)	47(3)	104(5)	-20(3)	-20(4)	-4(3)
C(13)	55(3)	77(3)	60(3)	-15(3)	12(2)	3(3)
C(14)	66(3)	58(3)	41(2)	-8(2)	7(2)	5(2)
C(15)	54(3)	65(3)	46(3)	-5(2)	6(2)	-3(2)
C(16)	69(3)	63(3)	50(3)	12(2)	-3(2)	7(3)
C(17)	62(3)	107(5)	88(4)	22(4)	31(3)	-6(3)
C(18)	54(3)	81(4)	112(5)	-32(4)	24(3)	10(3)
C(19)	47(3)	81(4)	71(3)	-3(3)	-2(2)	6(3)
O(13)	54(2)	153(4)	85(3)	-23(3)	29(2)	-10(3)
O(14)	117(3)	92(3)	47(2)	10(2)	2(2)	11(3)
O(15)	91(3)	108(3)	68(3)	-28(2)	32(2)	4(3)
O(16)	109(3)	85(3)	73(3)	35(2)	9(2)	-17(3)
C(20)	103(4)	47(3)	74(4)	-8(3)	-1(3)	-12(3)
C(21)	98(5)	87(4)	100(5)	27(4)	41(4)	-20(4)
C(22)	95(4)	59(3)	71(4)	19(3)	-14(3)	-10(3)
C(24)	152(8)	68(5)	223(12)	34(6)	-12(8)	4(6)

Table 16: Hydrogen coordinates (x 10^4) and isotropic displacement parameters ($Å^2$ x 10^3) for **43**.

	x	y	z	U(eq)
H(3A)	3920(4)	2055(5)	2390(2)	97
H(4A)	3701(4)	3756(6)	2819(2)	101
H(5A)	3887(3)	5317(5)	2282(2)	89
H(6A)	4225(3)	4546(4)	1533(2)	75
H(7A)	4247(3)	2531(5)	1606(2)	82
H(8A)	1730(5)	1163(4)	153(2)	97
H(9A)	2974(5)	704(4)	822(2)	95
H(10A)	2327(4)	721(4)	1552(2)	92
H(11A)	669(4)	1180(4)	1352(2)	88
H(12A)	291(4)	1472(4)	482(2)	99
H(17A)	-237(4)	2257(5)	1687(2)	125
H(17B)	-15(4)	3061(5)	2105(2)	125
H(17C)	-968(4)	3078(5)	1786(2)	125
H(18A)	200(4)	5402(5)	1942(2)	122
H(18B)	33(4)	5858(5)	1432(2)	122
H(18C)	-774(4)	5392(5)	1644(2)	122
H(19A)	-505(3)	3148(5)	682(2)	101
H(19B)	-1232(3)	3922(5)	823(2)	101
H(19C)	-425(3)	4388(5)	612(2)	101
H(20A)	2701(4)	6485(4)	1770(2)	114
H(20B)	2299(4)	7412(4)	1433(2)	114
H(20C)	1656(4)	6675(4)	1663(2)	114
H(21A)	3637(4)	5650(5)	967(2)	138
H(21B)	3046(4)	5451(5)	476(2)	138
H(21C)	3193(4)	6621(5)	670(2)	138
H(22A)	577(4)	5839(4)	639(2)	94
H(22B)	1213(4)	6058(4)	286(2)	94
H(22C)	568(4)	6214(4)	730(2)	94
H(22D)	1012(4)	5750(4)	331(2)	94
H(23A)	508(17)	7532(19)	800(9)	96
H(23B)	1697(7)	7287(8)	165(4)	96
H(24A)	1440(7)	8190(7)	266(4)	183
H(24B)	761(7)	8857(7)	557(4)	183
H(24C)	634(7)	8381(7)	695(4)	183
H(24D)	1245(7)	8742(7)	298(4)	183

Table 17: Atomic coordinates (x 10^4) and equivalent isotropic displacement parameters (A^2 x 10^3) for **45**.

U(eq) is defined as one third of the trace of the orthogonalized Uij tensor.

	x	y	z	U(eq)
Co(1)	6720(2)	6684(2)	3070(1)	60(1)
Co(2)	6774(1)	8244(2)	3346(1)	55(1)
Si(1)	7006(3)	7874(3)	1531(2)	62(1)
C(1)	5606(8)	7570(9)	2613(6)	42(3)
C(2)	6458(10)	7639(9)	2328(6)	46(4)
C(3)	8539(8)	7767(10)	1846(5)	117(7)
C(4)	6411(9)	7124(7)	743(6)	82(5)
C(5)	6600(15)	9014(9)	1249(8)	107(7)
C(6)	7081(19)	9274(13)	610(12)	139(9)
C(7)	6515(21)	9416(14)	-21(11)	178(11)
C(21)	6434(13)	9311(11)	3068(8)	71(5)
O(21)	6219(10)	10034(6)	2936(6)	97(4)
C(22)	6439(10)	8186(11)	4229(7)	61(4)
O(22)	6228(8)	8156(8)	4791(4)	94(4)
C(23)	8267(13)	8381(11)	3676(7)	72(5)
O(23)	9216(8)	8458(8)	3915(5)	98(4)
C(11)	6335(13)	6281(9)	3865(8)	72(5)
O(11)	6070(9)	6045(6)	4382(6)	93(4)
C(12)	6332(15)	5811(11)	2463(9)	80(6)
O(12)	6036(10)	5258(7)	2033(6)	110(4)
C(13)	8175(13)	6479(10)	3350(7)	70(5)
O(13)	9113(9)	6357(7)	3526(6)	104(4)

Table 18: Selected bond lengths [Å] and angles [deg] for **45**.

Co(1)-C(12)	1.73(2)	Si(1)-C(3)	1.853(10)
Co(1)-C(13)	1.78(2)	Si(1)-C(5)	1.864(14)
Co(1)-C(11)	1.783(14)	C(1)-C(2)	1.331(14)
Co(1)-C(1)	1.962(12)	C(1)-C(1A)	1.46(2)
Co(1)-C(2)	1.969(12)	C(5)-C(6)	1.53(2)
Co(1)-Co(2)	2.460(3)	C(6)-C(7)	1.19(2)
Co(2)-C(21)	1.74(2)	C(21)-O(21)	1.157(13)
Co(2)-C(22)	1.796(12)	C(22)-O(22)	1.143(11)
Co(2)-C(23)	1.81(2)	C(23)-O(23)	1.151(14)
Co(2)-C(1)	1.973(10)	C(11)-O(11)	1.156(14)
Co(2)-C(2)	2.023(12)	C(12)-O(12)	1.15(2)
Si(1)-C(2)	1.832(12)	C(13)-O(13)	1.145(14)
Si(1)-C(4)	1.834(10)		
		C(23)-Co(2)-C(1)	141.5(6)
C(12)-Co(1)-C(13)	96.8(8)	C(21)-Co(2)-C(2)	101.7(6)
C(12)-Co(1)-C(11)	99.3(7)	C(22)-Co(2)-C(2)	141.1(6)
C(13)-Co(1)-C(11)	101.9(6)	C(23)-Co(2)-C(2)	105.4(6)
C(12)-Co(1)-C(1)	103.8(6)	C(1)-Co(2)-C(2)	38.9(4)
C(13)-Co(1)-C(1)	142.5(6)	C(21)-Co(2)-Co(1)	151.4(5)
C(11)-Co(1)-C(1)	105.1(6)	C(22)-Co(2)-Co(1)	97.9(5)
C(12)-Co(1)-C(2)	100.4(6)	C(23)-Co(2)-Co(1)	98.4(6)
C(13)-Co(1)-C(2)	106.3(6)	C(1)-Co(2)-Co(1)	51.1(4)
C(11)-Co(1)-C(2)	143.0(6)	C(2)-Co(2)-Co(1)	51.0(4)
C(1)-Co(1)-C(2)	39.6(4)	C(2)-Si(1)-C(4)	110.1(6)
C(12)-Co(1)-Co(2)	152.2(5)	C(2)-Si(1)-C(3)	109.7(5)
C(13)-Co(1)-Co(2)	98.7(5)	C(4)-Si(1)-C(3)	109.6(6)
C(11)-Co(1)-Co(2)	99.8(5)	C(2)-Si(1)-C(5)	105.8(7)
C(1)-Co(1)-Co(2)	51.5(3)	C(4)-Si(1)-C(5)	111.3(6)
C(2)-Co(1)-Co(2)	53.0(4)	C(3)-Si(1)-C(5)	110.3(8)
C(21)-Co(2)-C(22)	102.1(7)	C(2)-C(1)-C(1A)	141.8(13)
C(21)-Co(2)-C(23)	97.4(8)	C(2)-C(1)-Co(1)	70.5(8)
C(22)-Co(2)-C(23)	101.6(5)	C(1A)-C(1)-Co(1)	132.7(5)
C(21)-Co(2)-C(1)	103.3(6)	C(2)-C(1)-Co(2)	72.6(8)
C(22)-Co(2)-C(1)	105.3(6)	C(1A)-C(1)-Co(2)	134.5(8)

Co(1)-C(1)-Co(2)	77.4(3)	C(7)-C(6)-C(5)	123(3)
C(1)-C(2)-Si(1)	150.5(10)	O(21)-C(21)-Co(2)	175(2)
C(1)-C(2)-Co(1)	70.0(8)	O(22)-C(22)-Co(2)	180(2)
Si(1)-C(2)-Co(1)	132.6(7)	O(23)-C(23)-Co(2)	177.3(14)
C(1)-C(2)-Co(2)	68.5(8)	O(11)-C(11)-Co(1)	178(2)
Si(1)-C(2)-Co(2)	129.1(7)	O(12)-C(12)-Co(1)	176(2)
Co(1)-C(2)-Co(2)	76.1(4)	O(13)-C(13)-Co(1)	179(2)
C(6)-C(5)-Si(1)	108.9(12)		

Table 19: Anisotropic displacement parameters ($Å^2$ x 10^3) for **45**.

The anisotropic displacement factor exponent takes the form:
$-2p^2$ [h^2 a^{*2} U11 + ... + 2 h k a* b* U12]

	U11	U22	U33	U23	U13	U12
Co(1)	53(2)	60(2)	64(1)	2(2)	14(1)	7(2)
Co(2)	43(1)	64(2)	54(1)	-1(1)	9(1)	-5(2)
Si(1)	52(2)	79(4)	58(3)	0(3)	22(2)	-2(3)
C(2)	51(8)	51(9)	45(9)	0(8)	21(7)	-3(9)
C(3)	49(9)	220(22)	89(10)	-2(12)	27(8)	-6(13)
C(4)	77(10)	107(14)	69(10)	-3(9)	36(9)	6(9)
C(5)	149(19)	120(17)	61(12)	-6(11)	42(12)	-32(14)
C(6)	147(24)	99(17)	168(24)	-5(20)	44(21)	75(16)
C(7)	241(32)	150(20)	127(19)	9(20)	33(21)	39(23)
C(21)	58(12)	84(13)	66(11)	12(12)	7(9)	7(13)
O(21)	106(10)	65(8)	119(10)	2(8)	31(8)	5(9)
C(22)	40(9)	84(11)	61(10)	33(11)	21(8)	24(10)
O(22)	98(8)	134(9)	59(6)	-3(9)	37(6)	-28(9)
C(23)	63(12)	70(11)	64(9)	5(10)	-8(9)	2(13)
O(23)	51(7)	136(10)	90(7)	-29(8)	0(6)	-29(9)
C(11)	84(13)	66(12)	72(12)	-6(10)	34(10)	-24(10)
O(11)	104(10)	87(8)	106(10)	22(8)	57(8)	10(8)
C(12)	72(14)	88(15)	69(13)	-3(11)	-9(11)	24(13)
O(12)	107(10)	82(10)	121(11)	-33(7)	9(9)	17(9)
C(13)	46(11)	77(14)	80(10)	-13(10)	10(9)	13(11)
O(13)	47(7)	121(11)	136(9)	20(8)	5(7)	4(8)

Table 20: Hydrogen coordinates (x 10^4) and isotropic displacement parameters (Å x 10^3) for **45**.

	x	y	z	U(eq)
H(3A)	8823(8)	7891(10)	1427(5)	175
H(3B)	8738(8)	7187(10)	2021(5)	175
H(3C)	8849(8)	8167(10)	2252(5)	175
H(4A)	6703(9)	7252(7)	328(6)	123
H(4B)	5618(9)	7186(7)	576(6)	123
H(4C)	6601(9)	6541(7)	912(6)	123
H(5A)	5797(15)	9064(9)	1075(8)	129
H(5B)	6881(15)	9396(9)	1682(8)	129
H(6A)	7848(19)	9323(13)	718(12)	167
H(7A)	5747(21)	9370(14)	-141(11)	213
H(7B)	6840(21)	9572(14)	-395(11)	213

Table 21: Atomic coordinates (x 10^4) and equivalent isotropic displacement parameters (A^2 x 10^3) for **72**.

U(eq) is defined as one third of the trace of the orthogonalized Uij tensor.

	x	y	z	U(eq)
Co(2)	800(1)	7041(1)	4073(1)	37(1)
Fe(1)	1263(1)	8169(1)	2764(1)	35(1)
Si(1)	4268(1)	6491(1)	2941(1)	39(1)
C(2)	2798(4)	7264(2)	3355(2)	34(1)
C(3)	2538(4)	7878(2)	4029(2)	34(1)
C(4)	2745(4)	8762(2)	4134(2)	38(1)
C(5)	1855(5)	9300(3)	4837(3)	55(1)
C(6)	4329(5)	9172(3)	3869(3)	51(1)
C(7)	5218(6)	5862(3)	3983(3)	67(1)
C(8)	5758(6)	7046(3)	2236(3)	64(1)
F(1)	3277(3)	5833(2)	2210(2)	74(1)
C(11)	353(5)	7499(3)	1810(3)	50(1)
O(11)	-195(4)	7067(2)	1188(2)	79(1)
C(12)	-384(5)	8925(3)	2884(3)	50(1)
O(12)	-1397(4)	9409(2)	2998(3)	78(1)
C(13)	2384(5)	8770(3)	1920(3)	48(1)
O(13)	3073(4)	9127(2)	1363(2)	79(1)
C(21)	1594(5)	6448(3)	5148(3)	55(1)
O(21)	2118(5)	6086(3)	5823(3)	92(1)
C(22)	-918(5)	7590(3)	4517(3)	54(1)
O(22)	-2025(4)	7917(3)	4797(3)	87(1)
C(23)	-148(5)	6149(3)	3346(3)	50(1)
O(23)	-718(4)	5600(2)	2902(3)	83(1)

Table 22: Selected bond lengths [Å] and angles [deg] for **72**.

Co(2)-C(22)	1.800(4)	Si(1)-C(2)	1.826(3)
Co(2)-C(21)	1.807(5)	Si(1)-C(8)	1.837(4)
Co(2)-C(23)	1.838(4)	Si(1)-C(7)	1.843(4)
Co(2)-C(3)	1.937(4)	C(2)-C(3)	1.352(5)
Co(2)-C(2)	2.015(3)	C(3)-C(4)	1.386(5)
Co(2)-Fe(1)	2.5494(7)	C(4)-C(5)	1.506(5)
Fe(1)-C(11)	1.781(4)	C(4)-C(6)	1.522(5)
Fe(1)-C(13)	1.795(4)	C(11)-O(11)	1.144(5)
Fe(1)-C(12)	1.812(4)	C(12)-O(12)	1.142(5)
Fe(1)-C(3)	1.997(3)	C(13)-O(13)	1.130(5)
Fe(1)-C(2)	2.012(3)	C(21)-O(21)	1.133(5)
Fe(1)-C(4)	2.335(3)	C(22)-O(22)	1.138(5)
Si(1)-F(1)	1.601(3)	C(23)-O(23)	1.124(5)

C(22)-Co(2)-C(21)	102.1(2)	C(13)-Fe(1)-C(2)	106.1(2)
C(22)-Co(2)-C(23)	103.0(2)	C(12)-Fe(1)-C(2)	150.0(2)
C(21)-Co(2)-C(23)	99.5(2)	C(3)-Fe(1)-C(2)	39.42(14)
C(22)-Co(2)-C(3)	107.5(2)	C(11)-Fe(1)-C(4)	167.2(2)
C(21)-Co(2)-C(3)	98.4(2)	C(13)-Fe(1)-C(4)	92.6(2)
C(23)-Co(2)-C(3)	140.3(2)	C(12)-Fe(1)-C(4)	91.1(2)
C(22)-Co(2)-C(2)	141.4(2)	C(3)-Fe(1)-C(4)	36.28(13)
C(21)-Co(2)-C(2)	103.0(2)	C(2)-Fe(1)-C(4)	71.53(13)
C(23)-Co(2)-C(2)	101.3(2)	C(11)-Fe(1)-Co(2)	91.93(13)
C(3)-Co(2)-C(2)	39.95(14)	C(13)-Fe(1)-Co(2)	156.85(13)
C(22)-Co(2)-Fe(1)	94.59(14)	C(12)-Fe(1)-Co(2)	102.85(13)
C(21)-Co(2)-Fe(1)	148.40(14)	C(3)-Fe(1)-Co(2)	48.59(10)
C(23)-Co(2)-Fe(1)	102.68(13)	C(2)-Fe(1)-Co(2)	50.78(9)
C(3)-Co(2)-Fe(1)	50.63(10)	C(4)-Fe(1)-Co(2)	78.93(9)
C(2)-Co(2)-Fe(1)	50.67(10)	F(1)-Si(1)-C(2)	106.9(2)
C(11)-Fe(1)-C(13)	92.4(2)	F(1)-Si(1)-C(8)	107.5(2)
C(11)-Fe(1)-C(12)	99.7(2)	C(2)-Si(1)-C(8)	110.2(2)
C(13)-Fe(1)-C(12)	98.8(2)	F(1)-Si(1)-C(7)	107.9(2)
C(11)-Fe(1)-C(3)	131.3(2)	C(2)-Si(1)-C(7)	111.0(2)
C(13)-Fe(1)-C(3)	114.2(2)	C(8)-Si(1)-C(7)	113.0(2)
C(12)-Fe(1)-C(3)	114.4(2)	C(3)-C(2)-Si(1)	144.9(3)
C(11)-Fe(1)-C(2)	95.7(2)	C(3)-C(2)-Fe(1)	69.7(2)

Si(1)-C(2)-Fe(1)	138.1(2)	C(3)-C(4)-C(6)	119.2(3)
C(3)-C(2)-Co(2)	66.9(2)	C(5)-C(4)-C(6)	113.2(3)
Si(1)-C(2)-Co(2)	128.9(2)	C(3)-C(4)-Fe(1)	58.5(2)
Fe(1)-C(2)-Co(2)	78.54(12)	C(5)-C(4)-Fe(1)	118.5(3)
C(2)-C(3)-C(4)	137.7(3)	C(6)-C(4)-Fe(1)	112.2(2)
C(2)-C(3)-Co(2)	73.1(2)	O(11)-C(11)-Fe(1)	178.3(4)
C(4)-C(3)-Co(2)	138.0(3)	O(12)-C(12)-Fe(1)	177.2(4)
C(2)-C(3)-Fe(1)	70.9(2)	O(13)-C(13)-Fe(1)	177.6(4)
C(4)-C(3)-Fe(1)	85.3(2)	O(21)-C(21)-Co(2)	178.7(4)
Co(2)-C(3)-Fe(1)	80.78(13)	O(22)-C(22)-Co(2)	178.3(4)
C(3)-C(4)-C(5)	123.3(3)	O(23)-C(23)-Co(2)	179.5(4)

Symmetry transformations used to generate equivalent atoms

Table 23: Anisotropic displacement parameters ($Å^2$ x 10^3) for **72**.

The anisotropic displacement factor exponent takes the form:
$-2p^2$ [h^2 a^{*2} U11 + ... + 2 h k a* b* U12]

	U11	U22	U33	U23	U13	U12
Co(2)	35(1)	37(1)	40(1)	1(1)	5(1)	0(1)
Fe(1)	34(1)	37(1)	34(1)	1(1)	-1(1)	4(1)
Si(1)	36(1)	38(1)	44(1)	-6(1)	3(1)	6(1)
C(2)	29(2)	36(2)	37(2)	2(2)	3(1)	0(1)
C(3)	33(2)	36(2)	32(2)	0(2)	-2(1)	4(1)
C(4)	40(2)	35(2)	36(2)	0(2)	-5(2)	2(2)
C(5)	63(3)	47(2)	54(2)	-13(2)	9(2)	4(2)
C(6)	47(2)	45(2)	60(3)	-6(2)	0(2)	-10(2)
C(7)	63(3)	66(3)	72(3)	12(2)	9(2)	24(2)
C(8)	54(3)	86(3)	55(3)	8(2)	19(2)	12(2)
F(1)	67(2)	63(2)	89(2)	-39(2)	-6(2)	1(1)
C(11)	45(2)	58(3)	46(2)	0(2)	-1(2)	-2(2)
O(11)	78(2)	97(3)	59(2)	-28(2)	-12(2)	-18(2)
C(12)	49(2)	53(2)	47(2)	5(2)	-2(2)	11(2)
O(12)	67(2)	85(3)	80(2)	2(2)	3(2)	41(2)
C(13)	48(2)	53(2)	43(2)	3(2)	-3(2)	0(2)
O(13)	82(2)	91(3)	66(2)	20(2)	18(2)	-16(2)
C(21)	55(3)	55(3)	56(3)	10(2)	12(2)	5(2)
O(21)	105(3)	97(3)	73(2)	38(2)	8(2)	24(2)
C(22)	45(2)	62(3)	57(3)	5(2)	10(2)	3(2)
O(22)	58(2)	107(3)	100(3)	-6(2)	32(2)	24(2)
C(23)	38(2)	45(2)	68(3)	-2(2)	6(2)	-3(2)
O(23)	66(2)	66(2)	118(3)	-30(2)	4(2)	-20(2)

Table 24: Hydrogen coordinates (x 10^4) and isotropic displacement parameters ($Å^2$ x 10^3) for **72**.

	x	y	z	U(eq)
H(5A)	2180(5)	9892(3)	4790(3)	82
H(5B)	2114(5)	9097(3)	5496(3)	82
H(5C)	705(5)	9252(3)	4672(3)	82
H(6A)	4291(5)	9783(3)	3980(3)	76
H(6B)	4474(5)	9063(3)	3189(3)	76
H(6C)	5223(5)	8927(3)	4272(3)	76
H(7A)	5984(6)	5462(3)	3747(3)	100
H(7B)	4393(6)	5552(3)	4293(3)	100
H(7C)	5771(6)	6247(3)	4450(3)	100
H(8A)	6524(6)	6634(3)	2022(3)	96
H(8B)	6324(6)	7473(3)	2643(3)	96
H(8C)	5206(6)	7321(3)	1672(3)	96